REACTION CHEMISTRY IN CARBON DIOXIDE SEQUESTRATION

by

Prashanth Mandalaparty

A dissertation submitted to the faculty of
The University of Utah
in partial fulfillment of the requirements for the degree of

Doctor of Philosophy

Department of Chemical Engineering

The University of Utah

August 2012

The University of UtahGraduateSchool

STATEMENT OF DISSERTATION APPROVAL

The dissertation of **Prashanth Mandalaparty**

has been approved by the following supervisory committee members:

Milind D. Deo	, Chair	**08/08/2011** Date Approved
Edward M. Trujillo	, Member	**08/08/2011** Date Approved
JoAnn S. Lighty	, Member	**08/08/2011** Date Approved
Brian J. McPherson	, Member	**08/08/2011** Date Approved
Joseph N. Moore	, Member	**08/08/2011** Date Approved

and by **JoAnn S. Lighty** , Chair of the Department of **Chemical Engineering**

and by Charles A. Wight, Dean of The GraduateSchool.

ABSTRACT

Storing carbon dioxide generated by fossil fuel utilization will provide means of reducing CO_2 emissions into the atmosphere as the transition to carbon-neutral energy technologies unfolds. The brine-rock-CO_2 interactions that govern the long-term fate of CO_2 under conditions relevant to the geologic storage of CO_2 are largely unknown. Batch experiments were conducted in high-temperature, high-pressure reactors to establish the types of brine–rock-CO_2 reactions, including mineral precipitations. The solids were analyzed using X-Ray Diffraction (XRD), Scanning Electron Microscope/ Back Scattered Electron images (SEM/BSE) and Energy Dispersive X-Ray Spectroscopy analysis (EDS). The brine compositions were measured using Inductively Coupled Plasma Mass Spectrometry (ICP-MS) for cations and Ion Chromatography (IC) for anions.

The three formations, limestone, sandstone, and arkose, were chosen because of their common occurrence and their proximity to coal fire power plants. Peridotite was chosen because of its high reactivity. The experiments with synthetic arkose and CO_2 yielded precipitation of calcite, analcime, kaolinite, and ankerite. In experiments with limestone, extensive dissolution was observed in limestone-brine-CO_2 experiments with no precipitation. Precipitation of calcite and kaolinite (products of feldspar carbonation) were observed in sandstone experiments. Peridotite experiments yielded growth of orthorhombic crystals of magnesite. Growth of hollow Ca-zeolite crystals, alteration of clays, and trace amounts of dolomite precipitates were the principal observations in the

experiments with retorted shale. In experiments with CO_2+SO_2 as the feed gas, pronounced dissolution of all minerals and precipitation of kaolinite and anhydrite were observed. Precipitation of ammonium zeolites and calcite were observed in experiments with CO_2+NH_3. Increase in brine-to-rock ratio increases the pace of the reactions.

Modeling was performed by using the Geochemists WorkBench (GWB). The degassing simulations capture quenching and the secondary reactions that might occur during the de-pressurizing of the reactor. There was good agreement between the modeling and experimental results in all the cases and for all the ions barring calcium. A full factorial parameter sensitivity analysis was carried out to determine the principal kinetic factors affecting the behavior of a mineral species in the brine-arkose-CO_2 reaction system. This study shows that permanent sequestration of CO_2 in saline aquifers through mineral carbonation is highly dependent on the resident mineral composition and on the composition of the injected gas.

To my family

TABLE OF CONTENTS

LIST OF TABLES

LIST OF FIGURES

ACKNOWLEDGEMENTS

First and foremost, I am extremely grateful to my supervising advisor, Professor Milind D. Deo, who provided knowledge, guidance, and support through some of the tough and challenging times. I am also grateful to the members of my dissertation committee – JoAnn S. Lighty, Edward Trujillo, Brian McPherson, and Joesph N. Moore– for their comments and suggestions in critiquing the final draft of this dissertation.

I am thankful to my friends at the Petroleum Research Center for their input and help during my research time. I would specially like to thank Dr. Joseph N. Moore, in particular, for helping me out with different aspects of geochemical problems and guiding me all the way through the completion of my research. I would like to thank all the faculty and staff of the Chemical Engineering Department for making my graduate study pleasant.

I wish to thank my friends in Salt Lake City, who I regard as family, for making my stay a memorable one. Finally, I would like to express my gratitude to my family members for their unconditional love and support and for giving me courage and motivation through the difficult and enjoyable times.

1. INTRODUCTION

1.1. Background

Carbon dioxide (CO_2) is a greenhouse gas, whose release into the atmosphere from combustion of fossil fuels contributes to global warming. Trace gases in the atmosphere like carbon dioxide, methane, and water vapor trap infrared radiation escaping into space. Without such naturally occurring gases in our atmosphere, the earth's average temperature would be -18^0C instead of the comfortable $+15^0$C it is today. However, problems may arise when the atmospheric concentration of greenhouse gases increases. Rising global temperatures are expected to raise sea level, and change precipitation and other local climate conditions. Changing regional climate could alter forests, crop yields, and water supplies. It could also threaten human health and many types of ecosystems.

Carbon capture and storage (CCS) has been identified as the principal approach to mitigate the contribution of fossil fuel emissions to global warming. The overall task of diverting CO_2 to deep geologic reservoirs consists of three steps: capturing the flue gas, compression and transport of the flue gas, and injection of CO_2 into different target formations (depleted oil and gas reservoirs, unmineable coal seams, and deep saline aquifers). Technology for injecting CO_2 has long been used in the oil and gas industry for Enhanced Oil Recovery (EOR). The scale and scope of a meaningful CO_2 sequestration project are much larger than CO_2 EOR projects currently underway. CO_2 EOR is

accompanied by production of oil, water and CO_2 (after breakthrough) as a result of which the operation dynamics and associated risks are different. Sequestration must provide reasonably secure storage of CO_2. Otherwise, the energy penalty incurred in separating and storing CO_2 may result in net CO_2 emissions into the atmosphere basically negating the original objective. Injection into coal seams was also extensively studied. However, the storage capacity of these formations may not be sufficient to meet long-term needs.

Deep saline aquifers have been identified as the most viable target formations. They provide no economic return for CO_2 injection, but they are widespread and geographically associated with fossil fuel sources. Because it is not necessary to identify and inject directly into closed structural traps, they are likely to have large volumes and suitable injection sites in close proximity to power plant sources of CO_2 [1]. Deep saline aquifers have the highest storage potential sufficient to hold many decades worth of CO_2 emissions [2]. The sequestration physical processes must be understood to ensure that the process is engineered correctly

1.2. Trapping Mechanisms

The cumulative effectiveness of geological storage of CO_2 depends on a combination of physical and geochemical trapping mechanisms of which the following are considered important.

1. Structural trapping by an impervious confining layer or cap rock
2. Stratigraphic trapping below a formation whose entry capillary pressure is greater than the capillary pressure of the CO_2 phase
3. Residual phase trapping as the nonwetting phase becomes disconnected in pores

or small clusters of pores

4. Solubility trapping by CO_2 dissolution into the aqueous phase in the pore space
5. Mineralogical trapping by chemical reaction with aqueous species and minerals to precipitate carbonate minerals

Once injected, CO_2 being more buoyant than water will rise within the reservoir or along faults until it hits an impermeable membrane or low permeability seal. Some free CO_2 will become disconnected and remain in the pores, other free CO_2 will be trapped and accumulate below the low permeability or high capillary entry pressure layers. CO_2 will dissolve in the formation water depending on a rate controlled by several factors such as the rate of CO_2 injection, the rate of CO_2 dissolution into the pore water, the surface area available for the reaction, and the rate of diffusion of the CO_2 into the pore water. CO_2 then forms carbonic acid, which dissociates to form carbonate and bicarbonate ion, leading to ionic trapping of CO_2. This weak acid results in the dissolution of primary minerals, due to the decreased pH, which leads to precipitation of carbonates permanently sequestering CO_2 [3]. Hence, mineral precipitation can be termed sequestration whereas other mechanisms can be termed as storage [4]. Mineral-brine reactions are governed by the mineral composition of the rock matrix and the temperatures and pressures. These mineral reactions are central to what transpires in the aquifer system over time. It may be argued that the dynamics of CO_2 movement (both free and dissolved CO_2) are more important at this stage than mineral-brine reactions, which tend to be slow. Near-wellbore rock-fluid interactions may result in dissolution or precipitation (of new minerals), causing either preferential pathways or blockage. The reactions thus govern the subsequent dynamics of CO_2 transport. Macroscale events such

as fault activation or seal breach and leakage may also be induced by weaknesses caused by dissolution. Carbonation of CO_2 is desirable since it would ensure permanent storage with no risk of leakage. Thus, the mineral reactions are central to this storage mechanism.

The carbon repository (geologic formations into which CO_2 is pumped) is a complex structural and stratigraphic package containing diverse geochemical environments, brine and ground water, and rock compositions. The stability of the overlying confining bed should be considered, as it is critical for long-term containment of CO_2. Significant research and large-scale demonstrations are required to certify this method (pumping CO_2 into geological formations) as a safe, reliable, and economically viable solution for CO_2 sequestration.

1.3. Factors Effecting CCS Process

Injection of flue gases into an aquifer significantly complicates the evaluation of the behavior of CO_2 sequestration. The highly heterogeneous mineral matrices induce significant changes in the subsurface geomechanical, and geochemical, behavior of the rocks at depth that must be thoroughly understood to design safe and reliable injection strategies. The major factors that affect the ultimate fate of CO_2 in the formation are:

1. Flue gas composition being injected into the formation
2. Brine to rock ratio in the formation
3. Brine chemistry in the formation
4. Geology/mineralogy of the formation

Even if CO_2 sequestration is feasible, a significant energy penalty is paid in terms of separation, compression, transportation, injection, and other operations. No matter to what extent the flue gases are treated, pre-injection and the application of new

combustion technologies for precombustion capture of CO_2, depending on the nature of the coal used for combustion, the flue gas stream contains nitrogen, water vapor, carbon dioxide, and small amounts of sulfur dioxide, carbon monoxide, ammonia, and other trace gases. The most expensive part of pre-injection sequestration technology is CO_2 capture and purification. These costs can be significantly reduced if we could understand the alteration that the flue gas mixtures cause once injected into the geologic formation. Limited experimental work has been carried out to investigate the significant changes that occur because of the introduction of these trace gases into the geochemical repository. Hence, the principal question that needs to be answered is –"should the trace gases be separated before injection or would sequestration technologies be able to handle minor amounts of SO_2, NH_3, and NOx."

Chemical reactions are affected by the system pressure, temperature, and salinity, which ultimately affect the speed at which the dissolution and reprecipitation reactions take place. One of the important factors is the brine to rock ratio in the formation. The amount of brine available for the CO_2 to dissolve into, at reservoir temperature and pressure, determines the acidity of the brine, which is the principal factor in triggering the complex set of sequestration reactions.

The geologic formations considered for sequestration may include formations with distinctly different mineralogies – ranging from sandstone, limestone, dolomite, or exotic rocks such as peridotite. The reactions between CO_2, brine, and the formation rocks determine pore level changes that could occur during injection and permanent mineralogical sequestration of CO_2. The reactions are slow and the changes are often difficult to measure. Systematic measurement of the progress of these reactions is one of

the main challenges in understanding the CO_2-brine-rock interactions. There is also a dire need to decipher these reactions using thermodynamic and kinetic models and back off relevant parameters as appropriate. Even if CO_2 sequestration is feasible, a significant energy penalty is paid in terms of separation, compression, transportation, injection, and other operations.

1.4. Purpose and Objective of Study

The principal purpose of this study is to obtain fundamental data that would be useful in determining the fate of CO_2 in deep saline aquifers over the short and the long term. The following steps describe the objective of this research, which is to understand the effect of various factors on the principal reactions in geological sequestration of CO_2:

1. Catalog and understand reactions between minerals, brine, and CO_2 at sequestration conditions
2. Understand the effect of the presence of co-contaminant gases (SO_2, NH_3) in the flue gas stream
3. Study the effect of brine to rock ratios on the sequestration reactions
4. Analyze the ultimate fate of CO_2 in different rock formations such as limestones, sandstones, and spent shale
5. Build a comprehensive geochemical model to simulate these sequestration reactions
6. Gauge the effect of different kinetic parameters on the outcome of the model by carrying out a full factorial parameter sensitivity analysis

To achieve the first four goals, a high-temperature, high-pressure experimental setup was built. A batch analysis helps us in understanding the effect of all the possible

parameters such as temperature, pressure, brine chemistry, gas compositions, and rock chemistry on the sequestration reactions. An experimental matrix, which includes conducting analysis at similar conditions varying one parameter at a time, helps us in identifying the key factors affecting the geological interactions. The choice of a base case temperature of 100^0C was selected to achieve a tradeoff between the thermodynamic and the kinetic constraints of the geochemical system considered. The principal purpose of this study is to catalogue the sequestration reactions and determine the detectable changes in the aqueous and solid phases on measurable time scales. The rocks used in this study were ground to 100 μm to provide ample reactive surface area and a sufficiently high temperature of 100^0C was chosen to accelerate the dissolution kinetics of the carbonate and silicate minerals in the system. The high temperature only alters the pace of the reactions, but the stability regimes of the minerals formed in these reactions remain relatively unaltered within the temperature ranges considered.

The sequestration reactions are very complex, but they can be simulated in chemical, physical, and geological terms that are used to describe the complex set of the geochemical alterations occurring within the reactor. Thus, modeling is a very important tool to get a quantitative and qualitative estimate of the changes occurring in the solid and aqueous phase chemistries over long reaction time periods. There are a number of simulation packages available but Geochemists WorkBench (GWB) was chosen because:

a) It has an extensive geochemical thermodynamic database that has been validated for a number of different applications
b) It includes most of the complex chemical reactions involved

c) It can be used for equilibrium, path of reaction, and kinetic modeling of CO_2-brine-mineral reactions.

Comparison of batch experimental results with a comprehensive batch reactor model has not previously been published. All the available literature has been either purely experimental or purely modeling. In this study, an attempt has been made to quantitatively compare the results from the experiments with a batch geochemical model.

A comprehensive literature review has been described in Chapter 2. This review includes experimental (both batch and flow), kinetic, and modeling studies principally referred to in this study. Modeling studies include both batch geochemical modeling and field modeling from which the primary kinetic parameters have been adopted for modeling in this study.

In Chapter 3, which is the experimental section, the experimental setup and the analytical procedures used are described in detail. The experiments to assess the rock compositional effects are described using five different rock types: limestone, sandstone, peridotite, arkose, and spent shale. The experiments to study the gas compositional effects are described using three different gas compositions: CO_2, CO_2+SO_2, and CO_2+NH_3. The brine to rock ratio effects are studied with three different brine to rock ratios: 10:1, 10.5:1, and 15.5:1.

In Chapter 4, the modeling approach, the modeling package used (Geochemists WorkBench), and the reason to use it are described. The kinetic parameters used in the simulation and the approach adopted for degassing simulations has also been described in detail. A comparison of the modeling results with the experimental results for the principal cases described in the experimental sections have been described in this chapter.

In the experiments using synthetic arkose as the starting material, there are multiple minerals involved. Hence, there are many different kinetic rate constants and reactive surface areas corresponding to each case, to be fed as input to the model in the Geochemists WorkBench. To evaluate the variation or the uncertainty in the model both qualitatively and quantitatively with the variation in these kinetic parameters, a full factorial sensitivity analysis is necessary. This analysis takes into account the contribution of each parameter to the desired output and weighs it on a pareto chart. Depending on the desired output chosen, the model gives us the principal parameter governing the output of the simulation.

2. LITERATURE REVIEW

Carbon dioxide (CO_2) is one of the most abundant (64%) greenhouse gases (GHG). The atmospheric concentration of CO_2 has increased from 280 ppm during the preindustrial period to 385 ppm with about half of this increase having occurred since the mid-1960s. In the United States, the majority of the CO_2 emissions are from power plants, which account for about 40% of the total emissions [5]. Carbon dioxide sequestration appears to be an important potential method by which emissions into the atmosphere can be reduced. In this method, anthropogenic CO_2 is injected into geologic formations such as saline formations, depleted oil reservoirs (CO_2 enhanced oil recovery), and unmineable coal seams (enhanced coal bed methane recovery). These formations are widely available and are often in close proximity to the majority of the point emission sources [6]. Injection of CO_2 deep underground is particularly promising because deep sedimentary formations have the potential to retain CO_2 in the subsurface for thousands to millions of years [1]. In the United States, the capacity of deep saline formations is greater than any other geologic environment [7-9], and they are also found within close proximity to power plants. Formations with salinities exceeding 10,000 mg/l total dissolved solids are excluded by the U.S. Environmental Protection Agency as underground sources of drinking water [10]. Hence, these form a primary target for the eventual disposal of CO_2.

2.1. Experimental Work on Mineralogical Changes

Very little attention has been paid to the mechanisms that adversely impact the integrity of a carbon repository. Some simple numerical models (using Darcy equation and Fick's law) have been employed by Lindeberg et al. [11]. Their models attributed the leakage of CO_2 to gravity migration with subsequent release through subvertical fractures and faults. The geologic formations with the highest CO_2 storage potential (saline aquifers) are often in close proximity to the majority of the point emission sources [6]. Injection of CO_2 deep underground is particularly promising because deep sedimentary formations have the potential to retain CO_2 in the subsurface for thousands to millions of years [1]. In the United States, the volumetric capacity of deep saline aquifers is greater than other geologic formations [12][13]. Aquifers with salinities exceeding 10,000mg/l total dissolved solids are excluded by the U.S. Environmental Protection Agency as underground sources of drinking water [10]. Hence, these form a primary target for the eventual disposal of CO_2.

The temperatures in these aquifers (50^0-80^0C) vary greatly depending on the depth and also the local geothermal gradients [1]. Typically, CO_2 is injected at depths greater than 800 m to ensure that it stays in the supercritical state or has sufficiently high density (critical temperature and pressure of CO_2 are 31^0C and 7.4 MPa, respectively) [14]. The notion of CO_2 disposal in aquifers has been discussed in the literature with specific aquifers as target; for example, in the Netherlands [15] and the Alberta Basin, Canada [16-19],[13] and the Sleipner west oil field of the North Sea [20].

Numerical simulations have been used to evaluate potential leakage through the confining rock or fractures. A few experimental studies examined geochemical reactions

in a saline aquifer in response to CO_2 injection. Gunter et al. [19] carried out numerical geochemical modeling studies that incorporated kinetic laws and some studies combining experiment and modeling, in which dissolution of silicate minerals in brine and precipitation of carbonate are reported. A major study in the identification of geochemical reactions within an experimental system at reservoir temperature and pressure was conducted by Kaszuba et al. [4][21].

Kaszuba et al. [4] carried out a study to determine the extent of fluid rock interactions, in addition to carbonate mineral precipitation, that may occur in an experimental system that simulates geologic storage and sequestration of CO_2. Reaction conditions chosen by them were 200^0C and 2000 psi. The experimental setup used was a flexible cell hydrothermal apparatus with an Au-Ti (gold-titanium) reaction cell with a sampling port [22]. The reactant mixture was synthetic arkose, which consisted of quartz, oligoclase, and microcline. Shale was used as an aquitard, the confining layer of the repository. The brine used was synthesized using laboratory grade salts to represent aquifer compositions in the Delaware basin. The brine + rock mixture was allowed to react for 59 days to achieve equilibrium and CO_2 was injected and then allowed to react for another 80 days. The solid phases were analyzed using Scanning Electron Microscopy (SEM), Energy Dispersive X-Ray Spectroscopy (EDS), and X-Ray Diffraction (XRD) analysis. The brine chemistry was analyzed using Inductively Coupled Plasma Mass Spectrometry (ICP-MS) for cations and Ion Chromatography for anions. The results were indicative of the geochemical reactions taking place in the repository. Clear euhedral crystals of magnesite were evident in the postreaction sample when analyzed by SEM. Siderite was seen growing on the shale surface. Microcline was seen to undergo severe

etching. Patchy crystals of halite were present. Analcime crystals were found in abundance in the experiment. The brine chemistry also changed significantly after the experiments. The concentration of Na and Cl ions decreased initially but stabilized thereafter and was constant throughout. The concentration of the trace ions Ca, Mg, Br, Fe, and SO_4 all increased during the reactions. This indicated that the minerals in the starting materials underwent dissolution, thus displaying evidence of participation in fluid rock reactions.

Kaszuba et al. [21] then carried out a study to analyze the effect of CO_2 injection on fluid rock reactions. For this study, they used the same experimental apparatus and starting materials as in their previous study. One experiment was with brine + rock without CO_2 injection and the other experiment was with CO_2 injection. Both the experiments were analyzed using the same techniques as their previous study. In this experiment, shale was used to model the aquitard. In the brine-rock experiment, the Na concentration initially decreased, then increased; then it continued to decrease throughout the remainder of the experiment. The Cl concentration decreased then increased before stabilizing for rest of the experiment. The pH decreased and then achieved a stable value. All the trace ions increased in their concentrations. In the experiment with CO_2, the concentrations of Na and Cl and the trace elements were similar to that of the brine-rock experiment. The exception was Mg, whose concentration was 3 to 10 times greater than the brine-rock experiment. The pH was lower because of the formation of carbonic acid. No carbonate precipitation was observed in the brine-rock experiment, but in the CO_2-brine-rock experiment, two types of carbonate precipitations were observed. Magnesite occurs as large, discrete bladed crystal visible to the naked eye. Siderite occurs as

euhedral crystal on the shale, indicating that the aquitard is also a reactive component of the carbon repository. So, shale reactivity may produce an increase in porosity and permeability, which increases the potential for the release of CO_2.

Precipitation of the hydroxyl-carbonate mineral dawsonite, predicted to be a stable carbonate phase [23][24], is not observed in any of the experimental studies. In the field, large volumes of dawsonite were observed in oil shales in the Green river formations, but their deposition is linked to highly alkaline solutions. A study of the stability of dawsonite was conducted by Hellevang et al. [25]. They concluded that dawsonite, when initially present, would become unstable as CO_2 pressures decrease following injection. Hellevang et al. [25] also measured dissolution rates of dawsonite at 80^0C as a function of pH from 3 to 10. Use of these dissolution rates in reactive transport calculations indicate that dissolution of dawsonite following a decrease in the CO_2 pressure out of its stability leads to the precipitation of kaolinite. They described the dawsonite dissolution using the reaction:

$$NaAlCO_3(OH)_2 + 4H^+ \leftrightarrow Na^+ + Al^{3+} + CO_{2(aq)} + 3H_2O \quad (2.1)$$

Thus, the stability of dawsonite can be attributed to aqueous CO_2 concentrations which itself can be related to partial pressure of coexisting CO_2 phase by the relationships:

$$CO_2(g/fl) \leftrightarrow CO_{2(aq)} \quad (2.2)$$

$$H_2O + CO_2 \leftrightarrow H_2CO_3 \quad (2.3)$$

$$H_2CO_3 \leftrightarrow H^+ + HCO_3 \quad (2.4)$$

The relative stability of dawsonite with respect to other Na and Al bearing phases can be assessed using logarithmic activity fugacity diagrams, which suggest that dawsonite stability increases with increasing aNa^+/aH^+ and fugacity of CO_2, but decreases with increasing temperature. Hence, at higher temperatures, higher CO_2 fugacities are required to stabilize dawsonite. So, following CO_2 injection, as injected CO_2 disperses, dissolves, or leaks, the CO_2 fugacity would decrease, potentially destabilizing dawsonite to other alumino-silicate phases like kaolinite or albite. When carbon dioxide dissolves in water, the pH decreases due to the formation of carbonic acid. The carbonate ion is provided by inducing calcite minerals or natural dissolution of calcite in the low pH state.

Soong et al. [26] reported the dominant state of carbonic acid with respect to solution pH. H_2CO_3 dominates at a low pH of 4, HCO_3^- at a mid-pH of 6, and CO_3^{2-} at a pH of 9. In terms of carbonate formation, a pH of 9 is advantageous because of the dominance of carbonate ion. Geologic abundance of cations in the aqueous phase may lead to mineral sequestration. Rosenbauer et al. [27] discussed the capacity for brine disposal with CO_2 removal. They reported that this high capacity of storage is possible due to scaling and a variation of porosity when CO_2 is injected into a deep aquifer. They also showed that more CO_2 might be trapped in a deep saline aquifer by the formation of bicarbonate ion (HCO_3^-). They provided insight into CO_2 sequestration by the dissolution and the formation of mineral carbonates:

$$H_2O + CO_2 \leftrightarrow H_2CO_3 \quad (2.5)$$

$$H_2CO_3 \leftrightarrow H^+ + HCO_3^- \quad (2.6)$$

The sequential reactions result in a decrease in pH. Dissociated hydrogen ion can dissolve calcite, mainly $CaCO_3$, to produce calcium ion and bicarbonate:

$$CaCO_3 + H^+ \leftrightarrow Ca^{2+} + HCO_3^- \quad (2.7)$$

The generation of bicarbonate will lead to additional CO_2 dissolution into the aqueous phase. Precipitation reactions can be also expected in the aqueous CO_2 phase. For instance, in arkosic sandstone, carbonate reacts with hydrogen ion to precipitate calcium carbonate:

$$2H^+ + CaAl_2Si_2O_8 + H_2O \leftrightarrow Ca^{2+} + Al_2Si_2O_5(OH)_4 \quad (2.8)$$

(Plagiclase fledspar) (Kaolinite)

$$Ca^{2+} + HCO_3 \leftrightarrow CaCO_3 + H^+ \quad (2.9)$$

$$CaAl_2Si_2O_8 + H_2CO_3 + H_2O \leftrightarrow CaCO_3 + Al_2Si_2O_5(OH)_4 \quad (2.10)$$

From the two different scenarios (carbonate dissolution and precipitation) above, we recognize that reactions of aqueous CO_2, brine, and rocks vary with their compositional differences, apart from temperature and pressure variance. Dissolution and precipitation of carbonates are simultaneously expected in complex rock environments. Therefore, we need to consider the net porosity changes caused by dissolution and precipitation reactions in host rock environment.

Tables 2-1 and 2-2 summarize the results by Rosenbauer et al. [27]. Their experiments were carried out at 25^0C and 120^0C and 100 − 600 bar using rock crushed to 100-200-mesh size. Brine with high sulfate ion generates the precipitation of anhydrite ($CaSO_4$) and the dolomitization of limestone, which decreases the net porosity.

Table 2- 1: Porosity changes in CO_2-brine-rock system

Brine	Minerals	Porosity	Observation

Low-Sulphate	Limestone	2.6%	
High-Sulphate	Limestone	4.9%	Precipitation of anhydrite and dolomotization of limestone

Table 2- 2: Solubility changes of CO_2 in brine

Minerals	Solubility	Temperature	Pressure (bar)
Limestone	9%	25^0C	200
	6%	120^0C	200
Arkosic Sandstone	5%	120^0C	300

Participating in the formation of carbonates resulted in increase of CO_2 solubility of up to 9 %. The experiments reacting high sulfate brine with limestone, both in presence and absence of supercritical CO_2, were characterized by the precipitation of anhydrite, dolomitization of limestone, and a final decrease in porosity of 4.5%. The concentration of the ions in the liquid phase showed a similar trend to that of the results showed by Kaszuba et al. [4] except that the concentrations of the ions were much less, which may probably be due to the lower temperature used in these experiments.

The reactions such as sulfate formation and ion exchange by magnesium ion are presented. Equation (2.13) shows the conversion from calcite to dolomite.

$$Ca^{2+} + SO_4^{2-} \leftrightarrow CaSO_4 \quad (2.11)$$

$$Mg^{2+} + CaSO_4 \leftrightarrow Ca^{2+} + MgSO_4 \quad (2.12)$$

$$Mg^{2+} + 2CaCO_3 \leftrightarrow Ca^{2+} + CaMg(CO_3)_2 \quad (2.13)$$

Druckenmiller et al. [28] reported the importance of pH to form carbonates. Carbonic species exist in three different dominant phases with respect to pH values. They concluded that the main parameters affecting the carbonate precipitation/dissolution process are:

1. Temperature
2. Pressure
3. Brine composition
4. Rock composition
5. pH

Temperature has greater influence on carbonate formation than pressure (increase in temperature increases the formation of carbonates). The trend of the fluid chemistry was similar to what was reported by Kaszuba et al. [4].

It has often been cited that slow reaction rates of mineral carbonates is disadvantageous for sequestration. Magnesium rich minerals may be viable to carbonation-base sequestration. For enhancing the reaction rate, Druckenmiller et al. [28] suggested the activation of magnesium rich minerals (serpentine). They presented a way to increase the pore volume of magnesium rich minerals using physical and chemical treatments. The major cost for mineral activation is the heating process to remove surface hydroxyl groups. One such method is the chemical treatment using sulfuric acid that results in high porosity of mineral with less magnesium in the surface. Geological abundance of magnesium minerals provides incentive for the study of carbonate sequestration.

Wolf et al. [29] developed a microreaction (0.1 cm^3) system to observe in-situ reactions relevant to CO_2 sequestration. They characterized the carbonation reaction using synchrotron X-ray Diffraction and Raman Spectroscopy. The objective of their microreactor built with moissanite windows is to understand the carbonation reaction, which will provide a cost-effective process design. The precipitation of magnesite in their study was described using the reaction:

$$Mg_3Si_2O_{6.76}(OH)_{0.48} + 3CO_2 \leftrightarrow 3MgCO_3 + 2SiO_2 + 0.24H_2O \quad (2.14)$$

Wellman and coworkers [30] suggested the permeability to porosity correlation:

$$k = k_0\left\{\frac{\phi}{\phi_0}\right\}^x \quad (2.15)$$

where k and k_0 are system and initial permeabilities, ø and $ø_0$ are system and initial porosity, respectively. x is fitting constant and they chose a value of 3.4 for their experiments.

Moore et al. [31] investigated the alterations caused by the neutralization of descending acidic waters at Karaha-Telaga Bodas, located on the planks of Galunggung volcano, Indonesia. It is a partially vapor-dominated geothermal system. These alterations have resulted in the appearance of argillic alteration characterized by alunite, other clay minerals and pyrite, anhydrite pyrite, and interlayered sheet silicates and carbonates. Magmatic gases also participated in these reactions, as indicated by the presence of tourmaline (a borosilicate mineral), fluorite, and native sulfur. Thus, natural

mineralogical reactions of gases containing SO_2 in natural environment have been studied and documented.

Jacquemet et al. [32] investigated the impact of H_2S-CO_2 mixtures on well cement and sequestration reactions. They concluded that it is the physical state of the mixture (supercritical, dry, or dissolved state) that has the major impact on the ageing reactions. The experiments were carried out at 200^0C and 500 bar where the crystalline structure of the minerals changed over a period of 15 days. In a recent paper, Bacon et al. [33] modeled the reactive transport of CO_2 and SO_2 injection in a deep saline formation. Their geochemical model showed significant differences in mineralogical reactions when pure CO_2 injection was compared to injection of mixtures of SO_2 and CO_2.

Taberner et al. [34] modeled the injection of supercritical CO_2 into a deep saline aquifer containing carbonate minerals (calcite and dolomite), with minor anhydrite. TOUGHREACT was used with Pitzer ion-interaction model implementation for handling high salinity brines. Their simulation-based conclusions were that the brine is further concentrated due to water dissolution into the CO_2 phase, pH is lowered from 5.5 to 3.1, halite (NaCl) and anhydrite ($CaSO_4$) precipitate, and the brine becomes $CaCl_2$−dominant. They also observed that calcite and dolomite dissolve as the CO_2 plume advances during injection. Anhydrite dissolves only slightly along the CO_2 front, but precipitates in higher proportions near the well bore. These findings are valuable for the assessment of injectivity changes and near well-bore stability of saline aquifers in carbonate formations during injection of CO_2.

O'Connor et al. [35] experimentally investigated the feasibility of aqueous mineral carbonation for mineral sequestration of CO_2. They combined brine consisting of

sodium bicarbonate and sodium chloride with different mineral reactants (magnesium silicates such as olivine or serpentine) and dissolved CO_2 into this slurry. They reported precipitation of magnesite from the carbonation of the magnesium silicate minerals. The optimum conditions for this process were determined and a method for mineral preparation for the process was developed. It was also found that these slow geological processes could be accelerated by increasing the reactive surface area, increasing the activity of carbon dioxide in solution, inducing imperfections into the crystal lattice through high energy attrition grinding, and also thermally activating the mineral. Kellemen et al. [36] measured the rates of peridotite rock (containing olivine and serpentine minerals) carbonation experimentally and the amounts of solid carbonates formed by natural weathering and carbonation of peridotite in the Sultanate of Oman.

2.2. Core Flooding Experiments

Izgec et al. [37] performed CO_2 core flooding experiments and observed changes in the permeability and porosity of the core samples using computerized tomography (CT) monitored laboratory experiments. CO_2 displacement in the core depends mainly on the following parameters:

1. Multiphase flow characteristics
2. Solution dissolution kinetics
3. Solute transport
4. CO_2 movement
5. Hydrodynamic instabilities due to the displacement of brine with less viscous CO_2

When CO_2 is injected, it dissolves in water. Minerals such as calcite dissolve readily, increasing porosity and permeability, leading to increased flow rate and increased

dissolution, forming wormholes in the core. This process of dissolution and the precipitation process are characterized by the dimensionless numbers: Peclet (Pe) and Damkohler (Da). The effect of these two dimensionless parameters is shown in Table 2-3. Experiments were carried out using sandstone cores and CO_2 saturated brine and characterization was done using an X-ray CT scanner at a temperature of 18^0C and a pressure of 500 psi. The composition of brine did not seem to effect the porosity and the permeability changes. The injection rate followed the same trend as predicted by the dimensionless numbers (Pe) and (Da). The effect of the flow direction (orientation of the core) plays a crucial role on rock property trends. For vertically oriented plugs, the permeability increased and then decreased after a certain pore volume. On the other hand, for the horizontally oriented core plugs, the permeability initially decreased and then after a certain injection period, stabilized. Porosity also showed the same trend. The difference may be due to the manner in which precipitated minerals block pore throats. Krunhansl et al. [38] performed both CO_2 core flooding and long-term static tests and made an attempt to validate their modeling results (carried out with TOUGHREACT). For the core-brine experiments, characterization was done using SEM analysis. Both the core and the static tests were carried out at 700 psi and 40^0C. The lithology of the sample consisted of fine grained arkosic sandstone with occasional petroleum stains. The main minerals identified were quartz, potassium feldspar, and dolomite. The brine chosen was collected from the West Pearl Queen reservoir. In the flow tests, no notable change in porosity was found. The reason for this decrease was not explained. In the static tests, the posttest fluid was captured and analyzed for cations by DCP and anions by IC. The dominant change was increase in salt content by 20%. The solids showed etching of the carbonate grains.

Table 2- 3: Effect of the two dimensionless parameters Pe and Da on dissolution and precipitation processes

Da large (Da >> 1)	Rapid chemical reaction
Da small (Da << 1)	Slow chemical reaction
Pe large and PeDa large	Wormholes are formed
Pe small and PeDa large	Reactions mainly occur at inlet boundary resulting in near inlet dissolution
At moderate Pe and PeDa numbers	Reactions are generally nonuniform with more in the upstream and less in downstream

Egermann et al. [39] performed similar core flooding experiments but at a higher pressure of 100 bar and 90^{o}C. The porosity measurements were done by the NMR technique. The effect of flow rate was analyzed by varying the flow rate of CO_2 saturated brine in the range of 2cm^3/hr to 500cm^3/hr. The results indicated that high flow rates favor wormhole dissolution patterns whereas low flow rates lead to compact dissolution patterns. The lateral extension of the wormholes seemed to be favored when sulfates had been removed from the brine. In the analysis of the test fluid, Ca^{2+} concentration increased continuously, which could be directly related to the calcite dissolution. The concentration of SO_4^{2-} decreased continuously.

Similar core experiments were performed by Bateman et al. [3] and Wellmann et al. [30], who investigated the changes in the porosity and permeability and the effect of the brine composition, orientation of core, and the injection rate on the reactions. The results were similar to those of Egermann et al. [39] and Krunhansl et al. [38].

2.3. Kinetics of Geochemical Reactions

Numerous authors have investigated kinetics of geochemical reactions. Reaction rates of different minerals such as kaolinite, dolomite, calcite, quartz, chlorite, and the effect of pH temperature and pressure have been reported in the literature.

Carroll et al. [40] measured the dissolution rates, k_r of the mineral kaolinite at 25^0C, 60^0C, and 80^0C, which were highly dependant on pH. The experiments were conducted by placing kaolinite into polypropylene reaction vessels, filled with 500 ml of different pH buffer solution to conduct the experiments at various pH. The solutions were analyzed for aluminum and silicon with a DCP emission spectrometer. At all three temperatures, k_r decreased from acid to near neutral pH and increased from near neutral to alkaline pH. The pH dependency of kaolinite dissolution is attributed to the net adsorption of H^+ and OH^- ions to aluminum and silicon reaction sites as well as to the formation of positively, neutral, and negatively charged alumino-silicate complexes at acid, neutral, and alkaline pH, respectively. The diffusion of the elements through an amorphous surface layer also affects the overall rate of dissolution. The activation energies of the reactions were calculated because the dissolution rate behavior is a function of temperature (and solution pH). The reactions at the mineral-solution interface were explained using transition state theory and surface-complex reaction theory. The temperature dependence of kaolinite dissolution was described using the classical Arrhenius equation and the activation energies of the reaction at different pH were calculated and compared with those already published in the literature.

Alkattan et al. [41] reported the dissolution rates of calcite and limestone as a function of pH from -1 to 3 and temperatures from 25^oC to 80^oC. The dissolution rates

were measured using the rotating disk technique proposed by Gregory and Riddiford [42], which employed a double glass walled rotating disk reactor. Rates were determined from the weight loss of the solid samples dissolved in HCl solutions. Three types of samples were considered: single calcite crystals, limestone, and compressed calcite powders. Two different limestones were used.

The dissolution rates listed were calculated from the relationship:

$$r = \frac{\Delta m}{stW} \tag{2.16}$$

where Δm represents the weight loss of the solid, s designates the geometric surface area of the disk, t represents the elapsed time, and W signifies the molecular weight of calcite (100.1g/mol). The transport rate constant for the rotating disk reactor at disk rotation speeds >> 0 is given by Gregory and Riddford [42], Pleskov et al. [43], and Alkattan et al.[41].

$$k_t = \frac{D}{\delta} = 0.62 D^{\frac{2}{3}} \vartheta^{\frac{-1}{6}} \omega^{\frac{1}{2}} \tag{2.17}$$

D stands for H^+ diffusion coefficient, δ signifies the thickness of the diffusion layer, ν corresponds to the kinematic viscosity of solution, and ω represents the disk rotation speed. For calcite dissolution, it follows that for a rotating disk reactor:

$$\frac{1}{r} = \frac{1}{k_2 c_{H^+} \gamma_{H^+}} + \frac{1}{0.62 D^{\frac{2}{3}} \vartheta^{\frac{-1}{6}} c_{H^+}} \omega^{\frac{-1}{2}} \tag{2.18}$$

where r is the overall dissolution rate and is a linear function of the reciprocal of the square root of the rotating disk speed $\omega^{-1/2}$. The intercept of this straight line can be used

to deduce k_2, the chemical rate constant, while its slope allows determination of the diffusion coefficient D. The variation of H^+ diffusion coefficients can be described by an Arrhenius equation and which allows the activation energies and the pre-exponential factor to be determined. The apparent rate constants and the H^+ diffusion coefficients increase substantially with increasing temperature.

Arvidson and Mackenzie [44] measured the rate of precipitation of dolomite and its dependence on temperature and solution composition. They quantified and modeled kinetics by the application of a rate law that represents rate as a simple function of saturation index (as stated by Lasaga [45]):

$$r = k(\Omega - 1)^n \tag{2.19}$$

where Ω is the saturation index of the solution with respect to ideal dolomite given by:

$$\Omega = \frac{a_{Ca^{2+}} a_{Mg^{2+}} a_{CO_3^{2-}}}{K_{T,Dol}} \tag{2.20}$$

This law was tested using a series of experiments by measuring the steady state rate of dolomite precipitation in a dolomite seeded flow reactor. The dependence of the kinetics on the fluid composition was determined by varying the saturation index from near saturation to 100. The temperature was also varied from 100^0C to 200^0C to solve for the reaction order and the Arrhenius rate constant $k = A\exp\left(\frac{-\varepsilon_a}{RT}\right)$ of this rate law. The experiments were conducted in a steady state plug flow reactor with recycle. The reactor was filled with a > 2μ m pore size (5g) dolomite seed material. The pressure was

maintained at 100 psi by a backpressure regulator. The overall precipitation reaction proceeds as:

$$Ca^{2+} + Mg^{2+} + 2CO_3^{2-} \leftrightarrow CaMg(CO_3)_2 \qquad (2.21)$$

Selective fitting of rate data gives values for the activation energy ϵ_A, pre-exponential frequency factor A, and reaction order n of 31.9 Kcal/mol, 101.05, and 2.26, respectively. The comparison of values for activation energy with those computed from other sources and with those estimated from a thorough consideration of heats of cation hydration suggests that Mg^{2+} dehydration represents a significant component of ϵ_A, the activation energy associated with cation ordering. The style of growth of the dolomite crystals varies according to the extent of super saturation, with lower values promoting simple migration of surface steps and kinks. Higher saturations are associated with the development of complex nucleation centers consisting of sub-micron sized nuclei. The effective dolomite precipitation rate is maximized in the absence of other carbonate phases like calcite. Thus, one can conclude that the overall rate of dolomite precipitation relative to the competing carbonate phases at surface temperatures determines the abundance of dolomite in a sedimentary regime.

Gautelier et al. [46] measured the rate of dolomite dissolution as a function of pH from -0.5 to 5 and temperature from 25^0C to 80^0C. The same experimental method as used by Alkattan et al. [41] (to measure the dissolution rates of calcite) was employed here. The use of the rotating disk techniques and the comparison of the experimental data with the equations reported by Gregory and Riddiford [42] yielded steady state

dissolution rates as a function of the solution pH adjacent to the dolomite surface. Rates at all temperatures and for 1 < pH < 5 were found to be consistent with the rate law:

$$r = k_1 a_{H^+}{}^n \tag{2.22}$$

where r refers to surface area normalized dissolution rate, k_1 is the reaction rate constant, and a_{H+} refers to hydrogen ion activity in the solution.

The variation of dolomite dissolution rates with temperature were described in terms of an Arrhenius equation in the form r = Aexp(−ϵ_a/RT). The apparent activation energy decreases dramatically with pH from 46 KJ/mol at pH = 0 to 15 KJ/mol at pH 5. The overall dissolution process was found to be surface reaction limited at pH< 1, but the effect of diffusional transport becomes increasingly significant with increasing pH.

Gautelier et al. [46] studied dolomite dissolution rates at 80^0C as a function of chemical affinity and solution composition. They used the dissolution mechanism proposed by Pokrovsky et al. [47], where the rates are controlled by the detachment of the $Mg(OH)_2^+$ species at the dolomite surface. The dolomite dissolution rates were described using the expression:

$$r = k_{Mg^+}\left[\frac{KCO_3{}^* K_{Ca}{}^*}{KCO_3{}^* K_{Ca}{}^* + K_{Ca}{}^* a_{CO_3{}^{2-}} + a_{CO_3{}^{2-}} a_{Ca^{2+}}}\right]^n (1-\exp(-n_A/RT) \tag{2.23}$$

where k_{Mg+} designates rate constant

K_{CO3}*, K_{Ca}* denote equilibrium constants

a_i refers to activity of subscripted aqueous species

A is the chemical affinity of the dissolving dolomite

n denotes the stoichiometric coefficient

Rates were calculated from the difference between the inlet and outlet solution calcium and magnesium concentrations. Ca and Mg were analyzed by atomic absorption spectrometry (AAS) or by complexometric titration with EDTA. The dolomite dissolution rates at 80^0C in the aqueous solution decreased with increased carbonate activity. The data are also found to be consistent with the Pokrovsky et al. [47] dolomite dissolution mechanism.

Liu et al. [48] did a comparative study on the dissolution rates of dolomite and limestone. For limestone under the condition of CO_2 partial pressures > 100 Pa dissolution rates increased significantly by a factor of about ten after addition of carbonic anhydrase (CA), which catalyzed the conversion reaction of CO_2, whereas CA had little influence on dolomite dissolution. Moreover, the dissolution of limestone was more sensitive to hydrodynamics (rotation speed) than dolomite dissolution. Measurements of the dissolution rates were performed at a fixed rotating speed and concentration of CA by measuring the increase in conductivity. The increase in the dissolution rate by addition of CA for limestone and dolomite were highly sensitive. Both carbonate rock dissolution rates increased with increase in P_{CO2}.

Pokrovsky et al. [49] measured the dissolution rates of calcite, dolomite, and magnesite at 25^0C and pH values from 3 to 4 as a function of salinity and partial pressure of CO_2. Experiments on calcite and dolomite (both crystals and powders of 100-200μm) were conducted in a batch reactor under controlled hydrodynamic conditions using the rotating disk technique. The in situ pH was measured using a solid contact electrode in a cell without liquid junction. The results indicate that the carbonate mineral dissolution

rates were proportional (weakly dependent) to PCO_2 but not H_2CO_3* (aq). For dolomite and magnesite, the surface complexation model (SCM) of Pokrovsky et al. [50][51] predicts dissolution rates at CO_2 pressures up to 50 atm with good accuracy.

2.4. Modeling Mineralogical Changes

Xu et al. [10] performed numerical simulations with the reactive fluid-flow and geochemical transport code TOUGHREACT to analyze mass transfer between sandstone and shale layers and CO_2 immobilization through mineral precipitation. Earlier, Xu et al. [52][53] modeled the interaction of aqueous solutions under high CO_2 partial pressures with three different rock types. The first rock was glauconite-bearing sandstone from the Alberta Sedimentary basin. The second rock type evaluated was a proxy for sediment from the United States Gulf Coast. The third rock type was a dunite, an essentially monomineralic rock consisting of olivine.

Xu et al. [52] performed reactive transport simulations of a 1-D radial well region under CO_2 injection conditions in order to analyze CO_2 immobilization through carbonate precipitation, using Gulf Coast Sandstones of the Frio formation of Texas. Most of the simulated mineral alteration patterns were consistent with the observations. However, quartz abundance declined over the course of the simulation, while quartz overgrowths were observed during diagenesis due to the release of SiO_2 during the replacement of smectite by illite in the adjacent shales.

Xu et al. [52][53] made many simplifications and approximations such as:

1. Treating the sandstone aquifer as if it were a closed system isolated from the enclosing shales

2. Not adequately representing the extremely complex process of kerogen

decomposition in deeply buried sediments

Xu et al. [10] carried out simulations using the nonisothermal reactive geochemical transport code TOUGHREACT [54]. A reactive geochemical transport model for a sandstone-shale system under high CO_2 pressures was developed. The model was used to analyze the mass transfer of aqueous chemical components, the alteration pattern of minerals, and sequestration of CO_2 by secondary carbonates and changes of porosity in a Gulf Coast aquifer.

Andre et al. [55] presented numerical results performed by TOUGHREACT for two CO_2 injection scenarios, first with CO_2 saturated water and second with pure supercritical CO_2. Simulations showed high reactivity of CO_2 saturated water with the porosity increasing up to 90%, associated with strong carbonate dissolution, in qualitative agreement with wormholing observed in some experimental investigations [39]. The second scenario shows much less geochemical activity. If the porosity increases by about 5% to 7% in most parts of the reservoir, then there is a decrease observed in the vicinity of the injector due to mineral precipitation.

Cipolli et al. [56] gathered geochemical data on spring waters through an extensive survey of the Gruppo di Voltri area and confirmed that progressive interaction between ultramafic rocks variably affected by serpentinization and meteoric waters produces $Mg{-}HCO_3$ waters first, in shallow aquifers open to CO_2 exchange, followed by the development of $Na{-}HCO_3$ and Ca−OH type waters, under closed system conditions with respect to CO_2. The reaction path modeling of high-pressure CO_2 injection into deep serpentine bearing aquifers appears to represent a feasible option to reduce anthropogenic CO_2 inputs into the atmosphere as these aquifers have a high CO_2 sequestration capacity,

mainly through mineral fixation as magnesite and subordinately through solution trapping.

Gaus et al. [57] performed numerical simulations to model the impact of reactive transport on the clay cap rock at Sleipner (North Sea) because of CO_2 injection. The simulations show that although initially some dissolution occurs, feldspar alteration is the dominant long-term reaction and the exact mineralogical composition of the plagioclase fraction in the cap rock plays a crucial role. Diffusion in the cap rock is a slow process and the section of the cap rock, which is exposed to geochemical interactions due to CO_2 injection, is limited to the rock adjacent to the reservoir. These reactions can cause a slight decrease in porosity.

Knauss et al. [24] evaluated the impact of CO_2, co-contaminant gas, aqueous fluid, and reservoir rock interactions on the geologic sequestration of CO_2. They simulated the results of CO_2 and co-contaminants into a specific heterogeneous rock formation (Frio formation in Texas) and calculated the mineralogical changes along the path by coupling a chemical model with a simplified fluid flow using the reactive transport code CRUNCH proposed by Steefel et al. [58]. They found that even relatively large amounts of co-injected H_2S should not prove problematic for a CO_2 injection process. In the case of SO_2, if conditions allow the S to be oxidized, only minor amounts of this gas could be tolerated due to the extremely low pH generated. Potential porosity loss due to the formation of anhydrite will also need to be assessed.

Lagneau et al. [59] simulated the chemical reactions likely to occur, when the system is coupled to reactive transport at large time and space scales. They used HYTEC, a reactive transport code initially developed for transport of chemical solutions and

colloidal matter in column systems. They concluded that transport controlled the dispersion of the dissolved CO_2 in the carbonated aquifer, with a rapid dissolution of the supercritical CO_2 bubble and a transport of the injected CO_2 bubble in the flow direction. In the case of a sandstone aquifer, the evolution is controlled by the reactivity of the dissolved CO_2 with the host rock minerals. They also concluded that despite the poor ionic solvent capacity of supercritical CO_2, its activity might not be negligible.

White et al. [60] simulated the reactive transport of injected CO_2 on the Colorado Plateau in Utah. They investigated the injection of CO_2 into nondome shaped geologic structures that do not provide the traps, which are traditionally deemed necessary for the development of artificial CO_2 reservoirs. They developed two TOUGH2/ChemTOUGH2 integrated finite difference models of the geology and ground water flow. They found that 1000 years after the 30-year injection period began, approximately 21% of the injected CO_2 was permanently sequestered as carbonate minerals, 52% was beneath the surface as gas or dissolved in the ground water, 17% had leaked to the surface, and leakage to the surface was continuing.

Zerai et al. [61] conducted equilibrium, reaction path, and kinetic modeling of CO_2 -brine-mineral reactions in the Rose Run Sandstone, one of Ohio's deep saline aquifers, to investigate the factors that are likely to influence the capacity of this formation to trap solid CO_2 as solid carbonate minerals. Geochemists WorkBench (GWB) version 3.2.2 was used for equilibrium, reaction path, and kinetic modeling of CO_2 -brine-mineral reactions. They concluded that dissolution of albite, K-feldspar, and glauconite and the precipitation of dawsonite and siderite are potentially very important for mineral trapping of CO_2. The stability of carbonate rocks is controlled by the brine to

rock ratio, reactive surface area, f_{CO2}, and porosity.

Battistelli et al. [62] described an EOS (Equation of State) module to handle the three component mixtures of water, sodium chloride, and a slightly soluble non-condensable gas.

Allen et al. [55] carried out geochemical modeling with GWB and PHREEQC to simulate the behavior of a geochemical repository at elevated CO_2 pressures and high salinities. Their results indicate that stand-alone solubility models that do not take mineral reactions into account will underestimate the total capacity of aquifers to sequester CO_2 in the long term through enhanced solubility and mineral trapping mechanisms. Technology for injecting CO_2 has long been used in the oil and gas industry for Enhanced Oil Recovery (EOR). Yousuf et al. [63], Jessen et al. [64], and Shtepani [65] conducted numerical simulations to evaluate the impact of CO_2 injection into depleted oil reservoirs. Injection into coal seams was also extensively studied [66-68].

3. EXPERIMENTAL SECTION

3.1 Experimental Setup

In order to investigate the effect of the primary parameters on these sequestration reactions, a batch experimental setup was designed. The experimental apparatus (Figure 3-1 and Figure 3-2) consists of a series of reactors made of 316 stainless steel rated to 30 MPa at 600^0C. The reactors are 1" in diameter and 6" long with high-pressure Swagelok fittings on each end. The reactors are heat wrapped along the core and are insulated with self-adhesive high-temperature silicon tape and glass wool along the core and the fittings. The system was pressure tested at 22 MPa (3200 psi) using high-pressure nitrogen. CO_2 was pressurized in the reactor using a single-piston cylinder high-pressure positive displacement pump (from DBR Associates Company, now Schlumberger-DBR). The flow of CO_2 into the reactor was controlled with high-pressure needle valves. CO_2 was siphoned from a cylinder at 25^0C. The temperature was controlled using a bench-top temperature controller with SPECVIEW as the interface via K-type thermocouples. High purity nano-filtered de-ionized (DI) water was used to prepare the brine samples. The reactors have provisions for retrieving rock samples after depressurization through a detachable bottom cap. The reactors are replaced by new sets after two experiments to avoid the corrosion produced by metal interaction to the brine.

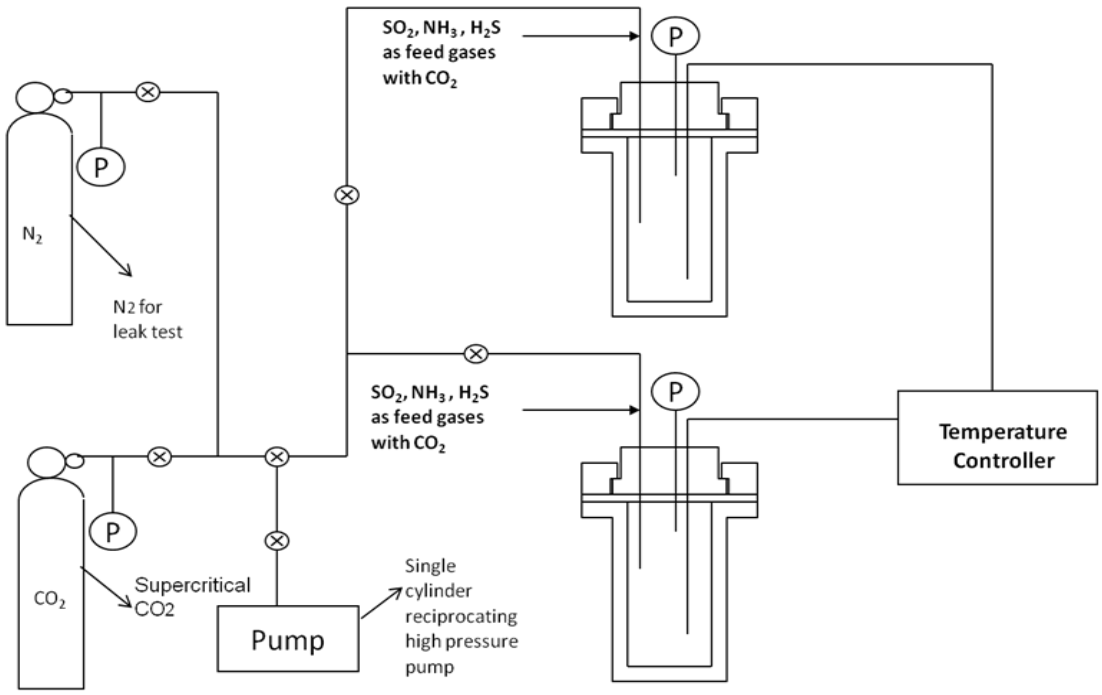

Figure 3- 1: Schematic diagram of the experimental setup

The rock is fed into the reactors at the beginning of the experiment. All the samples were crushed to 100 μm. A manual size distribution analysis revealed most of the particles to be in the range of 40 μm to 100 μm. The reactor is then loaded with brine and sealed with high-pressure swagelok fittings. Kaszuba et al. [4][21] proved that the rock-brine system is by itself reactive because of physical (leaching) and chemical (rock-brine interactions) phenomena. Hence, all the samples were allowed to equilibrate for 36 days before CO_2 was injected into the system. Identical reactor conditions were established in multiple reactors and reactions were carried out to different completion times. This procedure helps us avoid changes that occur due to sampling.

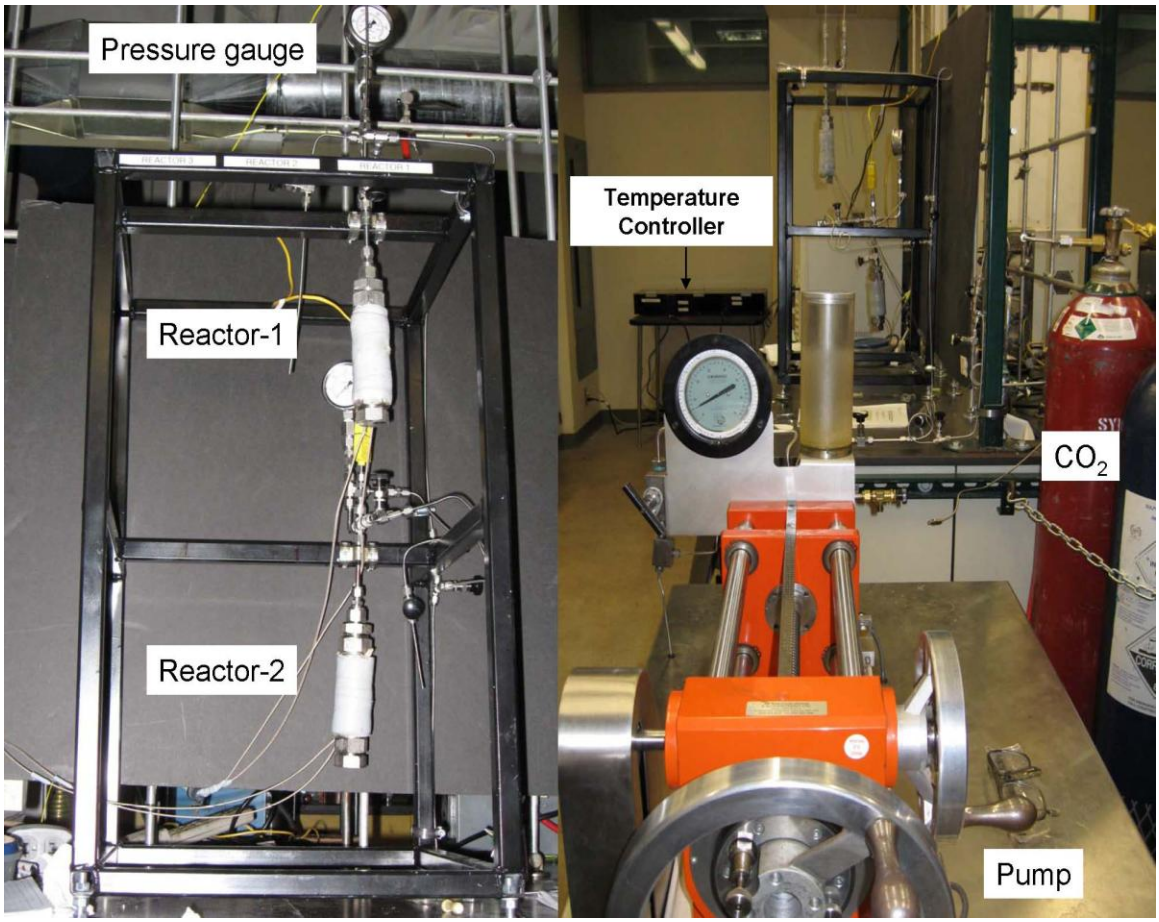

Figure 3- 2: Photograph of the experimental setup

The advantage of using such an apparatus over the previous experimental setup described by Seyfried et al. [22], which was adopted by Kaszuba et al. [4][21] and Rosenbauer et al. [27] is we can correlate the changes in mineralogy with the changes in brine chemistry at each stage the sample is collected. This provides a comprehensive picture of the geochemical interactions taking place. Sampling does not disturb the system, and mineralogical changes can be viewed in light of the changes in brine chemistry.

3.2 Analytical Methods

The samples are retrieved from the reactor by detaching the bottom (where the sample rests in a cap) and carefully taking the sample out without disturbing the minerals that might have precipitated on the sample surface. The samples are dried overnight at 60^0C, a temperature not high enough to alter the crystal structure of any minerals. The mineralogy of the rocks was determined by X-Ray Diffraction (XRD) analysis before and after the experiment and by Scanning Electron Microscope/Back Scattered Electron image analysis, (SEM/BSE). The SEM is equipped with Energy Dispersive X-Ray Spectroscopy analysis (EDS), which provides semiquantitative elemental analysis of the initial and reacted rock samples. The methodology for these procedures is described below.

Whole-rock and clay XRD analyses were performed on each sample in the XRD laboratory at the Energy & Geoscience Institute at the University of Utah, using a Bruker D8 Advance X-Ray diffractometer. Phase quantification using the Reitveld method was performed using the TOPAS software developed by Bruker Analytical X-ray Systems. The principal of the Rietveld method is that the intensities calculated from a model of the crystalline structure are fit to the observed X-ray powder pattern by a least squares refinement. This is done by varying the parameters of the crystal structures and of the peak profiles to minimize the difference between observed and calculated powder patterns. Because the whole powder pattern is taken into consideration, problems of peak overlap are minimized and accurate quantitative analyses can be obtained.

The following operating parameters were used when analyzing the powdered samples: Cu-K-α radiation at 40 kV and 40 mA, $0.02^o2\theta$ step size, 0.4 and 0.6 seconds

per step, for clay and bulk samples, respectively. Clay samples were examined from 2 to 45^{o}2θ, and the bulk from 4 to 65^{o}2θ. The instrument is equipped with a detector (lynx eye), which collects data over 2.6 mm, rather than at a point, greatly increasing X-ray counts collected, and decreasing acquisition time, as well as a rotating sample stage which increases the mineral grain orientations encountered by the incident electron beam and an automated sample exchanger capable of holding up to 45 samples.

Three analyses were conducted on each sample. First, samples are ground in a micronizing mill until fine enough to pass through a 325 mesh screen (particle size < 44 micrometers), after which it is split into two fractions: one for the bulk and one for the clay analyses. The fraction used for the bulk analysis was rolled approximately 50 times to randomly orient the mineral grains before being scanned. The clay fraction (less than 5 micrometer portion) was separated from the bulk sample using Stokes' Law for particle sedimentation, after treatment with a surfactant, which inhibits flocculation. An air-dried scan was performed. The sample was then allowed to interact with ethylene glycol vapors to induce swelling of susceptible clays, and a glycolated scan was performed. The air-dried and glycolated patterns were then compared to determine which, if any, expandable clays are present. After the clay minerals are identified, their abundances are determined from the Rietveld refinement of the bulk scans.

The materials characterization facility operated by the Material Science and Engineering Department at The University of Utah is equipped with a Hitachi S3000-N scanning electron microscope (SEM). The SEM has low vacuum and environmental capabilities. Additional features include EDS chemical analysis, as well as orientational image mapping (OIM) technology. This supports analysis and imaging of metals,

ceramics, polymers, and biomaterials. Since these rock samples are very fine grained (100 μm), they need to be coated with gold to make them conductive and suitable for SEM/EDS analysis. The samples are gold sputtered in an inert Argon environment for about 5 min before being subjected to analysis. Samples analyzed with the SEM are mounted on 1-inch round C planchets using C sticky tabs and coated with approximately 200 Å of C. The accelerating potential was 20 kV with beam current dependent on the application.

Brine analyses were performed by Inductively Coupled Plasma Mass Spectrometry (ICP-MS). After the experiments, the brine samples were diluted and filtered using Whatman 40 filter paper (retention capacity of 8μm) in a vacuum filtration setup. The sample was then divided into subequal fractions for cation and anion analyses. The sample was acidified by addition of sulfuric acid to prevent any precipitation. All the dissolved cations were analyzed using ICPMS and dissolved anions by ion chromatography (IC). The ICPMS/ IC analysis was performed at the Department of Geology and Geophysics at The University of Utah. The lab is equipped with an Agilent 7500ce, quadrupole mass-spectrometer with an octopole reaction system to preferentially remove polyatomic interferences; Autosampler Cetac AS 520 which is quartz Scott type, PTFE cyclonic and quartz double-pass spray chambers; platinum or nickel cones and a quartz shielded torch. ICP-MS analyses are performed for aqueous samples, although organic matrices can be considered.

In this study, the following procedure is followed for all the experiments.

- Initial SEM/EDS and XRD analysis of the rock

- Initial ICPMS analysis of the brine
- Final XRD analysis of the rock after the experiment and quantitative comparison of the mineral assemblage before and after the reaction
- Final SEM/EDS analysis of the rock and identification of the dissolution of the initial mineral matrix and newly precipitated phases
- ICPMS analysis of the brine after the reaction
- Correlation of the brine and rock chemistry results throughout the time scale of the experiment

3.3. Initial Experiments

The experiments were conducted with four-rock types: limestone, sandstone, synthetic arkose, and peridotite. The most common reservoir lithologies are sandstone, dolomite, and fractured basement rock [69]. Sandstone and carbonate reservoirs are the most common natural gas reservoirs. The significance of the frequency of dolomite ($MgCa[CO_3]_2$) reservoirs trapping CO_2, rather than the more commonly occurring limestone ($CaCO_3$) reservoirs, is not known. Dolomite can be naturally very porous as a result of the dolomitization process of limestone, and can occur early (soon after deposition).

These minerals as a group are common occurrences in all formations such as Cutler formation in southeast Utah, which is a calcareous sandstone [70]; Bakken formation in North Dakota, primarily a mixed assemblage (sandstone+carbonate+clay formation) [71]; Granite wash in Oklahoma, Permian formation, Supai in Springerville,

Utah [72]; and Coconian sandstone reservoir section in the Gordon Creek formation in Southern Utah.

There are numerous limestone formations, many of which are natural CO_2 reservoirs. The McElmo Dome located in southwestern Colorado is the best-documented natural analog site as well as the world's largest supply of commercially traded carbon dioxide. Carbon dioxide at McElmo Dome is trapped in a supercritical state within the Mississippian Leadville formation, a dolomitic carbonate unit averaging 100 m in thickness and 1,800 to 2,600 m deep.

Another example is the Triassic Sinbad limestone member of the Moenkopi formation - the Farnham Dome, Utah. This is a low-porosity, low-permeability, reservoir that ranges in thickness from 15 to 46 m (50 to 150 ft) in the Farnham Dome area (1400 m depth). Another example is the Kaibab limestone formation in Escalante, Utah, which is composed primarily of limestone and dolomite at an average depth of 720 m.

Sandstone reservoirs are the most common formations - occurring mainly as "dirty" sandstones, with traces of carbonates and other clay minerals. The clay minerals are a result of silicate weathering reactions. Hence, the formations away from sources such as Granite Wash will have higher amounts of clay and other phylosilicate minerals resulting from weathering reactions. Jackson Dome, located in central Mississippi in the onshore Gulf Coast province, is a good example. It is aeolian sandstone with complex porosity and permeability distribution controlled by authigenic illite clays. The St. Johns field in Springerville, Arizona contains CO_2 in the Permian Supai Formation, primarily fine-grained nonmarine sandstone, with intercalated siltstone, anhydrite, and dolomite. Well depths are relatively shallow (200 to 700 m). Multiple impermeable anhydrite cap

rocks are present, vertically segregating the carbon dioxide within multiple zones. Some other examples are in Cedar Mesa sandstone formation in Escalante, Utah.

Arkose or dirty sandstones, as mentioned before, are common occurrences in many geological formations [69]. Bravo Dome in New Mexico is a natural CO_2 reservoir with the primary producing zone (99% of CO_2) being Permian Sangre de Cristo (Tubb) arkosic to conglomeratic sandstone. The Gallup sandstone in Shiprock, New Mexico is also arkosic sandstone with quartz, K-feldspar, and carbonates (calcite and dolomite) [73]. The Cutler formation in southeastern Utah comprises rapidly deposited, poorly sorted, conglomeratic sandstone, limestone, and siltstone [70].

Rather than taking a pure mineral such as quartz and subjecting it to sequestration conditions, which would yield no carbonates, a synthetic rock was built by taking minerals which are common in many geological formations and used in the experiments to yield carbonates. The abundances of these minerals are relatively less important considering the thermodynamic equilibrium of the system. The importance of the amount of mineral present in the rock can be neglected provided that it is greater than the amount required to precipitate carbonates relative to the amount of CO_2 enriched brine in contact with the mineral. Hence, the variations of the amount of minerals in these formations from the amounts used to prepare the synthetic rock can be neglected.

Synthetic arkose was prepared by mixing equal amounts of pure minerals, calcite, dolomite, quartz, chlorite, andesine, and microcline. The following reasons dictated this selection:

1. This synthetic rock has a typical sedimentary mineralogy [73].

2. The abundances of minerals were controlled carefully and the heterogeneity was minimized.
3. Minerals chosen contain key ions for carbonation reactions (Al, Na, Mg, Fe, Si).
4. The sample had all the minerals in excess.
5. Possibilities of observing important CO_2 sequestration reactions were favorable due to the variety and abundance of ions.

The red color of the Cutler rocks resulted from the formation of hematite by intrastratal solution of iron-bearing minerals. This calcareous sandstone with traces of iron is very similar to the arkose used in the experiments in this study. The Coconian sandstone from the Gordon Creek-1 well also has a very similar composition to the synthetic arkose used in this study. The Ohio Rose run aquifer studied by Zerai et al. [61] and the rock from the wells in Bravo Dome, New Mexico also have a very similar composition as listed in Table 3-1.

Table 3- 1: Comparison of the synthetic arkose with rock compositions (XRD) from natural formations

Mineral	Synthetic Arkose	Gordon Creek-Coconino SS	Bravo Dome New Mexico	Ohio Rose Run Sandstone
Quartz	22.7	16	31	58
Andesine	13.1	9	11	5
Dolomite	12.5	14	18	13.8
Calcite	13.2	20	29	9
Illite/Chlorite	20.2	15	4	2
Microcline	22.5	8	6	8
anhydrite	-	7	-	-

3.3.1 Reactor Stability Study

The first objective of this study was to make sure that the reactor itself was stable through the duration of the experiment. The primary question was whether the corrosion of the 316 stainless steel reactors in the high temperature, high pressure, highly saline, and mildly acidic environment contributed to the changes occurring in the repository. To verify this, two sets of experiments were carried out. In the first set of experiments, the reactor was subjected to the experimental conditions without the rock and CO_2. This experiment set would provide us with an idea of the stability of the reactor under experimental conditions. The experiments were carried out for 147 days with sampling intervals of 14 days, 28 days, 64 days, 127 days, and finally, 147 days. The brine samples retrieved from the reactors were subjected to ICPMS analysis for cations and IC analysis for anions. Table 3-2 indicates the behavior of the system during the course of the experiment. As the table shows, the brine concentration remained relatively unchanged through the duration of the experiments. The concentrations of the major ions Na and Cl remained stable given their relatively very high concentration compared to the trace ions. Na concentration showed a maximum variation of +2.8% in the sample retrieved after 64 days. The Cl ion concentration showed a maximum variation of 1.1%. These variations were well within the analytical error of ICPMS, which is around 5%. Regarding the trace ions, Fe exhibited a maximum variation of 7% and silica also showed a variation of 15%. This evidence shows that the reactor was relatively stable for 147 days at 200^0C and 2000 psi. The second set of stability analyses was carried out at 200^0C 2000 psi with brine and CO_2. Table 3-3 illustrates the results of this analysis.

Table 3- 2: Stability analysis of the reactor at 200^0C, 2000 psi with 3wt% brine

	Initial	14 days	28 days	64 days	127 days	147 days
Na(mg/L)	23032	23154	23087	23678	23047	23064
Mg(mg/L)	1	1	1	1	1	1
K(mg/L)	<6	<4	<6	<6	<6	<6
Ca(mg/L)	<4	<4	<4	<4	<5	<6
Al(ug/L)	<8	<8	<8	<8	<8	<8
Mn(ug/L)	<1	<1	<1	<1	<1	<1
Fe(ug/L)	54	49	61	59	42	57
Ba(ug/L)	<2	<2	<2	<2	<2	<2
Si(mg/L)	0.4	0.1	0.4	0,4	0.7	0.4
S(mg/L)	<6	<6	<6	<6	<6	<6
Cl(mg/L)	26542	26672	26834	26493	26598	26762

With mildly acidic conditions in addition to the high temperatures and pressures the reactor remained stable (Table 3-3). The maximum variations in the principal ions Na and Ca were 3.1% and 1.1%, respectively. Of the trace ions, Fe ion concentration showed the maximum deviation of 9% even after the system reached equilibrium. Thus, even at the maximum acidic conditions in the reactor, the reactor remained stable.

3.3.2 Base Experiments

The initial experiments were carried out using dirty sandstone or synthetic arkose at 200^0C and 2000 psi. Arkose was selected as the reacting material because of its chemistry and common occurrence in a number of sedimentary basins [21]. Arkose used in our experiments is comprised of equal proportions of the minerals calcite, dolomite (primary carbonate minerals), quartz, microcline, andesine (primary silicate minerals), and chlorite (iron bearing sheet silicate) (Table 3-1). The mineral samples were crushed to 100 μm and mixed to create the arkose. All the mineral grains were angular to circular

Table 3- 3: Stability analysis of the reactor at 200^0C, 2000 psi with 3 wt% brine and CO_2

	Initial	14 days	28 days	64 days	127 days	147 days
Na(mg/L)	23032	23154	23162	23781	23763	23368
Mg(mg/L)	1	1	1	1	1	1
K(mg/L)	<6	<4	<6	<6	<6	<6
Ca(mg/L)	<4	<4	<4	<4	<5	<6
Al(ug/L)	<8	<8	<8	<8	<8	<8
Mn(ug/L)	<1	<1	<1	<1	<1	<1
Fe(ug/L)	54	59	57	48	45	61
Ba(ug/L)	<2	<2	<2	<2	<2	<2
Si(mg/L)	0.4	0.1	0.4	0,4	0.7	0.4
S(mg/L)	<6	<6	<6	<6	<6	<6
Cl(mg/L)	26542	26684	26848	26674	26782	26465

in shape and ranged in size from 80-100 μm. The primary objective of these experiments was to compare the results from these reactions with those in the literature.

All the experiments were carried out with 3g of rock. For the arkose, the initial sample was prepared by mixing equal proportions of each mineral (0.5 grams each). The initial composition of the arkose is shown in Table 3-4. The brine to rock ratio in the experiments was 10:1. Brine was prepared from laboratory grade NaCl with the initial composition shown in Table 3-5. Injection of approximately 7cc of CO_2 into the reactor increases the pressure of the experimental system to 2200 psi. Subsequently, the pressure decreased to 2000 psi over a period of 37 hrs. The total pressure of the experimental system stabilized around 2000 psi for the duration of the experiment with the exception of a few fluctuations that can be attributed to changes in the ambient temperature in the laboratory.

Table 3- 4: Composition of the synthetic arkose

Rock	Quartz	Andesine	Dolomite	Chlorite	Microcline	Calcite
Formula	SiO_2	$Na_xCa_yAlSi_2O_8$	$CaMg(CO_3)_2$	$(Fe, Mg, Al)_6(Si, Al)_4O_{10}(OH)_8$	$KAlSi_3O_8$	$CaCO_3$
Class	Silicates	Silicates	Carbonates	Silicates	Silicates	Carbonates
Group	Quartz	Feldspar	Dolomite	Chlorite	Feldspars	Calcite
Wt % (XRD)	22.7	13.1	8.5	20.2	22.5	13.2

Table 3- 5: Initial composition of the brine for all the experiments (<=detection limits)

Na	Mg	K	Ca	Al	Mn	Fe	Ba	Si	S	Cl
mg/L	mg/L	mg/L	mg/L	µg/L	µg/L	µg/L	µg/L	mg/L	mg/L	mg/L
23032	1	<6	<4	<8	<1	54	<2	0.4	<6	26542

Initial examination of the rock surface was carried out using XRD and SEM/EDS analysis. The EDS analyses identified the clay minerals, plagioclase feldspar and illite (Figure 3-3) and chlorite to be the major silicate minerals and calcite and dolomite as the carbonate minerals in the starting material. The SEM analysis was performed at different resolutions to measure the exact chemical composition of the mixture and to ensure uniform composition.

Figure 3-4 shows the XRD patterns for two initial rock samples. Overlap of the spectra indicates the two samples had the same initial compositions. The initial sample XRD analysis shows the peaks of the minerals used to prepare the sample. These peaks serve as a reference for the analysis of the reacted sample.

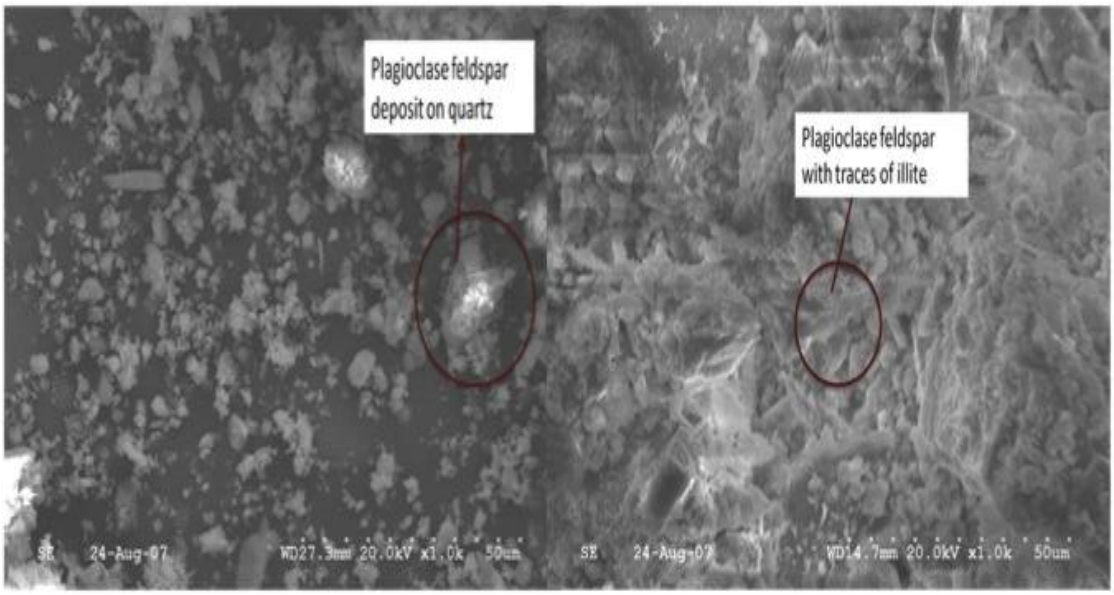

Figure 3- 3: SEM image of the host rock at 1kx magnification showing plagioclase feldspar deposits on quartz and branching aggregates of plagioclase feldspar with minor quantities of illite

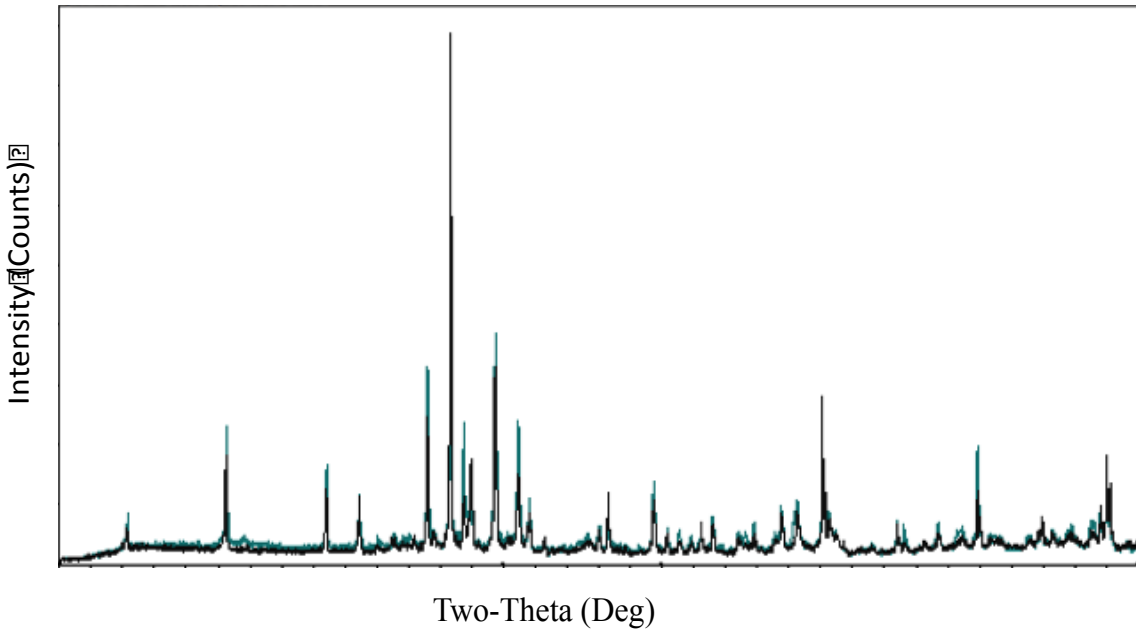

Figure 3- 4: Initial XRD patterns of the initial rock sample

The experimental conditions were similar to those of Kaszuba et al. [4][21]. Under these high-temperature (200^0C) and high-pressure (200 bar) conditions, the rates of silicate dissolution are accelerated. However, the aqueous solubility of CO_2 is generally lower at elevated temperatures and salinity and greater at elevated pressure. Using SUPCRT92, the maximum dissociation of carbonic acid dissolution occurs at 50^0C, above which log K decreases continuously with increasing temperature; the initially weak acid becomes increasingly weaker at elevated temperatures [27]. Consequently, the experiments at ~200^0C were carried out for a relatively longer time period (123 days) to increase the opportunity for detectable changes in the host rock. Several changes were observed. Andesine and dolomite dissolved, calcite, quartz, and chlorite precipitated. The precipitation of quartz was not conclusive since the change in its abundance was within the uncertainty in XRD measurement. This XRD analysis gives a preliminary picture of the changes that are occurring and a preview of what to expect in the SEM/EDS analyses. To study the surface chemistry and to identify the precipitation or dissolution patterns of the dominant minerals in the samples, the initial and the reacted samples were analyzed using SEM. The sample is mounted on a carbon tape and is gold coated in an inert (argon) environment to charge the surface. SEM analysis requires careful observation of the surface of the sample at a very high resolution. Figure 3-5 compares the initial and reacted rock samples. The silicate phases, andesine and microcline, underwent dissolution due to the increase in acidity of the brine, caused by the injection of CO_2.The primary carbonates, calcite and dolomite, dissolve during the initial stages of the experiment but calcite concentration increases in the final analysis

(Figure 3-6) as a result of the secondary precipitation reactions and carbonation of feldspars (equations 3.1 and 3.2).

$$Ca^{2+} + CO_3^{2-} \leftrightarrow CaCO_3 \quad (3.1)$$

$$CaAl_2Si_2O_8 + H_2CO_3 + H_2O \leftrightarrow CaCO_3 + Al_2Si_2O_5(OH)_4 \quad (3.2)$$

(Andesine) (Kaolinite)

Growth of calcite is shown in Figure 3-7. Due to the increased acidity caused by the formation of carbonic acid, dolomite and calcite undergo dissolution. The released calcium cation should be from dolomite or calcite, because the XRD analyses reveal the dissolution of these minerals. The calcium ion thus liberated into the solution forms calcite by the secondary precipitation reactions with the carbonate ion from the acid consuming one mole of CO_2 in the process. Calcium carbonate deposition is a clear indication of the consumption of CO_2 in this reaction. The acidity of the solution also decreases as the primary carbonates undergo dissolution in the system. This decreases acidity and also favors secondary precipitation reactions. The feldspars, which are sensitive to these relatively abrupt changes in pH, also undergo dissolution as the pH increases. Dissolution of feldspars also provides the required cations for these secondary precipitation reactions. Hence the brine, which is now cation rich and also has relative abundance of anions (through carbonate dissolution reactions), facilitates the precipitation reactions depending on the saturation states of the minerals in the brine. Crystals of halite were seen deposited on the mineral surface (Figure 3-8).

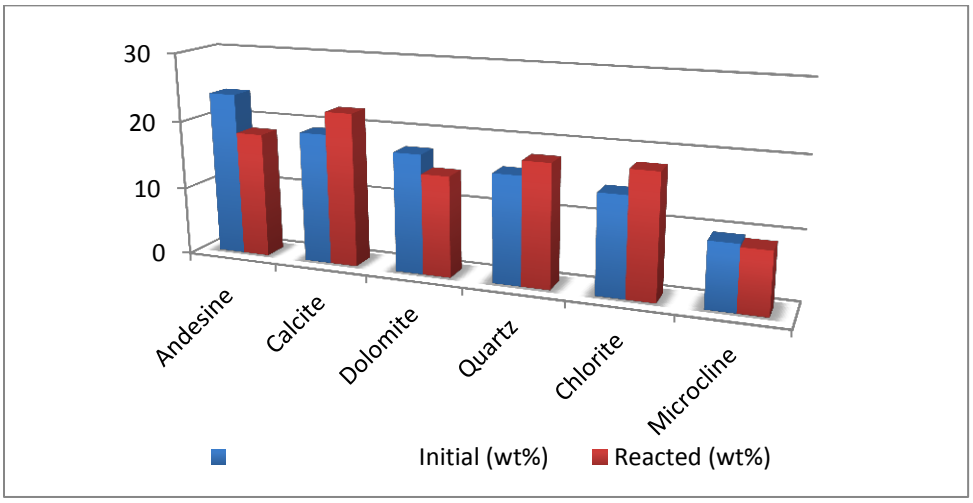

Figure 3- 5: Quantitative comparison of the XRD analyses of the initial and reacted phases. Y-Axis indicates the composition by wt%

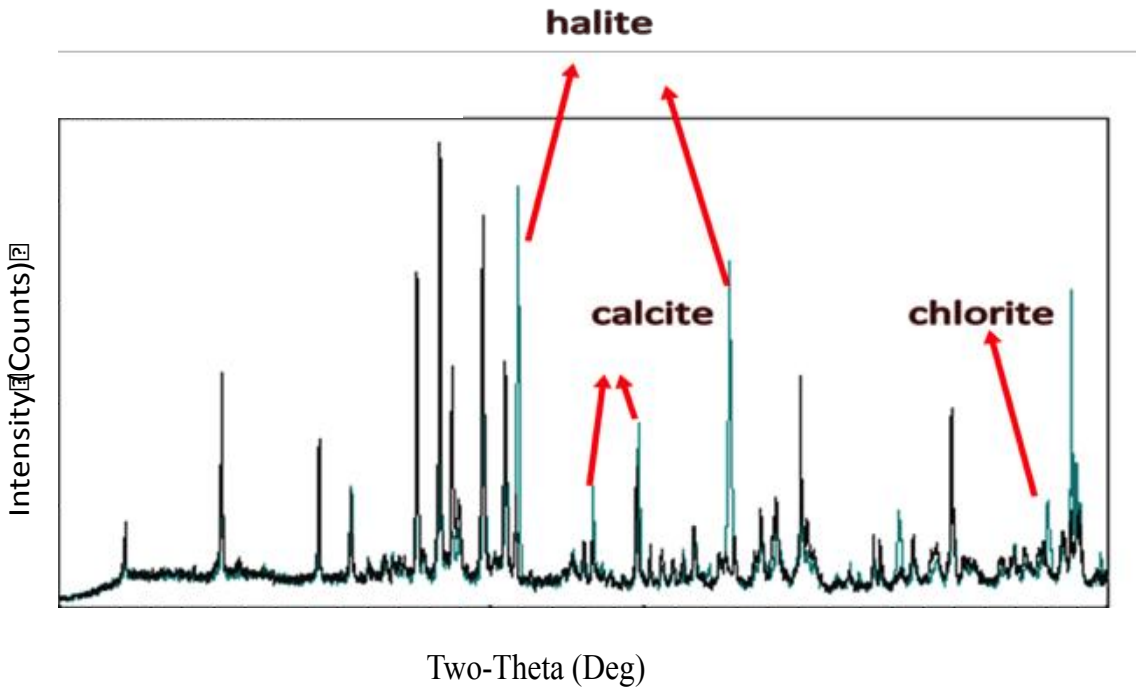

Figure 3- 6: XRD patterns of the initial and reacted samples for the experiment at 200°C and 2000 psi. Halite and chlorite and calcite peaks are labeled

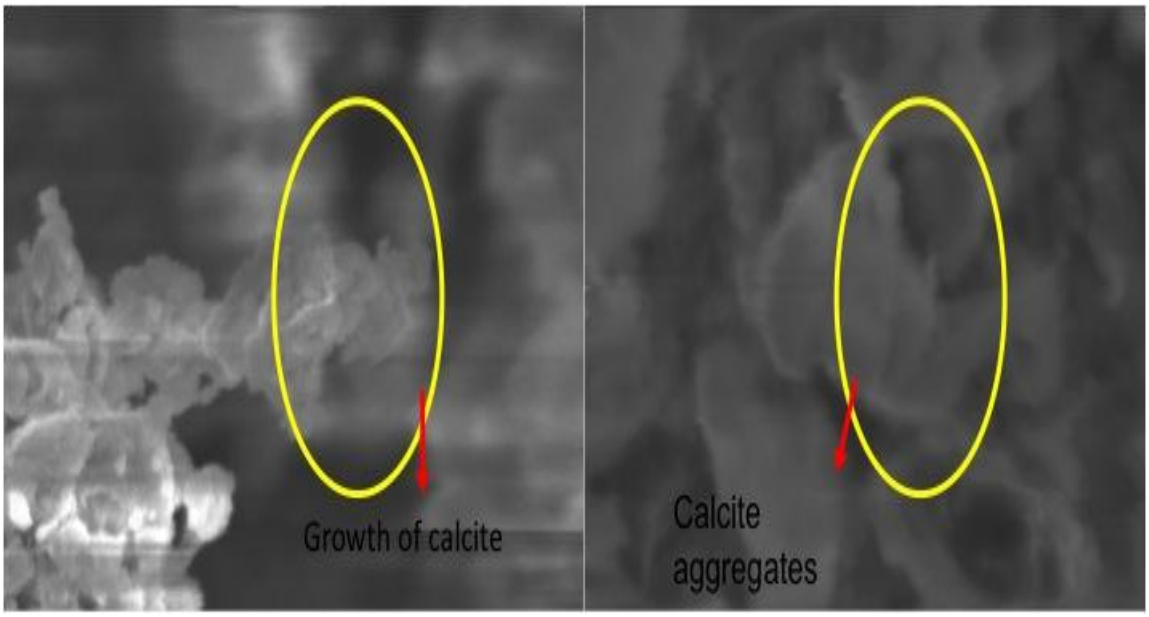

Figure 3- 7: SEM image at 6kx magnification (left) showing growth of calcite as layers and 12kx magnification (right) showing precipitation of calcite aggregates on quartz

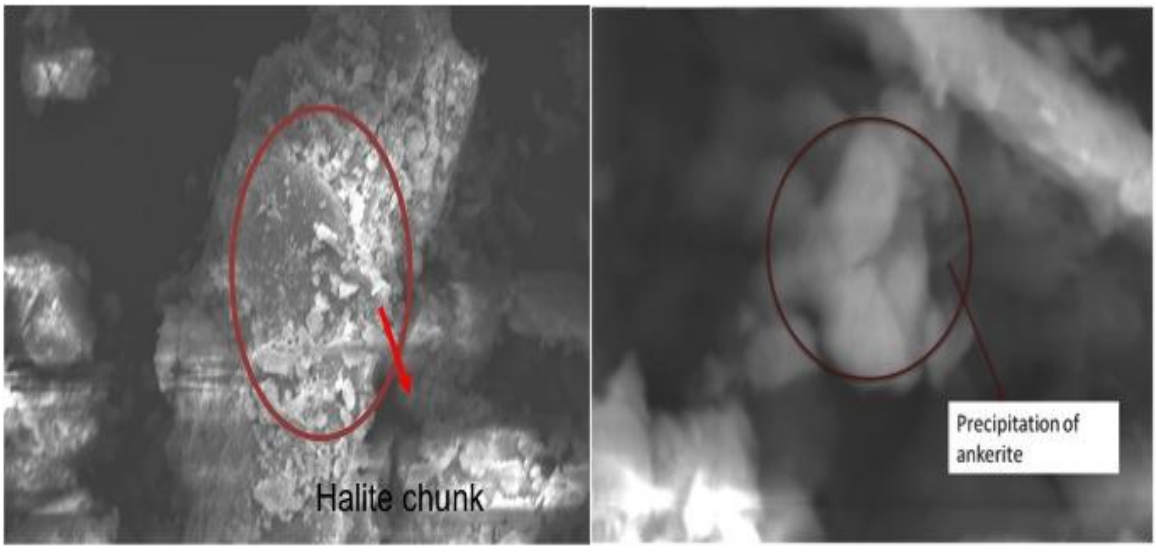

Figure 3- 8: SEM image at 3kx magnification (left) showing deposition of halite and Ankerite growth (right) in the final sample

Ankerite, (iron carbonate) was seen growing as aggregates in the pore spaces (Figure 3-8). The source of iron for ankerite was the dissolution of chlorite, magnesium rich phase in the initial sample. The XRD analysis, which shows the dissolution of chlorite, supports this comclusion. The qualitative analysis by EDS confirmed the identification of ankerite, which was absent in the initial mineral assemblage

3.4. Rock Compositional Effects

One of the main factors governing this complex geological environment is the initial mineral assemblage. Obviously, reservoir rock type will have a strong influence on rock-fluid interactions and the trapping mechanisms of CO_2. In a limestone reservoir, for example, the principal methods of trapping are structural and ionic. Zerai et al. [61] used geochemical models to simulate the effect of rock composition on the ultimate fate of CO_2 in subsurface formations. Continuous dissolution was reported in limestone, and in sandstone and mixed rock types (sandstone + carbonate), mineral trapping was predicted. This study provides experimental data to reexamine these important findings. To evaluate the effect of rock composition on these complex geochemical reactions, the following rocks that usually form the base minerals in saline aquifers were selected.

1) Limestone
2) Sandstone
3) Peridotite
4) Arkose
5) Spent shale

Peridotite was included because of its relatively high reactivity.

Limestone, sandstone, and arkoses are commonly occurring geological mineral bases for most of the saline aquifers chosen as potential sequestration sites. All the samples were crushed to 100μm and mixed to create the arkose. All the crushed rock fragments were angular to circular in shape and ranged in size from 80-100μm. Peridotite is an olivine-rich rock $(MgFe_2)SiO_4$, which is relatively scarce compared to the above-mentioned rocks. When producing oil from shale in-situ, the shale is retorted underground without mining to the surface. There has been debate on the ability of the processed shale to sustain sequestration reactions. Hence, conducting the experiments using spent shale as the initial rock would throw more light on the possibility of utilizing spent shale as potential CO_2 sequestration sites.

All the experiments were carried out at 100^0C and 2000 psi with the brine composition indicated in Table 3-5. The temperatures in these formations will vary depending on the depth of injection and local geothermal gradients. For this study, a temperature of 100^0C was chosen. With increase in temperature, the kinetic rates of these constituent minerals increase, but the solubility of CO_2 in brine decreases. Hence, an initially weak acid becomes progressively weaker with increasing temperature. The acidity of the brine is the principal factor that triggers the complex sequence of these sequestration reactions. Hence a temperature of 100^0C was chosen as a trade-off to achieve a balance between the thermodynamic and kinetic constraints of the system.

3.4.1. Experiments with Limestone

Initial XRD and SEM analysis (Figure 3-9) of the limestone revealed it to be 98.4 calcite, 1.2% dolomite, and 0.4% quartz. During the experiment, which lasted for a

period of 42 days, the pressure increased to 2060 psi after 17 days and 2090 psi after 42 days. This can be attributed to a four-step process indicated by the reactions listed below:

$$CO_2\,(g) \quad \leftrightarrow \quad CO_2\,(aq) \tag{3.3}$$

$$H_2O + CO_2 \quad \leftrightarrow H_2CO_3 \tag{3.4}$$

$$H_2CO_3 \quad \leftrightarrow H^+ + HCO_3^- \tag{3.5}$$

$$CaCO_3 + H^+ \leftrightarrow \; Ca^{2+} + HCO_3^- \tag{3.6}$$

The carbon dioxide dissolves in water to form carbonic acid (equations 3.3, 3.4). This leads to a decrease in pH. pH decreased from a value of 5.4 to about 4.9 after 28 days and increased to 5.2 after 42 days. The CO_3^{2-} concentration will be higher under slightly basic conditions than under acidic ones for the same Ca concentration. Concentrations (and thus activities) of calcium and carbonate in solution increase when calcite dissolves congruently. The moderate value of pH causes most dissolved carbonate to become bicarbonate. Hence, the activity of CO_3^{2-} is two orders of magnitude lower than that of Ca. Because of this increased acidity, calcite, which is sensitive to changes in pH, undergoes dissolution to release carbonate and bicarbonate ions (equation 3.5, 3.6). The absence of feldspars and clays, which serve as a source of cations for secondary precipitation of carbonates, rules out the possibility of any precipitants and also mineral sequestration of CO_2. XRD analysis revealed a reduction in both calcite and dolomite, indicating that significant dissolution of these components has occurred (Figure 3-9). The acid attack on limestone leaves pronounced dissolution patterns on the surface. These dissolution patterns are omnipresent (Figure 3-10) throughout the sample and visible in the SEM images. The primary cations tracked here are Ca and Mg (Figure 3-11). The Mg

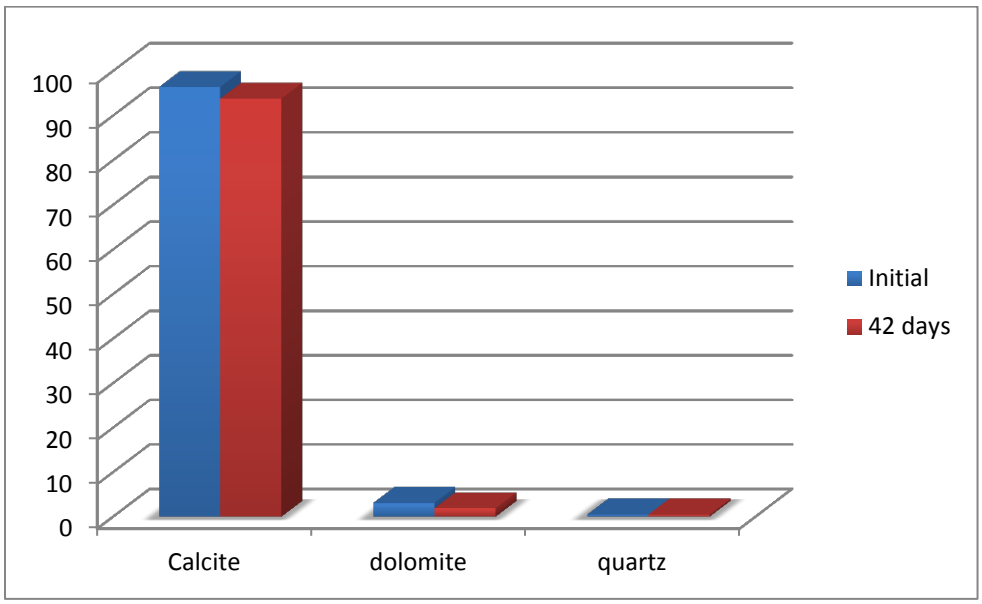

Figure 3- 9: Quantitative XRD analysis in wt% of limestone before and after the experiment. Y-Axis indicates the composition by wt%

derived from dolomite, which was present as traces in the initial mineral assemblage. The continuous increase in the concentrations of both the principal ions indicates continued dissolution of calcite and dolomite. The pH of the system initially decreased due to CO_2 dissolution in the brine and increased subsequently because of carbonate dissolution (equation 3.6). Carbonate chemistry buffers the brine by consuming H^+, which decreases the acidity of the system. The relative scarcity of cations nullifies the possibility of precipitation reactions. The primary modes of sequestration in these aquifers are structural trapping and ionic trapping.

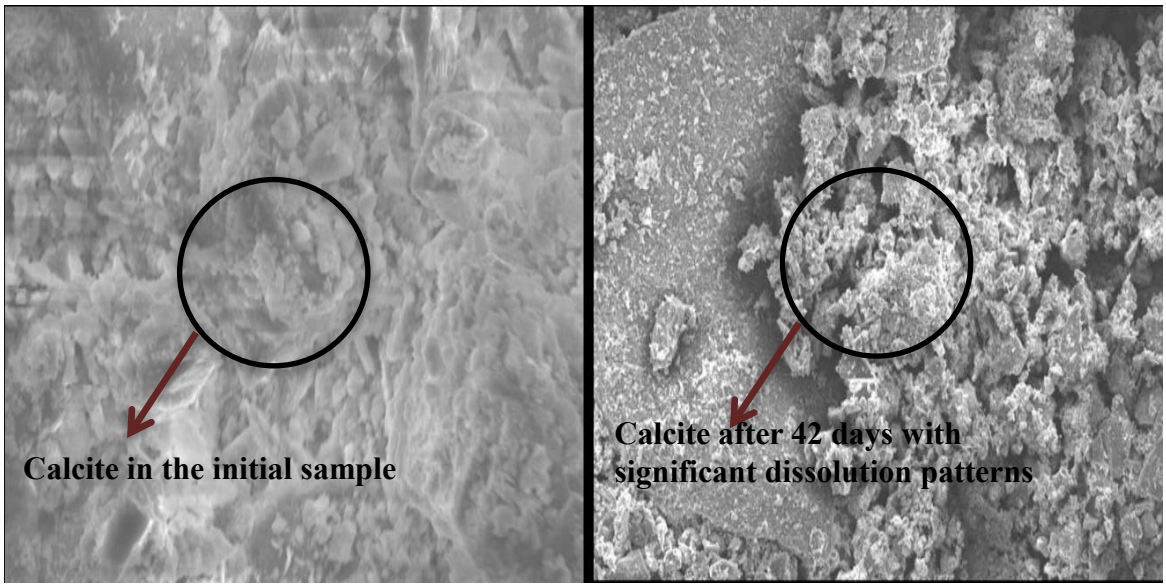

Figure 3- 10: SEM images of initial calcite (left) and the reacted calcite after 42 days; dissolution has produced deep etching and rough edges of the surfaces

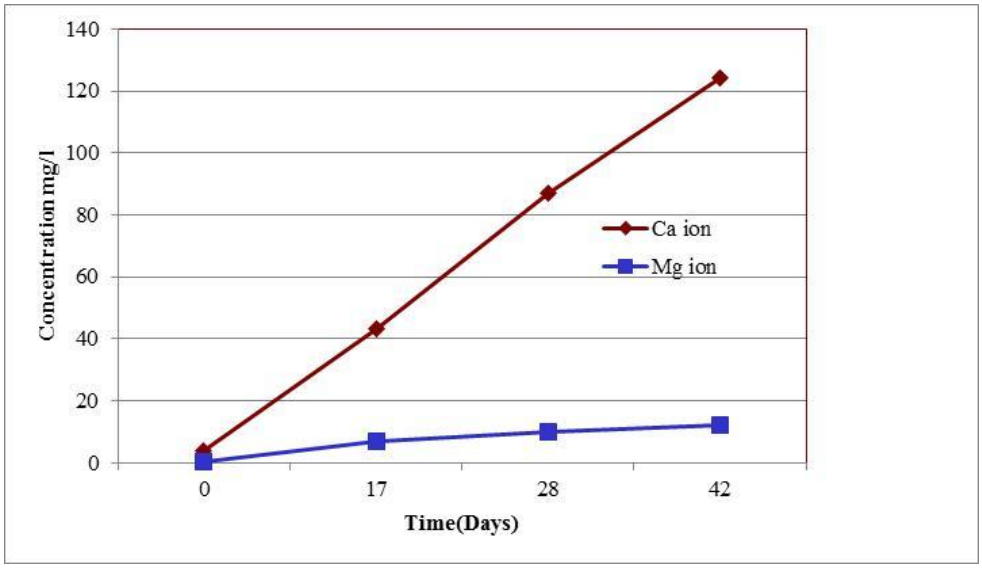

Figure 3- 11: Changes in brine chemistry during limestone experiments

3.4.2. Experiments with Sandstone

Initial XRD analysis of the sandstone revealed 44-wt% calcium feldspar, 26.2-wt% Na feldspar, and the rest K-feldspar. During the experiments, the pressure was constant around 2000 psi after 17 days and remained stable for the rest of the experiment. The pH increased from a value of 5.4 to about 5.9 after 28 days and 6.4 after 42 days. The principal reactions in this case can be formulated as follows:

$$2H^+ + CaAl_2Si_2O_8 + H_2O \leftrightarrow Ca^{2+} + Al_2Si_2O_5(OH)_4 \quad (3.7)$$

$$CaAl_2Si_2O_8 + H_2CO_3 + H_2O \leftrightarrow CaCO_3 + Al_2Si_2O_5(OH)_4 \quad (3.8)$$

$$NaAlSi_3O_8 + 3\ H_2O \leftrightarrow NaAlSi_2O_6.H_2O + H_4SiO_4 \quad (3.9)$$

$$2KAlSi_3O_8 + 9H_2O + 2H^+ \leftrightarrow Al_2Si_2O_5(OH)_4 + 2\ K^+ + 4H_4SiO_4 \quad (3.10)$$

Dissolution of feldspar also decreases the acidity of the brine (equation 3.7), which turned acidic because of the formation of the carbonic acid (equation 3.1). This leads to the next sequence of reactions: precipitation of calcite and kaolinite. At these temperatures and pressures, albite reacts with water (equation 3.9) to precipitate analcime, which was detected in the XRD analysis. Dissolution of K-feldspars (equation 3.10) also leads to precipitation of kaolinite. The primary product of these dissolution reactions is silica. This results in the brine becoming saturated, and in some cases, supersaturated with amorphous silica. Hence when the samples are retrieved for analysis heterogeneous deposition of amorphous silica occurs on the surface of the minerals in the sample, which was evident in the EDS analyses of all reacted samples. There was also precipitation of halite on these samples (Figure 3-12, 3-13 and 3-14). Halite precipitates as the sample dries out and NaCl is concentrated.

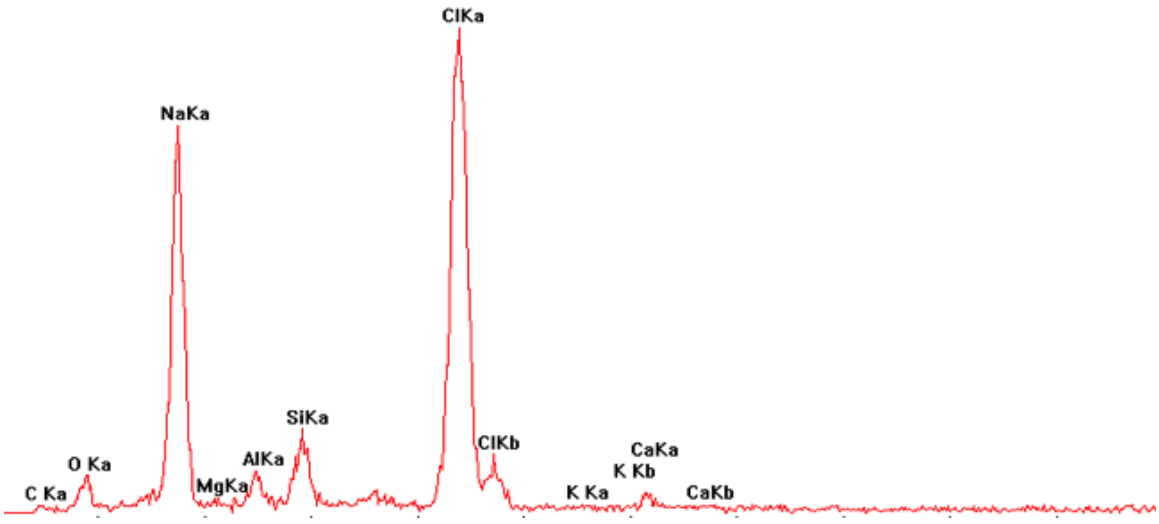

Figure 3- 12: EDS analysis of halite

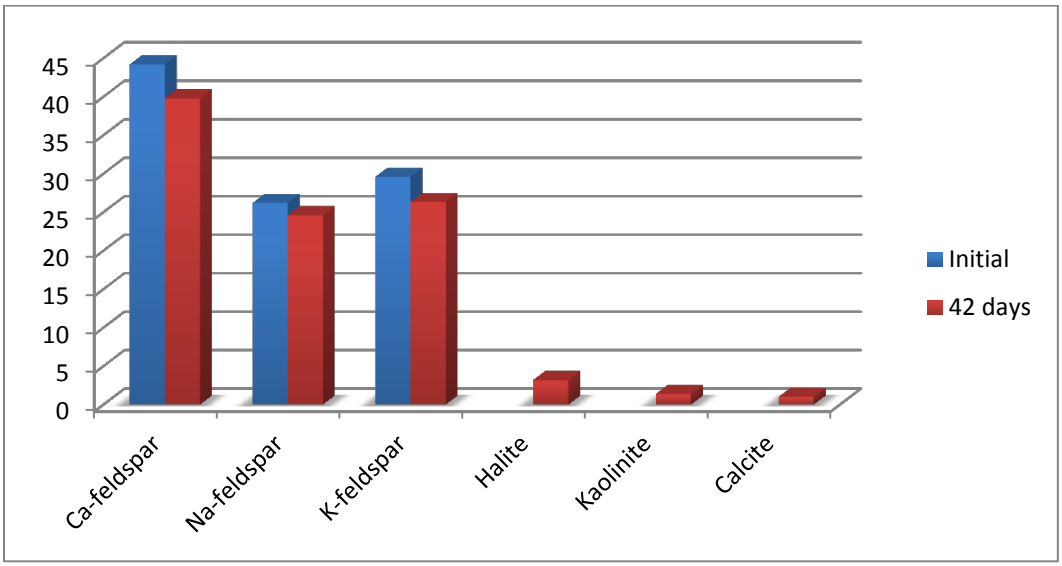

Figure 3-13: Quantitative XRD comparisons of sandstone before and after the experiment. Y-Axis indicates composition by wt%

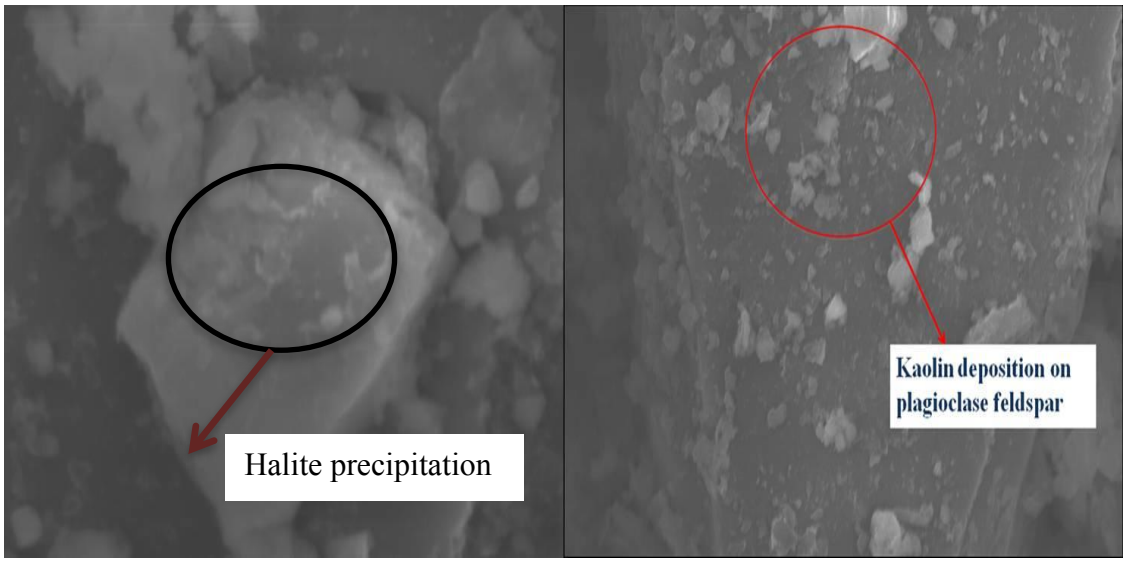

Figure 3- 14: Halite (left) and kaolinite on plagioclase feldspar (right). Kaolinite formed from the dissolution of potassium feldspar and was absent in the initial mineral assemblage

Though the carbonation of feldspars yields calcite, which was absent in the initial mineral assemblage, and in the final XRD analysis, it was not detected in the SEM analysis of the reacted sample. The reason for this was the amount of calcite-precipitated being very small.

Figure 3-15 shows the trend of the principal ions Ca, K, Al, and Si in the brine with plagioclase feldspar and microcline being the primary aluminosilicates in the initial rock matrix. The decrease in Al reflects precipitation of kaolinite, an aluminosilicate hydroxide. Analcime was detected in the XRD analyses but its precipitation was not observed in the reacted samples during the SEM analyses. Si concentrations increased continuously in the samples because of the dissolution of the aluminosilicate minerals.

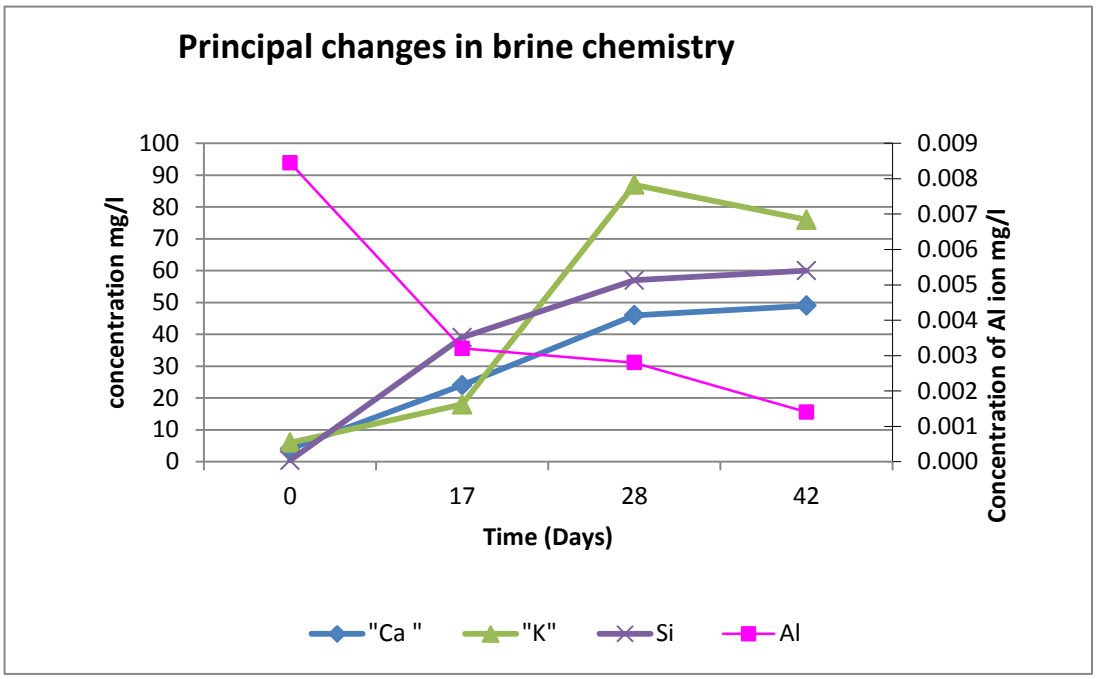

Figure 3- 15: Principal changes in brine chemistry for sandstone experiment

3.4.3. Experiments with Peridotite

Peridotite is composed largely of the minerals olivine [$(Mg,Fe)_2SiO_4$] and pyroxene [$(Ca,Mg,Fe)_2Si_2O_6$], which react with CO_2 and H_2O near the earth surface to form hydrous silicates (serpentine), iron oxides (magnetite), and carbonates (calcite, magnesite and dolomite). These reactions can be formulated as:

$$2Mg_2SiO_4 + Mg_2Si2O_6 + 4\,H_2O \leftrightarrow 2Mg_3Si_2O_5(OH)_4 \quad (3.11)$$

(Mg-olivine) (Mg-pyroxene) (serpentine)

$$Mg_2SiO_4 + 2CO_2 \leftrightarrow 2MgCO_3 + SiO_2 \quad (3.12)$$

(Mg-olivine) (Magnesite) (quartz)

$$Mg_2SiO_4 + CaMg_2Si_2O_6 + 2CO_2 + 2H_2O \leftrightarrow Mg_3Si_2O_5(OH)_4 + CaCO_3 + MgCO_3 \quad (3.13)$$

(Mg-olivine) (Ca-Mg-pyroxene) (serpentine) (calcite) (magnesite)

Evidence for natural, low-temperature hydration and carbonation of peridotite can be found in springs and associated travertines in catchments composed of peridotite and in outcrops of altered peridotite with abundant carbonate veins [36]. High alkalinity, stable isotope ratios, and the formation of travertine and carbonate cemented conglomerates in springs indicate serpentenization involving meteoric water occurring at low temperature. Ground water reacting with peridotite in near-surface, open systems forms water rich in Mg^- and HCO_3^-, which leads to precipitation of abundant magnesite and dolomite as veins. The resulting waters become progressively richer in Ca and OH^-. These waters emerge near the surface to mix with Mg-HCO_3^- waters or react with the atmosphere where they precipitate abundant calcite and dolomite in near surface veins. Enhanced natural processes such as dissolution, followed by the carbonation of feldspars, may provide an important alternative to mineral carbonation.

Peridotite was obtained as green crystalline granules from the deposits in the Samail Ophiolite, Sultanate of Oman. Kinetics of these carbonation reactions is very slow unless olivine and serpentine reactants are ground to a fine powder and held at elevated pressures and temperature. Hence, these rocks were ground to very fine powder. A size distribution analysis revealed that the grains in the crushed sample ranged from 60-100 microns in size. 3 gms of peridotite was fed into a 40CC reactor along with 20CC of brine prepared by mixing 3 gms of laboratory grade NaCl in 20CC of distilled water and brine was allowed to saturate the sample for about 2 days. CO_2 was then fed into the

reactor at a pressure of 2000 psi and the temperature was maintained at 100^0C. The reactor was isolated and the experiment was carried out for 47 days. The pressure in the reactor first decreased and then stabilized around 1980 psi for the rest of the experiment with minimal fluctuations, which can be attributed to changes in ambient conditions. The pH change was very similar to the results in experimental set B. It increased from a value of 5.4 to about 5.7 after 28 days and 6.2 after 42 days.

XRD analyses of the initial sample revealed that olivine was the major component in the sample. The sample was composed of 97.8-wt% olivine and 2.2-wt% pyroxene (Figure 3-16). Hence, we can conclude from the reactions mentioned above that carbonation of this sample will mainly yield magnesite and serpentine. Because of the presence of excess CO_2 in the reaction setup, carbonation of peridotite will dominate hydration and hence magnesite precipitation should be dominant.

Figure 3-17 shows the XRD analyses of the initial and reacted samples. Olivine and pyroxene underwent dissolution, siderite, and magnesite precipitated. The EDS analysis of the reacted rock (Figure 3-18) indicates the presence of $MgCO_3$ in the sample. This occurs due to the carbonation of the peridotite to form magnesite and silica. The presence of silica is also revealed in the analysis. The SEM analysis of the product revealed the precipitation of magnesite as orthorhombic crystals (Figure 3-19) with pitted rough faces. It can be concluded that the brine was undersaturated with respect to magnesite at the conclusion of the experiment. The dissolution of the calcium and magnesium silicate minerals produces silica. This silica precipitates (Figure 3-19) as amorphous silica when the experiment is terminated and the temperature is decreased because the brine becomes increasingly supersaturated with respect to amorphous silica.

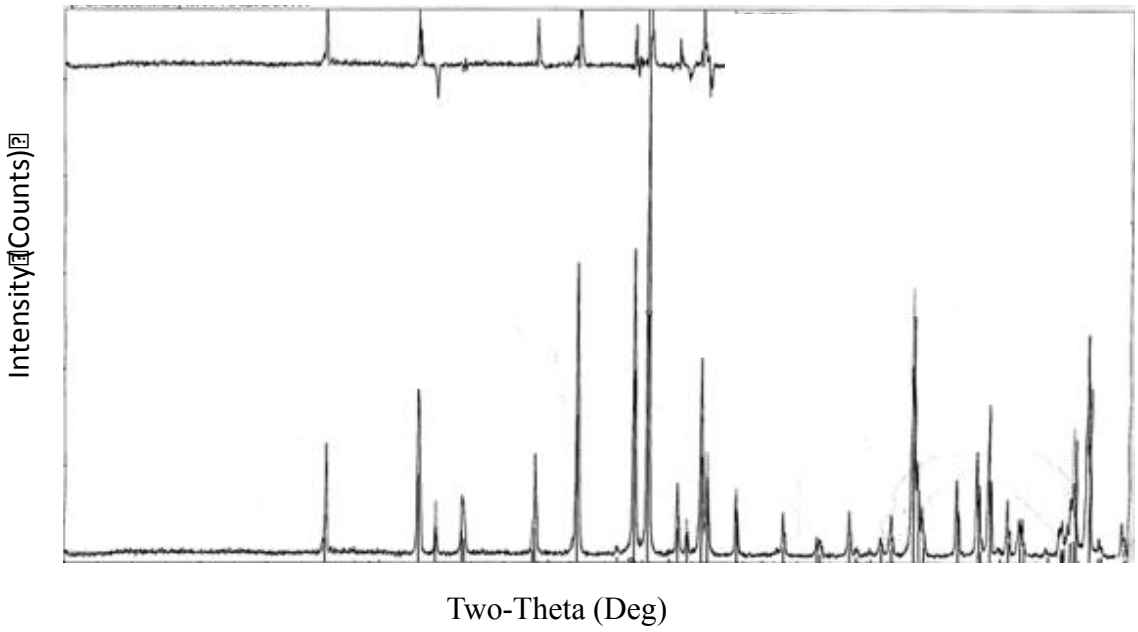

Figure 3- 16: XRD analysis of the initial peridotite sample

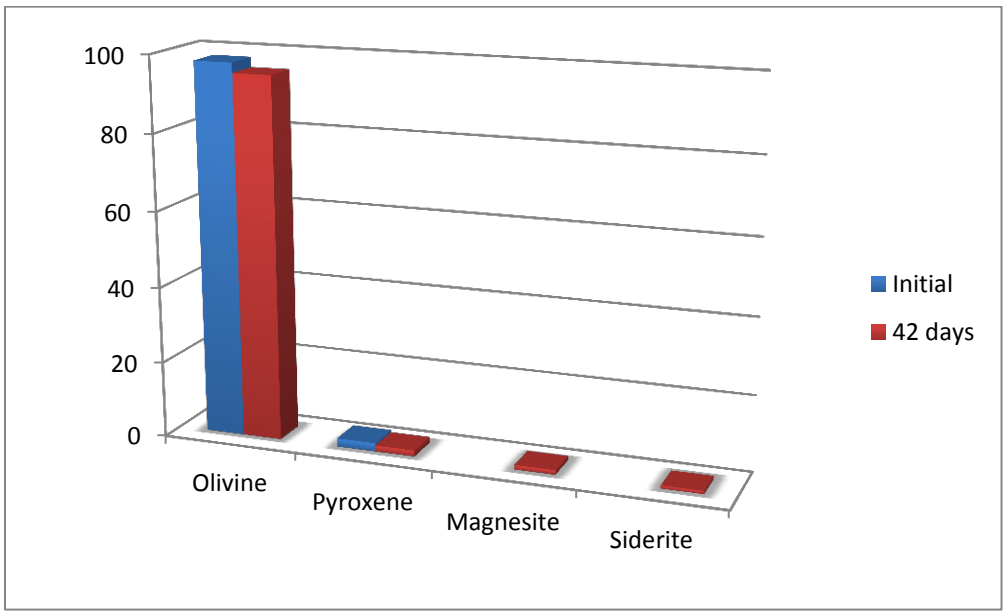

Figure 3- 17: Quantitative comparisons of XRD analyses of peridotite before and after the experiment. Y-Axis indicates composition by wt%

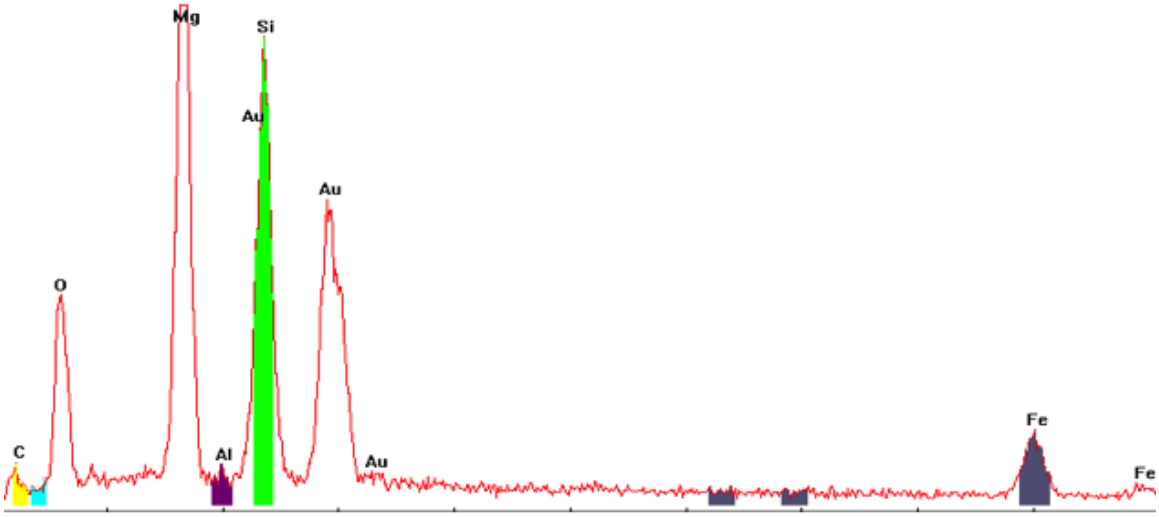

Figure 3- 18: EDS analyses of the reacted rock

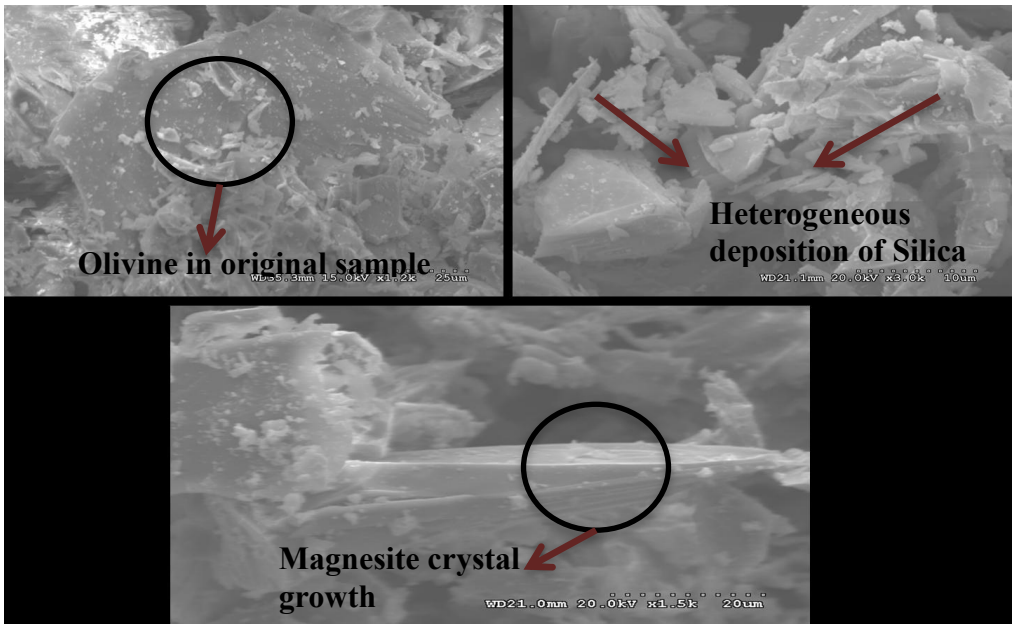

Figure 3- 19: SEM (point) analyses of the initial rock (top left) reveals the presence of olivine in the samples. (Top right) Figure showing trace amounts of silica on the surface of host peridotite. (Bottom) Figure shows the growth of magnesite due to carbonation

The initial increase in the primary ions Mg, Ca, and Si (Figure 3-20) reflects the dissolution of the aluminosilicates, which leads to a decrease in the pH of the solution. This leads to the carbonation reactions (favored at higher pH) dominating the hydration reactions. The carbonation of peridotite leads to the precipitation of magnesite and siderite. The steep increase in the concentration of Si is a result of the dissolution of the silicate minerals. The reacted samples were characterized by the deposition of silica, which precipitated from the brine when the reactor was degassed.

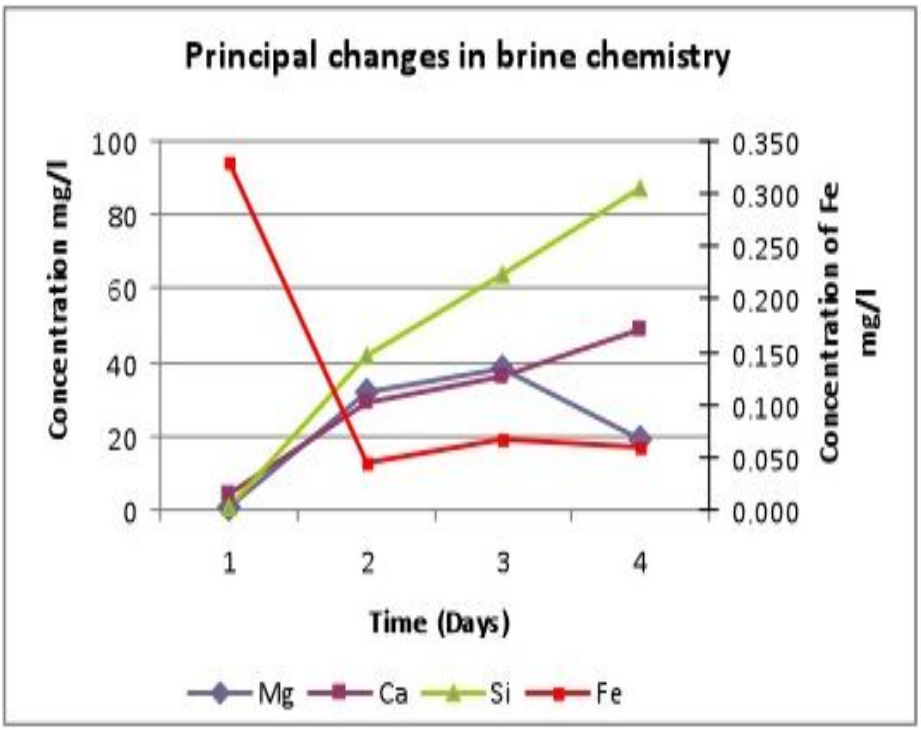

Figure 3- 20: Principal changes in brine chemistry in peridotite experiments

3.4.4. Experiments with Arkose

All the constituent minerals in the arkose (Table 3-1) can participate in the water-rock reactions. Dolomite and feldspars (microcline and andesine) are the most affected. While dissolution dominates the XRD analysis after 62 days, precipitation patterns dominate after 134 days. Dissolution of calcite and feldspar and subsequent precipitation of calcite and analcime are the principal characteristics of this experimental set. There is also evidence of abundant clay minerals (smectite and illite) on the surface of plagioclase feldspars. These results are in good agreement with the brine chemistry analysis and also the SEM/EDS analysis for the rock as explained below.

The quantitative estimates of the mineral abundances before and after the experiments were obtained by XRD analysis. Since very small amounts of precipitates were formed, attempts to quantify the abundances of precipitated solids proved difficult. Hence, the changes in the initial and reacted mineral assemblages were calculated. These changes are constrained by the SEM/EDS analyses. Using these data, a reaction mechanism leading to the precipitation of new minerals can be postulated. In the above analysis all the participating minerals were observed to participate in the reaction. The change in quartz abundance was not expected, as dissolution of quartz usually does not occur at pH 5. Figure 3-21 shows the comparison of the mineral assemblage after 134 days. While dissolution dominates the XRD analysis in the sample after 62 days, precipitation dominates after 134 days. Calcite was found precipitating while dolomite and quartz composition decreased in the final experiment.

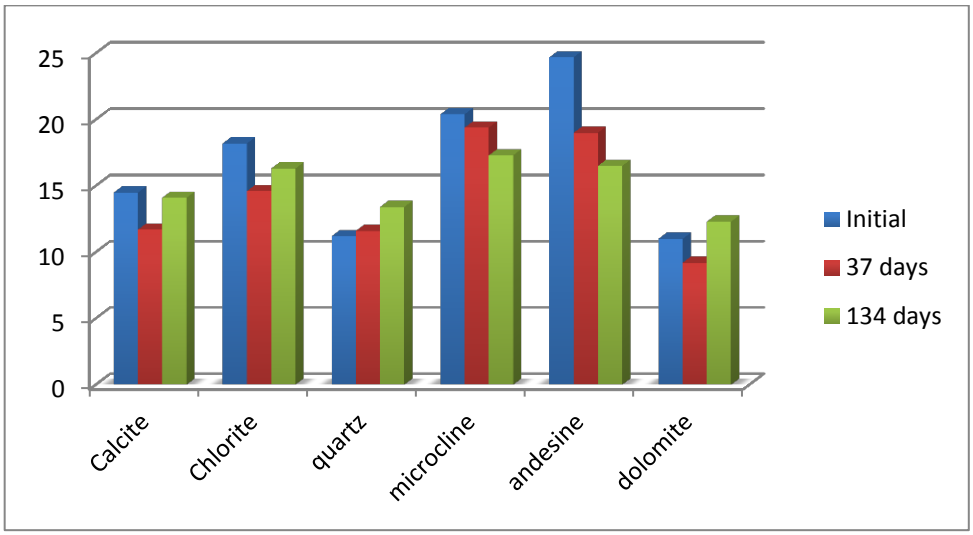

Figure 3- 21: Quantitative estimates of changes in the abundances of the minerals (wt%) before and after the experiment, based on XRD analysis after 37 days and 134 days. Y Axis indicates composition by wt%

Figure 3-21 shows the XRD analysis of the reacted sample after 37 days and 134 days. The calcite in the initial samples serves as a standard to examine precipitation and dissolution at different stages of the experiments. The precipitate from the experiment for 134 days was chosen because it was a reaction in which calcite precipitated as determined by the XRD. Figure 3-22 shows the pronounced dissolution in the sample after 62 days. Although there were numerous angular pits in the initial calcite grains, these pits are more enlarged and distinct in the reacted samples after 62 days. The actual grain shape changed and the number of pores also increased in the sample after 62 days. These changes result from a series of reactions triggered initially by the increased acidity of the brine. Carbon dioxide reacts with water to produce carbonic acid (equation 3.4). The carbonic acid dissociates to bicarbonate ion in the equilibrium aqueous phase (equation 3.5). Equation 3.4 is the dissolution of CO_2 in water, which is highly dependent on temperature pressure and salinity [26][74]. CO_2 solubility increases with increase in

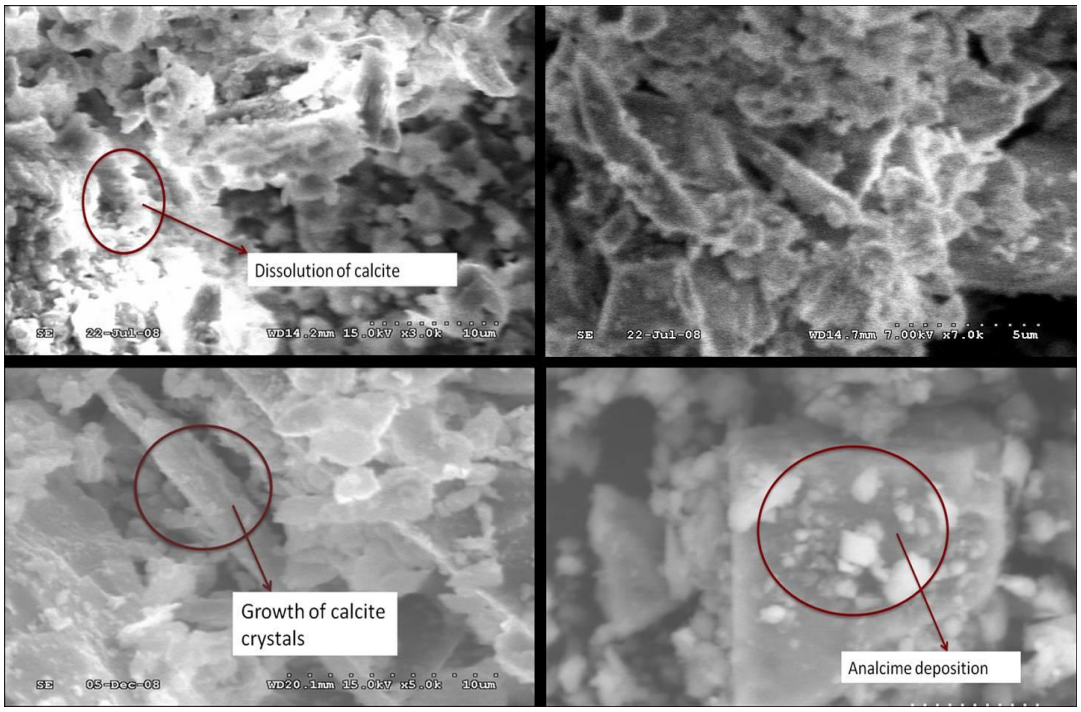

Figure 3- 22: (Top left) SEM image showing calcite dissolution after 62 days. (Top right) SEM image showing the growth of calcite after 134 days indicative of mineral precipitation. Calcite crystals growing (bottom left) in interstitial spaces between plagioclase feldspar. SEM image (bottom right) showing the growth of analcime on the surface.

pressure, and decreases with increase in temperature and salinity. CO_2 then reacts with water to from carbonic acid. This acid dissociates to liberate protons and bicarbonate ion. The sequential reaction in equation 3.6 results in increasing pH value because of carbonate geochemistry. Dissociated hydrogen ion can dissolve calcite (mainly $CaCO_3$) to produce calcium ion and bicarbonate.

Dissolution is represented by a few deep etch pits and some shallow ones. Dissolution occurs relatively quickly, followed by precipitation as seen in Figure 3-22 (experiment carried out for 134 days).

This precipitation of calcite can be postulated from several reactions. The cations liberated (due to the increased acidity) react with the carbonate ion to precipitate secondary carbonates, thus consuming CO_2 in the process (equation 3.1).

$$Ca^{2+} + CO_3^{2-} \leftrightarrow CaCO_3 \quad (3.1)$$

Calcite formation can also be postulated by another mechanism: dissolution of the feldspars and subsequent carbonation of feldspars in the initial mineral matrix. For example, arkosic sandstone as a carbonate reacts with hydrogen ion to precipitate calcium carbonate (equations 3.14, 3.15, 3.2).

$$2H^+ + CaAl_2Si_2O_8 + H_2O \leftrightarrow Ca^{2+} + Al_2Si_2O_5(OH)_4 \quad (3.14)$$

$$Ca^{2+} + HCO_3^- \leftrightarrow CaCO_3 + H^+ \quad (3.15)$$

$$CaAl_2Si_2O_8 + H_2CO_3 + H_2O \leftrightarrow CaCO_3 + Al_2Si_2O_5(OH)_4 \quad (3.2)$$

The above reaction also shows kaolin deposition, which was evident in the reacted samples (from EDS analysis). This indicates that plagioclase feldspar is an active reactant in this geochemical repository. Calcite is seen growing as a tightly packed polymorph of calcium carbonate. These layers of calcite are seen growing as an amorphous mass intergrown with the starting minerals (especially quartz). These calcite crystals (Figure 3-22) are highly irregular in shape and show no consistency in size. One calcite crystal had a width of about 10 mm, but most appear much smaller. Hence, it can be concluded that not all precipitates were collected when the brine was filtered (with a filter paper of 4μm retention capacity). Figure 3-22 shows the deposition of a new phase analcime or kaolinite on the reacted surface.

The formation of analcime from albite (from the plagioclase feldspar) is represented by the reaction:

$$NaAlSi_3O_8 + 3\ H_2O \leftrightarrow NaAlSi_2O_6.H_2O + H_4SiO_4 \quad (3.9)$$

Kaolinite formation from albite (from the plagioclase feldspar) can be formulated as:

$$NaAlSi_3O_8+CO_2+5.5H_2O \leftrightarrow Na^+ + HCO3^- + 2\ H_4SiO_4 + 0.5\ Al_2Si_2O_5(OH)_4 \quad (3.16)$$

Analcime occurs as large connected aggregates on the surfaces of other minerals (quartz). Kaolinite was not identified in the XRD analyses because it shares the same primary peak with one of the minerals in the initial assemblage, chlorite. However, it was identified in the reacted assemblage. It was seen in the interstitial spaces between the primary minerals, especially quartz. Amorphous silica was seen growing on the surfaces of other minerals.

The brine chemistry for this set of experiments is shown in Figure 3-23. Ca concentrations increased by about 90% after 14 days and continued to increase for the next 42 days, after which it decreased with the final concentration being approximately 47% less than the highest concentration measured. K concentration exhibited a similar trend to that of Ca ion with its concentration increasing abruptly and continuing to increase for 62 days, after which it decreased. The increase in the Ca concentration can be attributed to the dissolution of the primary carbonate minerals, calcite and dolomite, liberating Ca to the brine. The K ion concentration increase was due to the dissolution of the microcline, (a potassium feldspar), and the silicate dissolution reactions are relatively the fastest in a low pH geochemical system. Mg concentration increased by approximately 52% for 27 days, and then continued to increase for 62 days, after which it

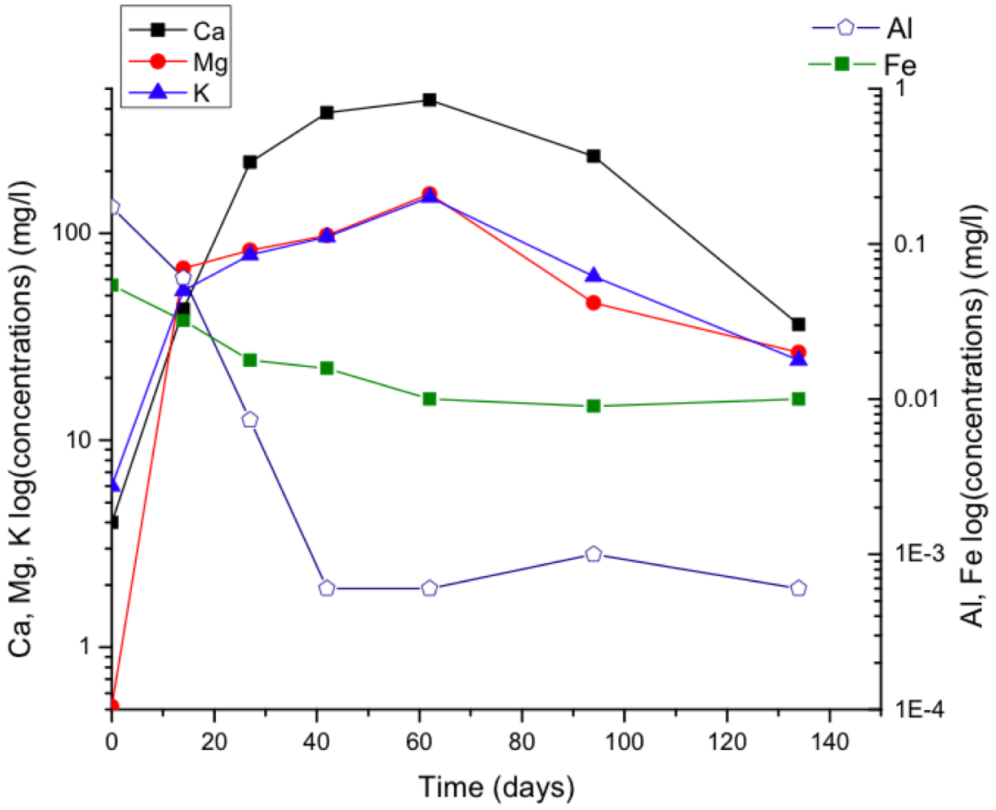

Figure 3- 23: Changes in the concentration of principal ions for experiments with arkose

decreased with a final concentration 42% lower than the initial concentration measured at 27 days. This increase was mainly due to the dissolution of dolomite and chlorite. Fe concentration decreased throughout the experiment and ended up approximately 27% lower than the initial concentration. The decrease in the concentrations of the Ca, Mg, and K ions by 47%, 42%, and 27% in the latter stages of the experiment are an indication of the fact that new minerals with the primary composition of these ions are precipitating in the solid phase. The Si concentration followed a unique trend. It increased by 14% after 27 days, then decreased slightly (2%), and finally increased by about 32% at the termination of the experiment. Since the increase of 2% was within the experimental and analytical uncertainty, the concentration can be considered stable from 27 days to 42

days. The Si concentration increase can be attributed to the dissolution of feldspars, microcline and andesine, which are the most sensitive minerals to decrease in pH [74]. Hence, silicate dissolution dominates the geochemical reactions in the system. This is evident from the fact that there is a silica coating seen on all the samples analyzed in the SEM with a distinctive Si peak in the EDS analyses. This is due to the deposition of Si when the solid sample was dried prior to the analysis. The samples collected at the end of 62 days and 134 days were selected to represent these changes and Ca was chosen as the principal ion undergoing the change. At the end of 62 days and also through the first 62 days, Ca concentrations increased in the brine, indicating the dissolution of primary calcite and dolomite. It is clearly seen in the SEM analysis of the rock sample that is collected at the end of 62 days where calcite dissolution pattern dominates. From 62 days through 134 days, the Ca ion concentration decreases, which implies that Ca bearing minerals were precipitating. This is clear from the SEM analysis of the sample collected at the end of 134 days where layers and crystals of calcite can be seen.

The complex trend in the brine chemistry provides a measure of the geological complexity of the system. The presence of carbonates and feldspars favors the precipitation of carbonates, thus permanently sequestering carbon dioxide. For this experiment, dissolution of carbonates and feldspars and carbonation of plagioclase feldspar and microcline occurred, accompanied by the precipitation of calcite, analcime, and kaolin. These changes were recorded by the changes in brine chemistry.

3.4.5. Experiments with Spent Shale

There has been debate on the viability of the processed shale formations to sustain the sequestration reactions. Hence, experiments were conducted to determine if this rock type has the potential for CO_2 sequestration. The mineral composition of these spent shales varies greatly depending on the source of the shale. Carbonaceous shales, siliciclastic shales, or shales rich in clays were used in this study. All, irrespective of their mineral compositions, were expected to actively participate in these geochemical reactions. The siliciclastic shales and the clay-rich shales are of notable interest because of their geochemical diversity and complex geochemistry. Relative abundance of reactive cations (e.g., Mg, Fe, Na, Ca) available in these environments makes them ideal target sites for CO_2 injection.

The mineralization of CO_2 is limited by slow reaction kinetics for most saline aquifer systems. Oil shale production zones are different from most saline aquifer systems because in-situ production of oil shale heats the rock to high temperatures. At higher temperatures, reaction kinetics are much faster and consequently, the potential to trap CO_2 as carbonate minerals is greater. Similarly, magnesium silicate minerals react readily with elevated concentrations of dissolved CO_2 to form carbonate minerals after being preheated [29]. The extent of CO_2 mineralization should increase at high temperature, because silicate minerals dissolve faster and provide more cations needed to form carbonate minerals for carbon sequestration.

The objective of the current study is to explore the possibility of using the (spent) shale repository as a potential source for geological sequestration of CO_2. Shale samples from the Green River formation were used. The sample was subjected to pyrolysis as a

core ¾" diameter at 350^{0}C for 24 hrs. This experiment had an oil yield of 4.8% by weight and 12.61% weight loss. A similar experimental setup was used by Kaszuba et al. [21]. They used oil shale as a reactant to model an aquitard and examined its reactivity post-CO_2-injection. They found that shale was a reactive component in the aquifer with siderite precipitation occurring on the shale.

Initial XRD analysis of the raw and spent shale samples from Green River formation reveal carbonates, quartz, and feldspars as the principal mineral components.

The XRD analysis on the initial sample revealed the following composition (Figure 3-24):

Quantitative Analysis - Rietveld

- Phase 1: Illite 3.8 wt%
- Phase 2: Dolomite 69.0 wt%
- Phase 3: Quartz 87.9wt%
- Phase 4: Albite 10.8 wt%
- Phase 5: Orthoclase 6.4 wt%
- Phase 6: Analcime 2.1wt%

Interlayered chlorite/smectite (or C/S) are also observed in the clay sample but not in the bulk sample, since it is below the detection limit (~1 wt%).

After 2 weeks, signs of Ca-zeolite precipitates in the reacted sample were evident in the sample (Figure 3-25). The presence of substantial quantities of dolomite, which undergoes dissolution in the acidic environment in the reactor, provides ample Ca for the precipitation of Ca-zeolites when the sample turns slightly alkaline due to dissolution of the feldspars. Zeolite precipitation is not unusual in nature. Zeolites usually precipitate

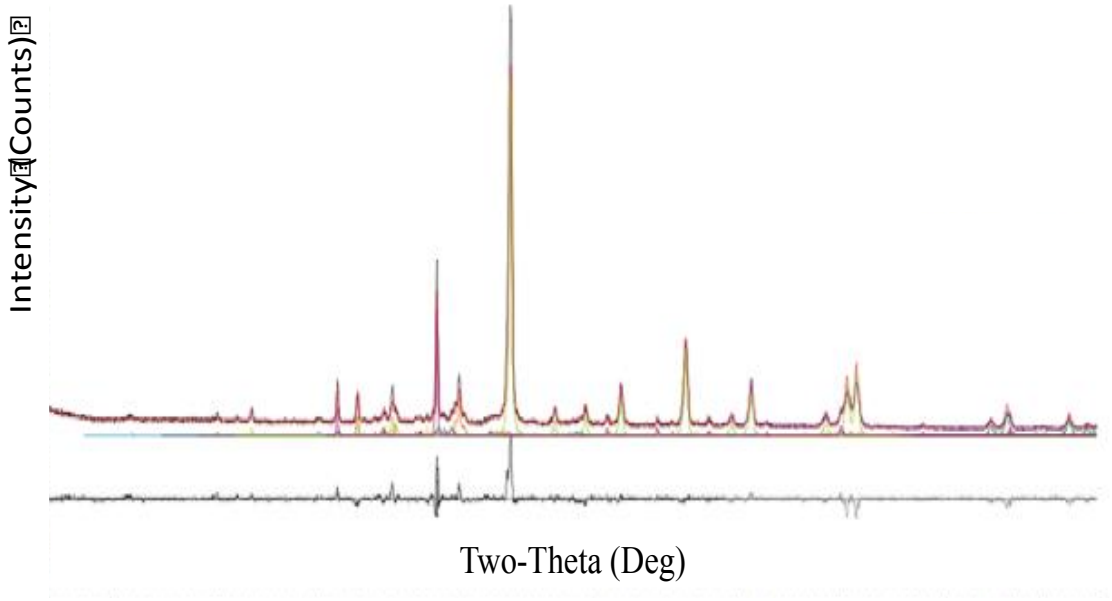

Figure 3- 24: XRD analysis of the initial spent shale sample

when alkaline groundwater reacts with volcanic ash. Zeolites usually do not occur individually. They occur as binding materials for quartz and other carbonates. Since the resolutions at which we are looking in this study are pretty high, we can isolate them as individual minerals. These zeolites have very complex chemical composition, which can only be determined by the EDS analysis (Figure 3-26). These zeolite precipitates (Figure 3-27) were seen as an amorphous mass grown into crystals on weathering orthoclase. The occurrence of these zeolites is common in natural analogs where brackish waters react with complex carbonaceous shales.

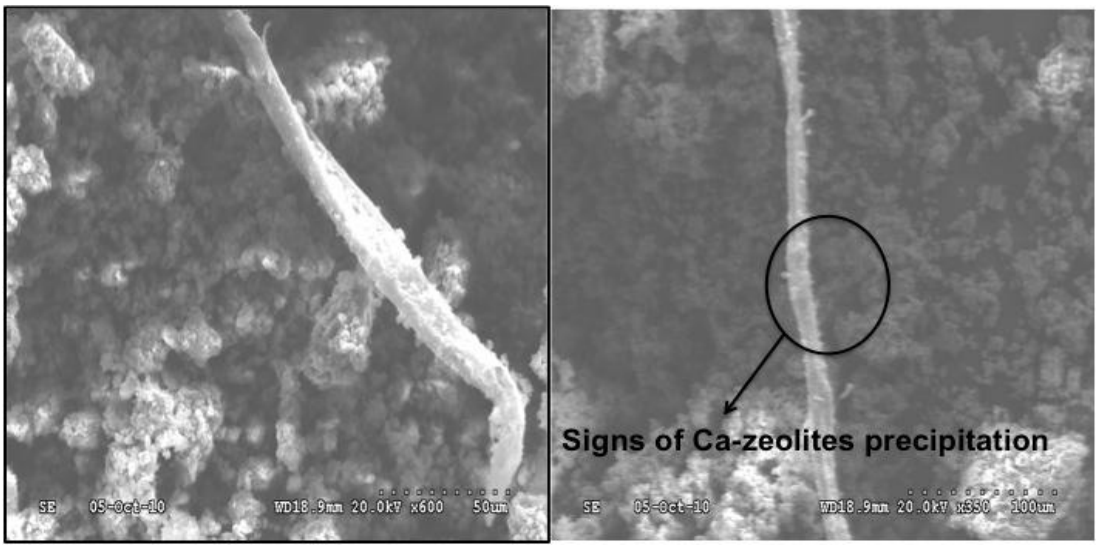

Figure 3- 25: Presence of woody fragments (left) and calcium zeolite (right)

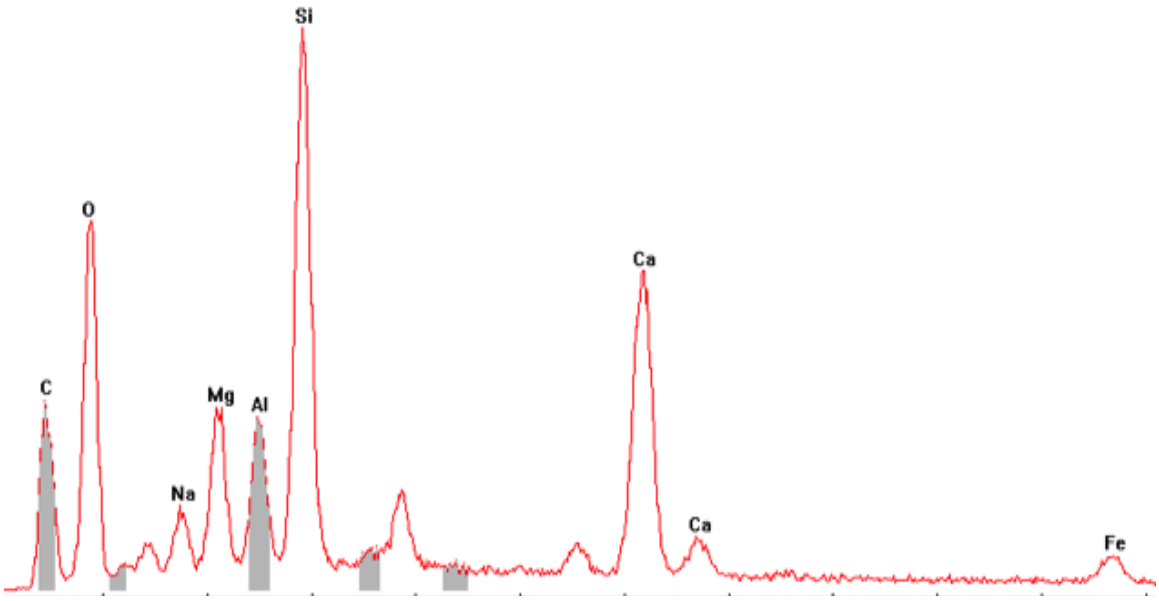

Figure 3- 26: EDS analysis of the Ca-zeolite

Figure 3- 27: Hollow prism of calcium zeolite 3 weeks after the start of the experiment

Alteration of clays is very common in complex geologic environments. The cation exchange capacity of illite is pretty low (10-40 milliequivalents/100g). However, due to the relative abundance of cations, these phase changes are observed (Figure 3-28). Re-precipitation of some carbonate phases such as dolomite and magnesite were observed in the sample after 4 weeks (Figure 3-29). These carbonate phases precipitate only when the brine becomes sufficiently alkaline to favor precipitation (decrease in pH of the brine). The pH decreases after the dissolution of the primary carbonate minerals in the shale (dolomite in this case). In the case of siliciclastic shales, dissolution of feldspars contributes to the decrease in the pH of the system. But the pH decrease in carbonaceous shales is quicker, owing to the relatively fast dissolution rates of carbonates in acidic environments.

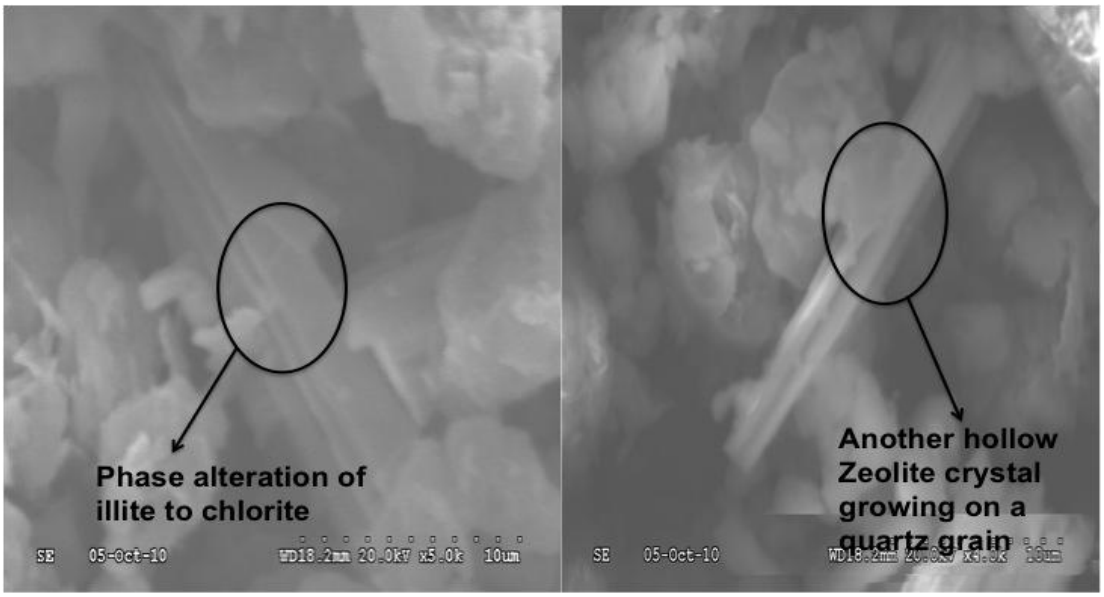

Figure 3- 28: After 3 weeks: Alteration of illite to chlorite (left) and zeolite prism (right)

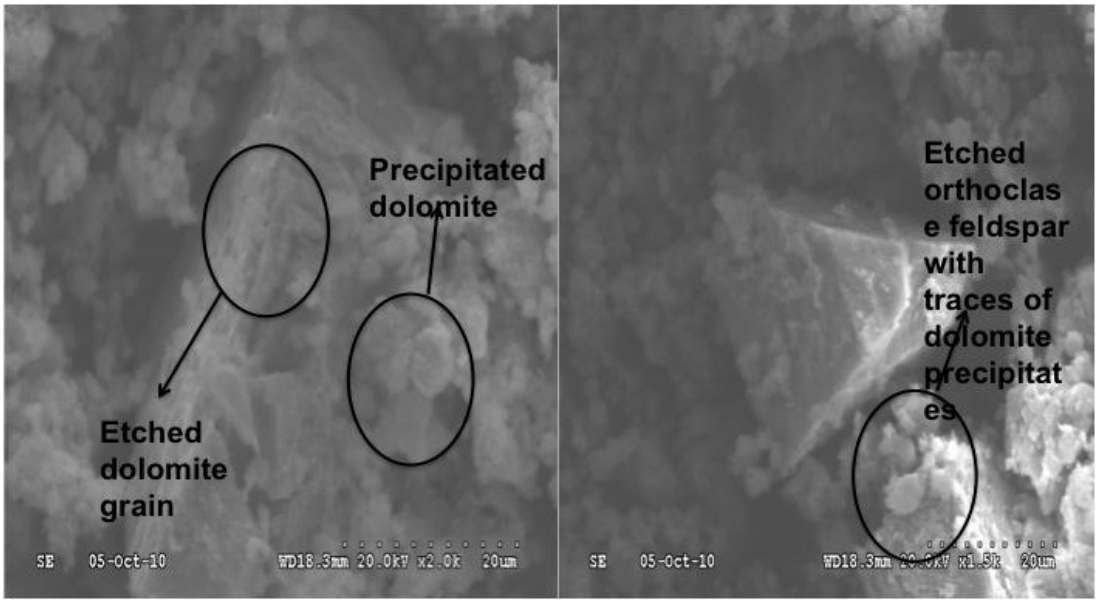

Figure 3- 29: Traces of dolomite precipitates in reacted sample after 4 weeks

Changes in concentrations of the principal ions reflect the changes in rock chemistry (Figures 3-30 and 3-31). The concentration of Ca increases in the initial stages of the experiment where the carbonate phases undergo dissolution and in the latter stages, decreases because of precipitation of dolomite and Ca-zeolite. The Si concentration increases continuously because of the dissolution of alumino-slicate minerals. Mg concentration follows a similar trend to that of Ca. Fe concentration decreases in the latter stages because of the phase alteration of illite to chlorite. K concentration decreases in the latter stages, which suggests the precipitation of some K-bearing phases like K-zeolites. These phases were not identified in the SEM analyses.

This study proves that spent shale has the required geo-chemical complexity to initiate and sustain the sequestration reactions. The precipitation of new phases indicates that the ultimate fate of carbon dioxide in the spent shale formation is mineral precipitation.

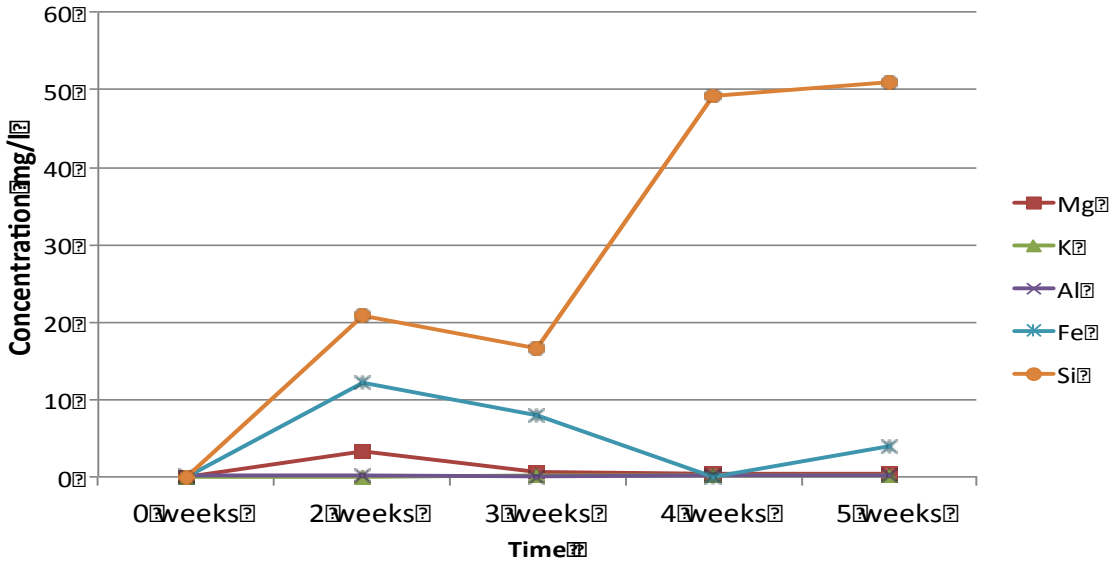

Figure 3- 30: Changes in principal ions in the brine chemistry with time in the spent shale experiments

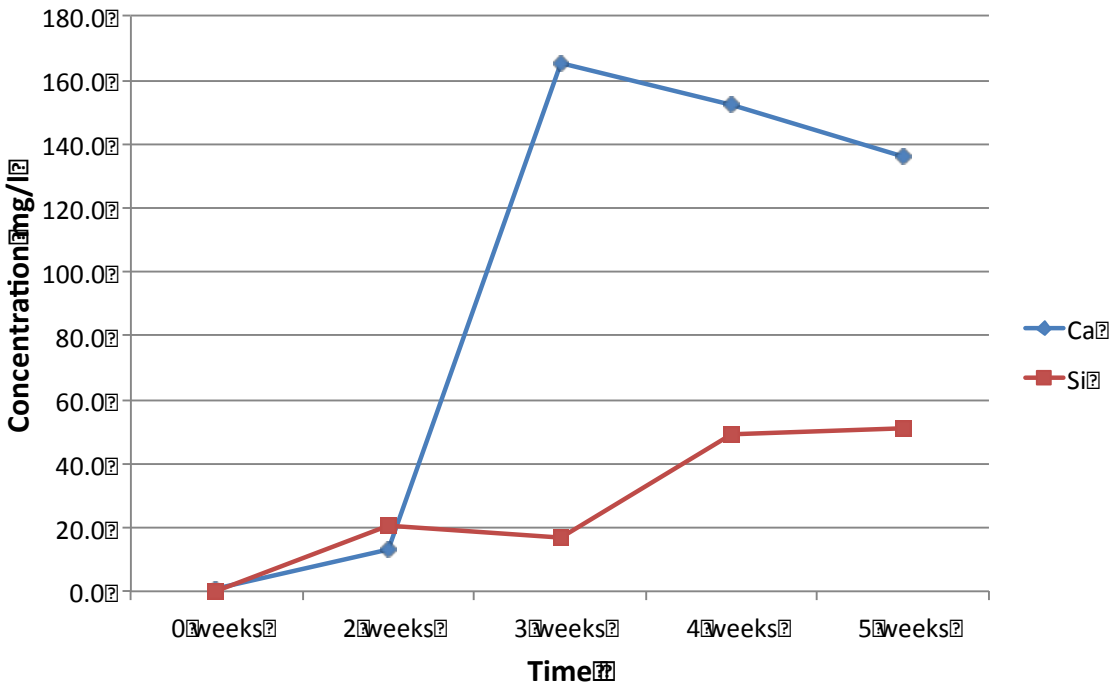

Figure 3- 31: Changes in concentration of Ca ion and Si ion with time in spent shale experiments

3.5. Gas Compositional Effects

To evaluate the effect of gas compositions on fluid-rock interaction reactions, the following gas mixtures were selected.

1) CO_2+ SO_2
2) CO_2+NH_3

No matter to what extent the flue gases are treated prior to injection, and the application of new combustion technologies for precombustion capture of CO_2, the flue gas stream will contain nitrogen, water vapor, carbon dioxide, and small amounts of sulfur dioxide, carbon monoxide, ammonia, and other trace gases. The most expensive part of preinjection sequestration technology is CO_2 capture and purification. These costs can be significantly reduced if the flue gas mixtures can be injected into the geologic

formation. Limited experimental work has been carried out to investigate the changes that occur due to the introduction of these trace gases into the geochemical repository. Hence, this experimental study contributes to understanding the effects of injecting CO_2 and the co-contaminant gases to reduce sequestration costs. These experiments were also performed using the same experimental setup as described in Figure 3-1. A 90% CO_2 and a 10% SO_2 gas mixture provided by AIRGAS was used for these experiments. The solubility of NH_3 in the brine at the temperature and pressure of interest was calculated and was added to the autoclave. All the analytical techniques employed in the experiments with pure CO_2 were used for this set of experiments.

3.5.1. Base Experiments with Brine-Rock and No CO_2

Arkose was selected as the host rock for this study for reasons mentioned before. Experiments were carried out with brine-rock and no CO_2 at 100^0 C to understand the path to equilibrium of the brine+rock mixture. Figure 3-32 shows the XRD results for the arkose after 7 days, 14 days, and 32 days, respectively.

None of the constituent minerals in the experiment exhibit detectable changes greater than the analytical uncertainty for XRD.

The SEM analysis of the reacted samples shows no detectable changes (Figure 3-33). Figure 3-34 shows the changes in brine chemistry for this experiment. The principal ions Ca, Al, Si, and K, exhibit very minor changes in concentrations on the order of 1%. Hence, after 32 days, it can be concluded that the brine+rock system had reached equilibrium.

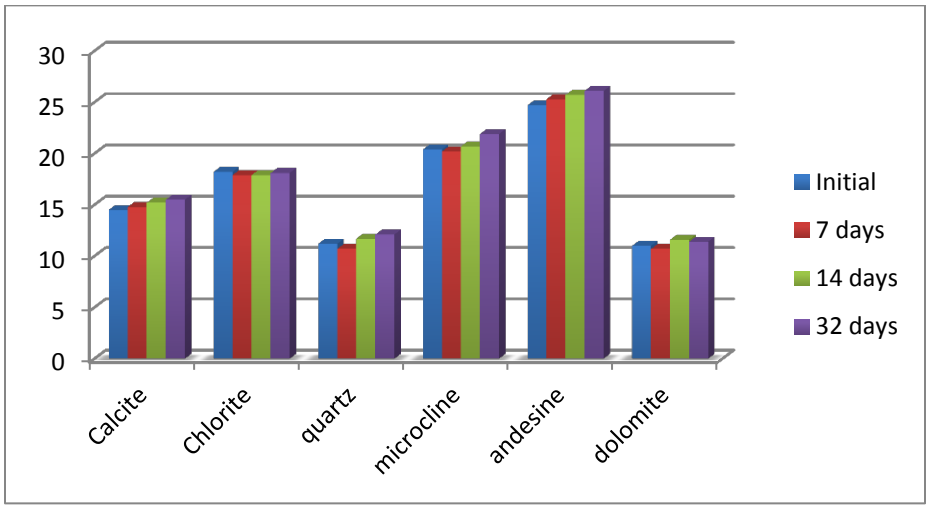

Figure 3- 32: Quantitative comparison of XRD results for arkose-brine interaction in the experiment without CO_2. Y- axis indicates composition by wt%

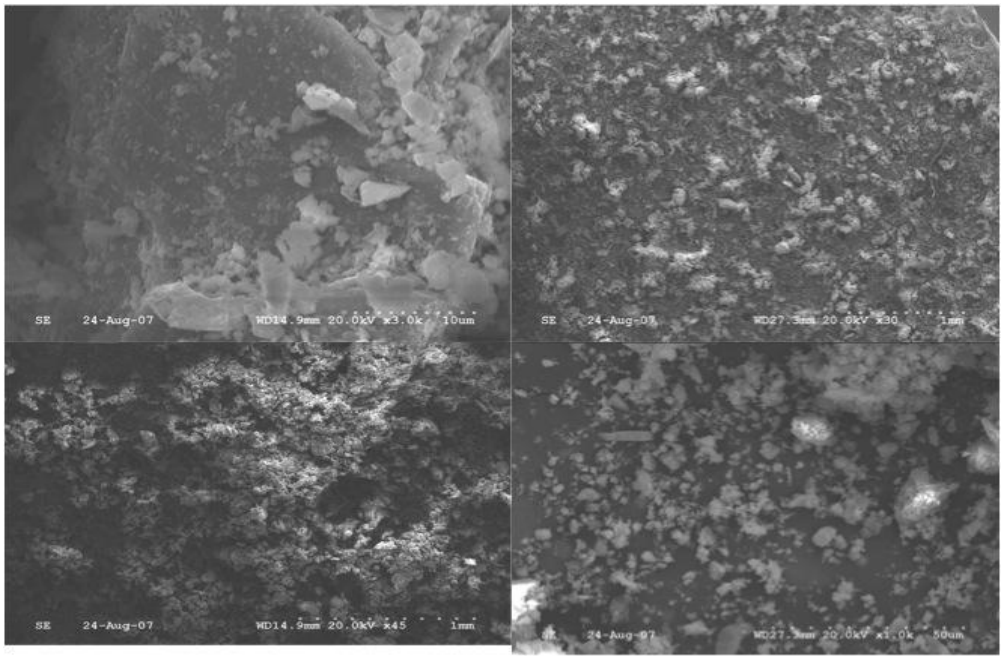

Figure 3- 33: SEM analysis of initial sample (top left), 7 days (top right), 14 days (bottom left) and 32 days (bottom left). No discernable changes were observed

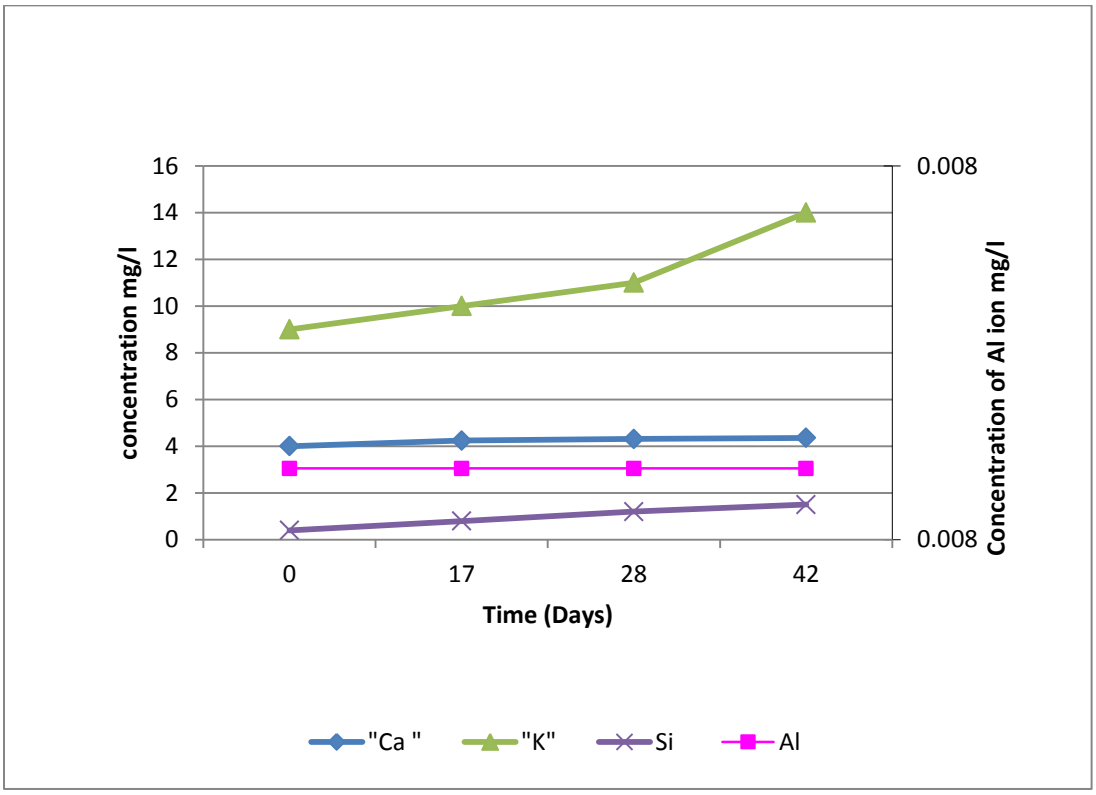

Figure 3- 34: Principal changes in brine chemistry for the arkose-brine experiment without CO_2

3.5.2. Experiments with Brine-Arkose with CO_2

The results for this case have been described in Section 3.3.4. Figure 3-35 shows the correlation of the brine chemistry results with rock chemistry, with Ca as the yardstick. The Ca concentration increases initially due to dissolution reactions. The dissolution patterns are omnipresent in the sample after 62 days. Then, due to the increased pH, and secondary precipitation reactions, calcite reprecipitates and as a result, the concentration of Ca in the brine decreases.

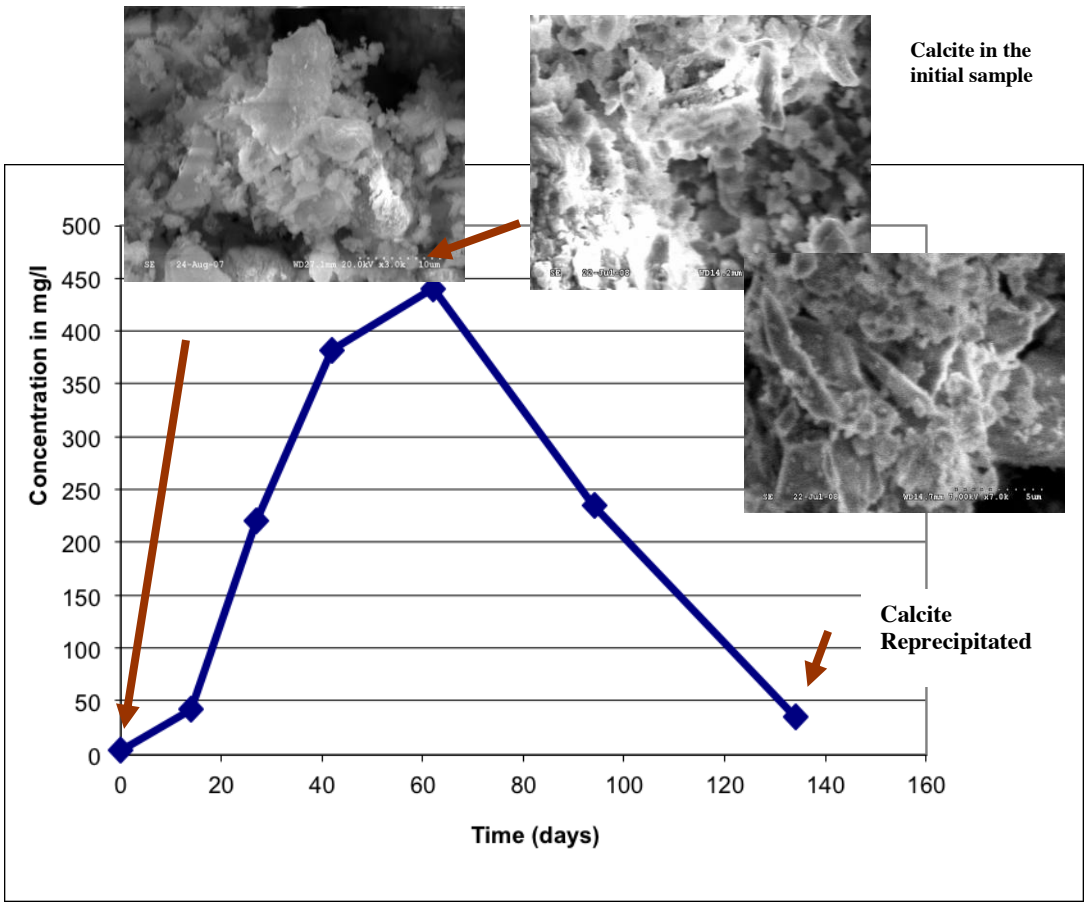

Figure 3- 35: Rock chemistry results correlated with brine chemistry

3.5.3. Experiments with Brine-Arkose with CO_2+SO_2

These experiments were carried out with a gas mixture containing 90% CO_2 and 10% SO_2. The five experiments in the set were terminated at 14, 21, and 37 days with the experiments performed at 14 and 37 days being repeated for consistency. The gas is a calibrated mixture provided by AIRGAS in cylinders with a maximum deliverable pressure of 600 psi. There were three reactors running under identical conditions. The rock was equilibrated with brine for a period of 36 days at the reaction temperature of 100^0C and then the gas was injected into the system. Comparison of the XRD analysis of the reacted sample (37 days) with the initial rock composition is shown in Figure 3-36.

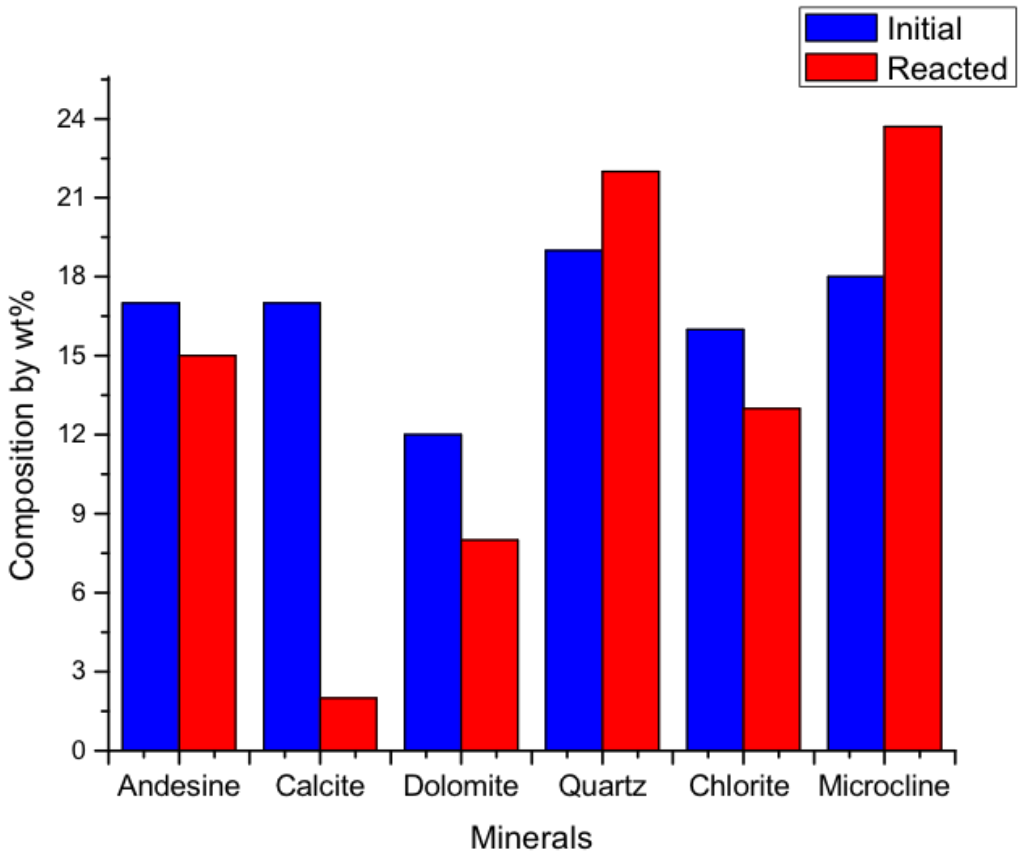

Figure 3- 36: Quantitative estimates of changes in abundances of the minerals (wt %) before and after the experiment after 37 days based on the XRD analyses

The XRD patterns show almost a uniform distribution of the primary minerals in the host rock. Dissolution of carbonate, silicate, and clay minerals was observed in the reacted samples.

The dissolution mechanisms postulated in Section 3.3.4 are also applicable to these results (with much lower pH due to the presence of SO_2). The XRD patterns show the precipitation of hydrated calcium sulfate (gypsum), bassanite, and anhydrite and loss of calcite and dolomite.

The SEM analyses of the host rock after the experiment showed pronounced dissolution of all the primary minerals and also widespread deposition of anhydrite

(Figure 3-37). These crystals were distinct and were seen growing either on the surface of quartz or in the interstitial spaces between the feldspars - anorthite and microcline. The final pH measured of the system was 1.9 after 14 days and 2.48 after 37 days. Dissolution of feldspars appears to buffer the solution to a certain extent.

The formation of anhydrite and gypsum can be formulated as:

$$Ca^{2+} + SO_4^{2-} \leftrightarrow CaSO_4 \quad (3.17)$$

$$CaSO_4 + 2H_2O \leftrightarrow CaSO_4.\ 2H_2O \quad (3.18)$$

Anhydrite occurs as large discrete bladed crystals usually 6-8μm wide. The crystal faces of anhydrite were pitted and rough, which suggests that anhydrite was undersaturated when the sample was analyzed. EDS analysis confirmed the presence of $CaSO_4$, which was absent in the initial mineral assemblage. Due to the increased acidity following the injection of the gas mixture, primary calcite and dolomite underwent dissolution and this led to secondary precipitation of anhydrite. The formation of anhydrite is possibly due to acidity in the brine and the presence of the CO_2 phase, which led to rapid crystal nucleation and growth [28]. Amorphous silica was deposited on the anhydrite crystals (Figure 3-37). The increased acidity led to rapid dissolution of silicate bearing phases, i.e., plagioclase and potassium feldspar, which led to the release of silica into the brine. The silica masses are 2-10μm in cross section. Most of the primary minerals display some evidence of dissolution in addition to the precipitation of anhydrite. Figure 3-38 gives evidence of calcite dissolution, which is also evident from the increase in the calcium ion in the brine, discussed below. The alteration of the silicate phases occurs as the dissolution of primary feldspars, the plagioclase feldspar, and also

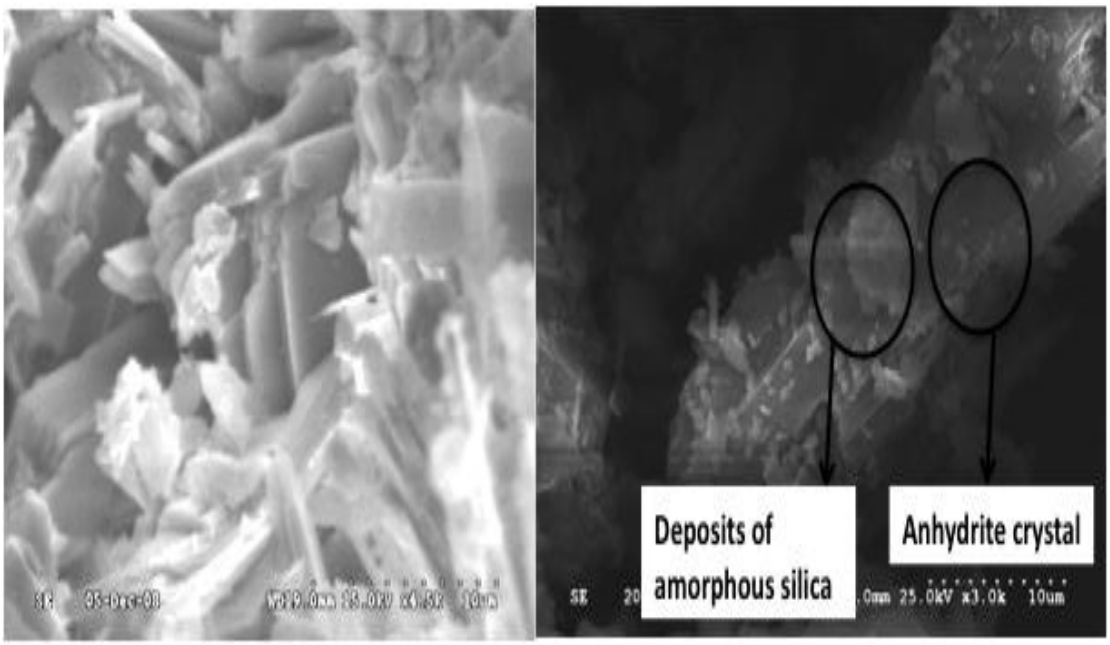

Figure 3- 37: Growth of anhydrite crystals after 37 days, and anhydrite + amorphous silica (right)

the potassium feldspar (microcline). These reactions are not parallel. Their dissolution rate constants at these temperatures are quite similar [57]. Dissolution patterns of calcite and dolomite were ubiquitous in addition to the precipitated anhydrite crystals. All the mineral surfaces were rough and pitted. There were other minerals, which were found as traces in the XRD analysis, but their presence was confirmed in the subsequent EDS analysis. Kaolinite was observed growing in the interstitial spaces of the host rock growing as hollow crystals as reported by Moore et al. [72], in their characterization of natural carbonate reservoirs in Colorado plateau. From the sample collected after 14 days, the dissolution patterns dominated with only traces of new mineral precipitation whereas after 37 days, there was more prominent precipitation and also more pronounced dissolution.

Figure 3- 38: Pronounced dissolution of calcite after 14 days

The presence of SO_2 in the feed gas stream along with CO_2 significantly alters the brine chemistry to a great extent (Figure 3-39). Na concentration increased by about 8% after 14 days and decreased for the remainder of the experiment. Prior to the termination of the experiment, there was a 6% decrease when compared to the initial concentration. The Cl concentration decreased by about 11% before increasing in the latter part of the experiment. Ca increased throughout the experiment with a final increase of almost 80%, interlinked to continued dissolution of calcite, dolomite, and Ca-feldspar in the system. The solubility of anhydrite is very low in these environments [34]). Hence, the contribution of anhydrite to the increase in Ca concentration in brine is relatively low. This increase is almost 1.5 times greater than the increase observed in experiments with CO_2 as pure gas. Mg ion concentration decreased by about 18% in the final sample collected, in contrast to the base case experiment wherein Mg was found to increase. The correlation between brine chemistry and the changes observed in the SEM images is shown in Figure 3-40.

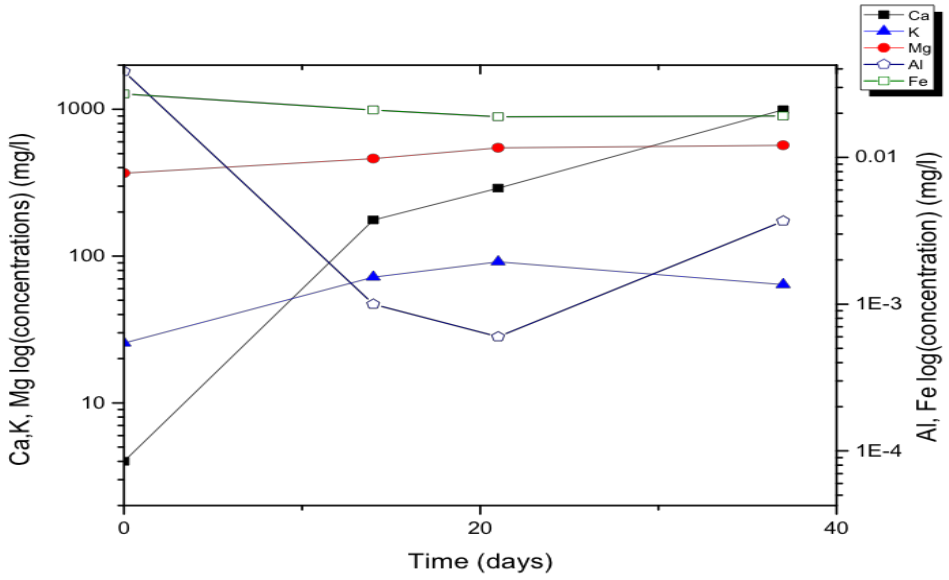

Figure 3- 39: Changes in the brine chemistry of principal ions during the experiment

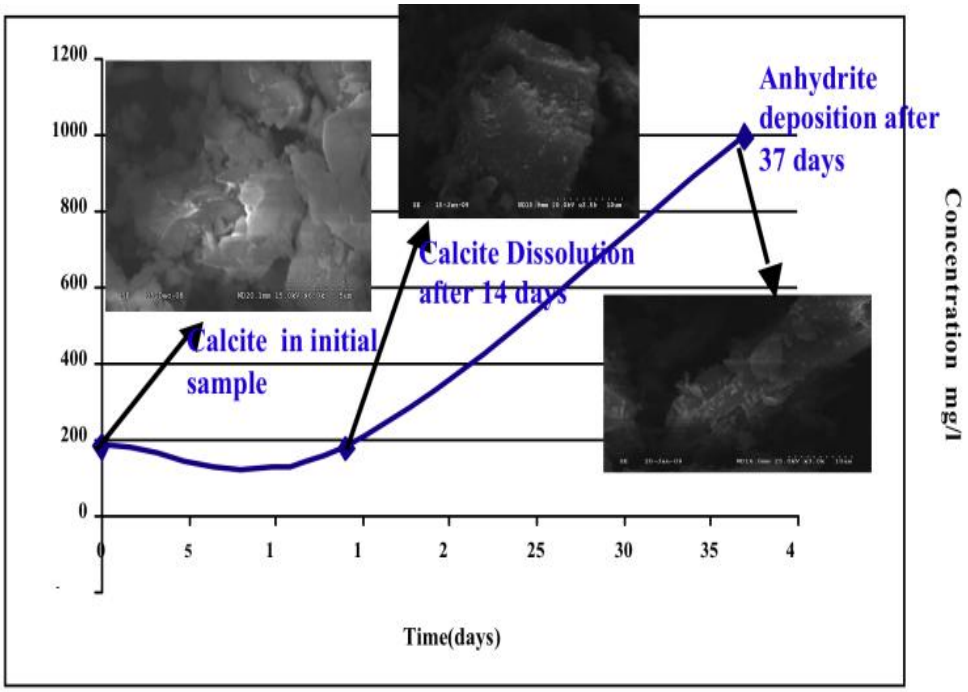

Figure 3- 40: Rock chemistry results correlated with brine chemistry for CO_2+SO_2 experiment. Y-Axis is concentration in mg/l

The decrease in Mg is less than the increase in Ca, which implies that Mg is precipitating in a phase other than dolomite. This might be due to two reasons, the first being the dissolution of calcite or dolomite and the second being the dolomotization of calcite. Dolomotization of calcite can be explained by the following mechanism. Mg liberated by the dissociation of dolomite reacts with anhydrite and calcite to give magnesium sulfate and dolomite:

$$Mg^{2+} + CaSO_4 \leftrightarrow Ca^{2+} + MgSO_4 \quad (3.19)$$

$$Mg^{2+} + 2CaCO_3 \leftrightarrow Ca^{2+} + CaMg(CO_3)_2 \quad (3.20)$$

The slight decrease in magnesium concentration leads us to the conclusion that dolomotization of calcite may be dominant.

The Al concentration decreased by about 1% and then there was a steep fall in its concentration, followed by a slight rise in the latter stages of the experiment. This trend was similar to that seen in the earlier experiment, but decrease was greater in this case. Fe concentrations decreased throughout the experiment. K ion increased abruptly because of the feldspar dissolution reactions, then decreased.

The behavior of silica in these experiments is similar to that of the base case studies with pure CO_2 as the feed gas. Quartz dissolves very slowly in waters with a pH<3. Amorphous silica behaves the same way. Hence, the acid attack on the feldspars and other silicates releases silica into solution causing the solution to become supersaturated with respect to amorphous silica. A decrease in the temperature or neutralization of the solutions can cause the precipitation of amorphous silica. Analcime is usually a high temperature alteration product. However, Neuhoff et al. [75] showed

that analcime precipitation can be achieved at temperatures as low as 50^0C when the solution has high silica concentrations. In the experiment, the brine was supersaturated with silica during the latter stages of the experiment because of the dissolution of feldspar. The heterogeneous deposition of amorphous silica on the retrieved reacted sample also serves as a proof for the same.

Bacon et al. [33] proposed a redox mechanism for the formation of anhydrite. The experiments performed in this study were performed with no oxygen. Nevertheless, they concluded that the addition of SO_2 to a CO_2 charged fluid results in the precipitation of anhydrite. This study confirms the formation of anhydrite, but postulates a different mechanism for its formation.

Taberner et al. [34] showed that anhydrite formation is possible in brines containing significant SO_4 concentrations. The experimental results in this paper show that anhydrite formation is also possible when SO_2 is present in the injection gas. A possible mechanism for this to occur is also presented.

3.5.4. Experiments with Brine-Arkose with CO_2+NH_3

This set of experiments was carried out with a gas mixture containing CO_2 and NH_3. The five experiments in this set were terminated at 14, 28, and 37 days, respectively, with the experiments for 14 and 37 days being repeated for consistency. The rock was equilibrated with brine for a period of 36 days at the reaction temperature of 100^0C and then the gas was injected into the system. Comparison of the XRD analysis of the reacted sample after 37 days with the initial rock composition is shown in Figure 3-41.

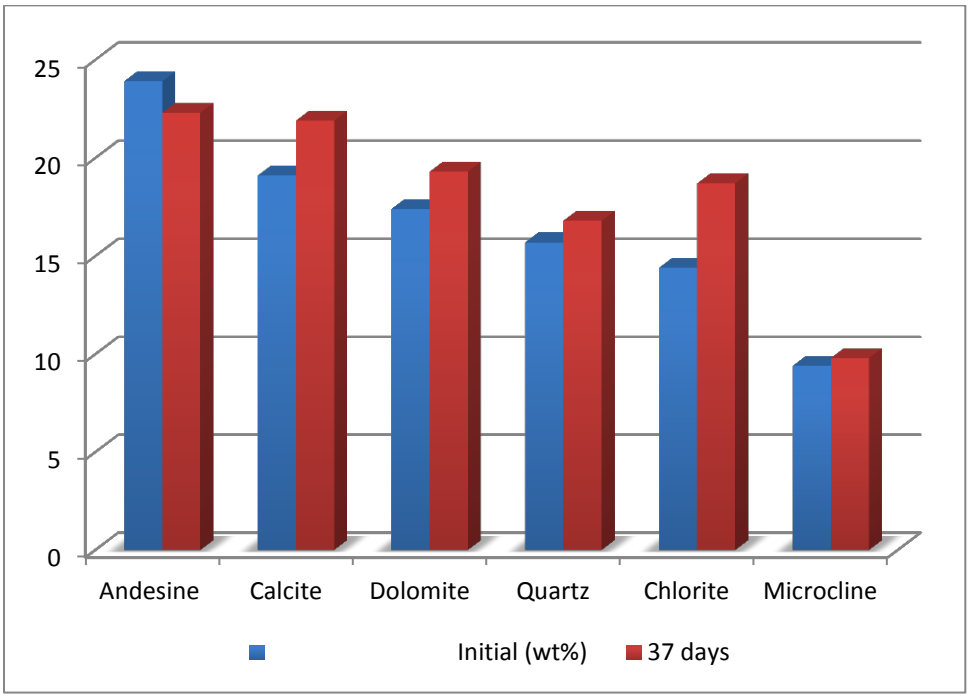

Figure 3- 41: XRD analyses of initial and reacted samples in brines containing CO_2+NH_3. Y-Axis is composition by wt%

In these experiments, a pH increase was observed because of the presence of ammonia. This pH increase facilitates precipitation of secondary carbonates. Calcite increases after 37 days, as does dolomite. These changes are interpreted on some precipitation and dolomatization reactions (equation 3.20) The feldspars undergo dissolution in the initial stages of the experiment before their concentration stabilizes.

The reacted sample is characterized by the growth of ammonium zeolite as acicular crystals (Figure 3-42). As mentioned earlier, zeolites are very commonly produced by reactions involving alkaline groundwater.

Calcite growth is also observed to grow as layers in the reacted samples after 37 days (Figure 3-43). This calcite can be from the carbonation of feldspar, a secondary precipitation reaction in alkaline environment.

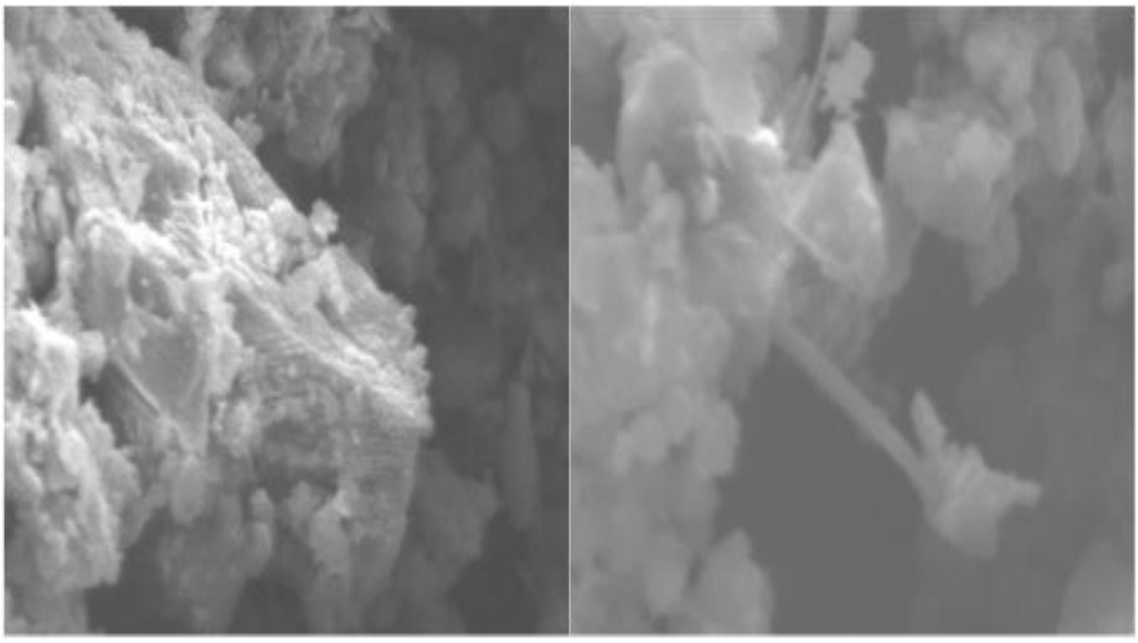

Figure 3- 42: SEM images showing calcite in the initial samples (left) and an ammonium zeolite in the reacted sample (right) after 14 days

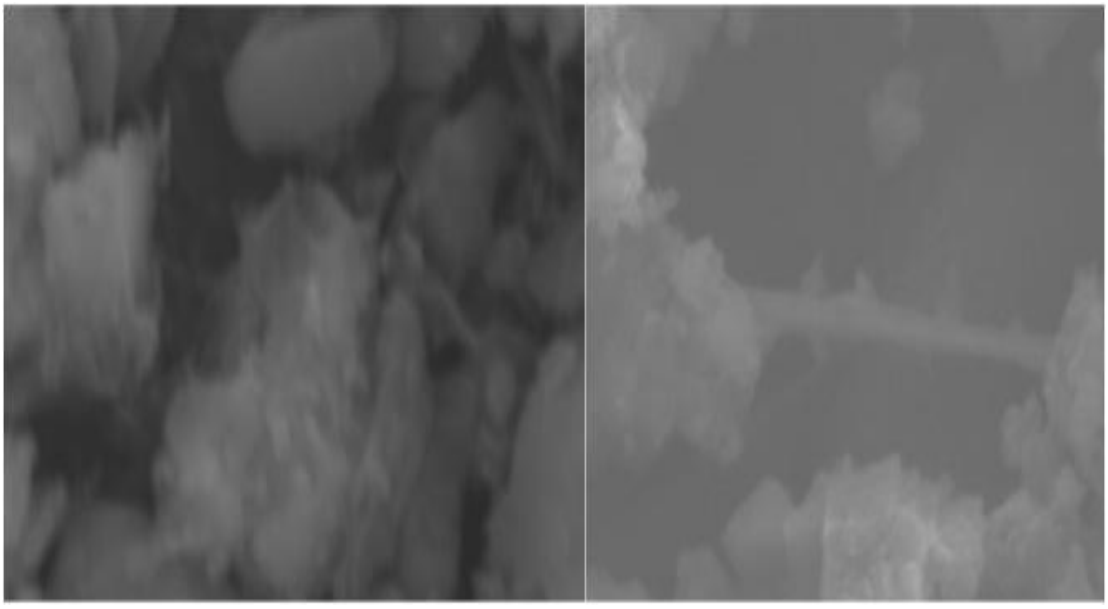

Figure 3- 43: SEM images showing layers of calcite in the reacted samples and Ammonium zeolite in the reacted samples after 37 days

Figure 3-44 shows the trend of Ca, K, Al, and Si in the brine, with plagioclase feldspar and microcline being the primary alumino silicates in the initial mineral matrix and calcite and dolomite being the primary carbonate minerals. The decrease in Al suggests its precipitation in a solid phase, possibly kaolinite. The Ca and Mg concentrations increase initially and then decrease, suggesting the precipitation of calcite and (or) dolomite.

3.6. Effect of Brine to Rock Ratio

To evaluate the effect of the brine to rock ratio (B/R), three different ratios of 10:1, 10.5:1, and 15.5:1 were employed. Zerai et al. [61] carried out geochemical simulations using Geochemists WorkBench to evaluate the effect of brine to rock ratios on the sequestration reactions and found that an increase in the brine to rock ratio

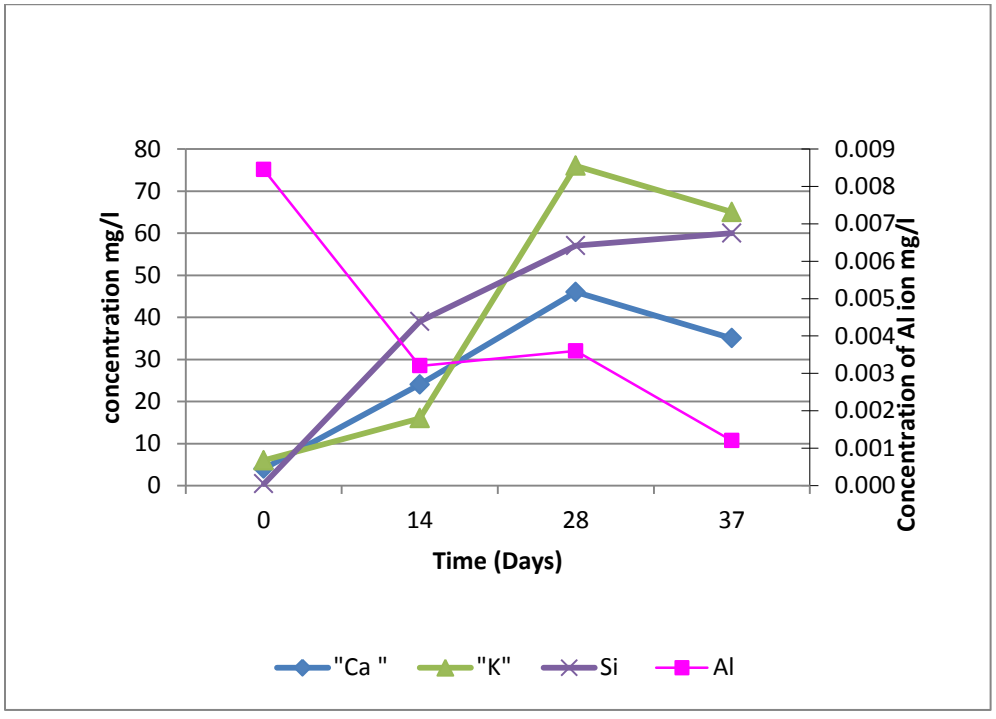

Figure 3- 44: Changes in brine chemistry in CO_2+NH_3 experiments

increases the amount of CO_2 that is sequestered. This experimental study tests this conclusion. Brine to rock ratio governs the amount of rock in contact with the brine, which indirectly effects the total reactive surface area of the geochemical system. Hence, this study will be helpful in evaluating the extent of precipitation or dissolution (mineralization reactions in geological environments) with three brine to rock ratios.

The brine samples were prepared with the same brine shown in Table 3-5. Arkose was selected as the reacting material for reasons already discussed. The brine to rock ratio was varied by varying the amount of water used to prepare the brine and the quantity of rock was maintained at 3g (0.5 g of each constituent in the arkose). Experiments were carried out for 64 days with samples collected at 14, 32, and 47 days. CO_2 was used as a feed gas for all these experiments.

Figure 3-45 compares the three B/R ratios after 64 days. As the B/R ratio increases, the dissolution of feldspars and carbonates increases. This can be attributed to more rock to fluid contact area, which enables enhanced reactive surface areas for these dissolution reactions. Chlorite exhibits a reverse trend, because as the B/R ratio increases, the osmotic barrier for the cation exchange between the clay and the brine increases, which inhibits the clay dissolution rates.

Figures 3-46 and 3-47 show the concentrations of Ca and Mg in the brine through the duration of the experiments. These changes can be correlated with changes in rock chemistry. Calcite and dolomite dissolution rates increase with the increase in B/R ratio. Hence the concentrations of Ca and Mg also increase in the brine with increasing B/R ratio.

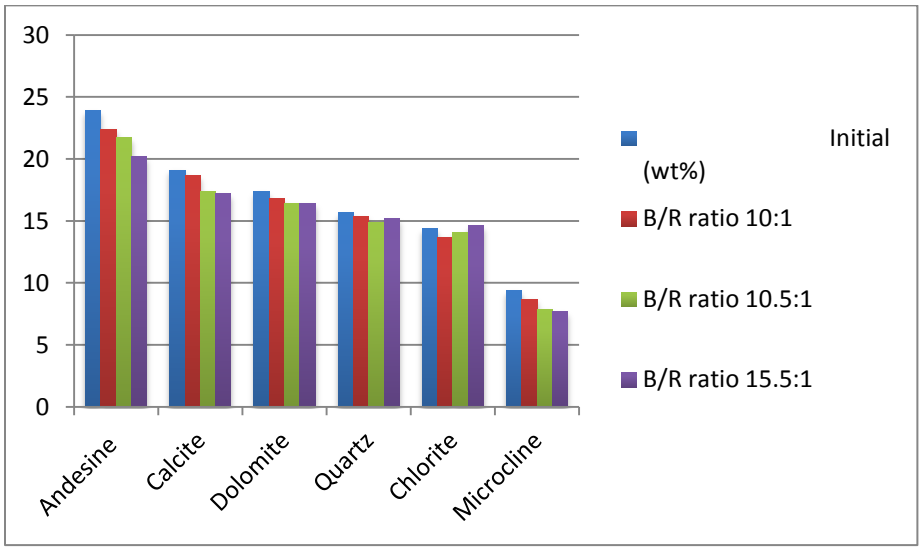

Figure 3- 45: Quantitative XRD analysis of arkose for 3 B/R ratios after 64 days. Y-Axis indicates composition in wt%

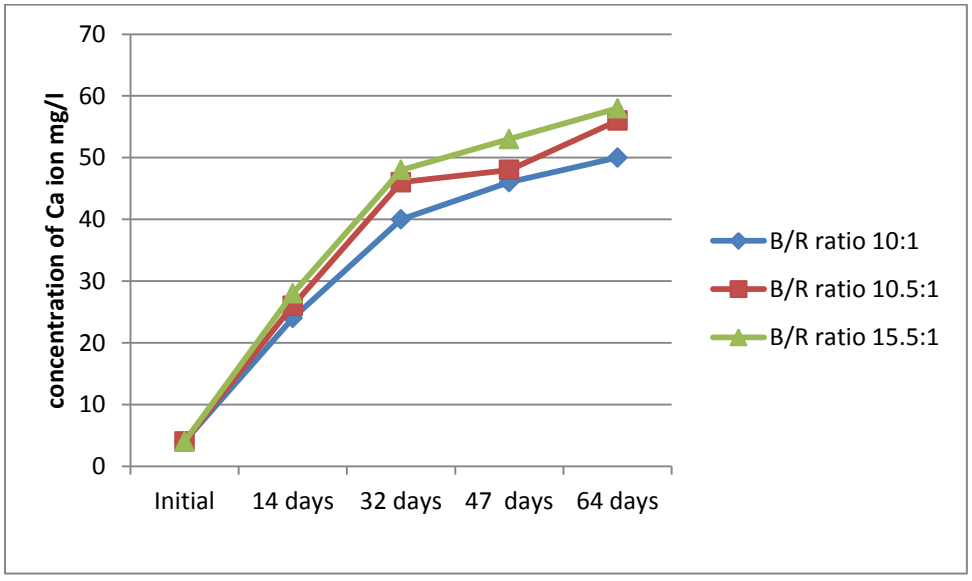

Figure 3- 46: Ca concentration for three B/R ratios

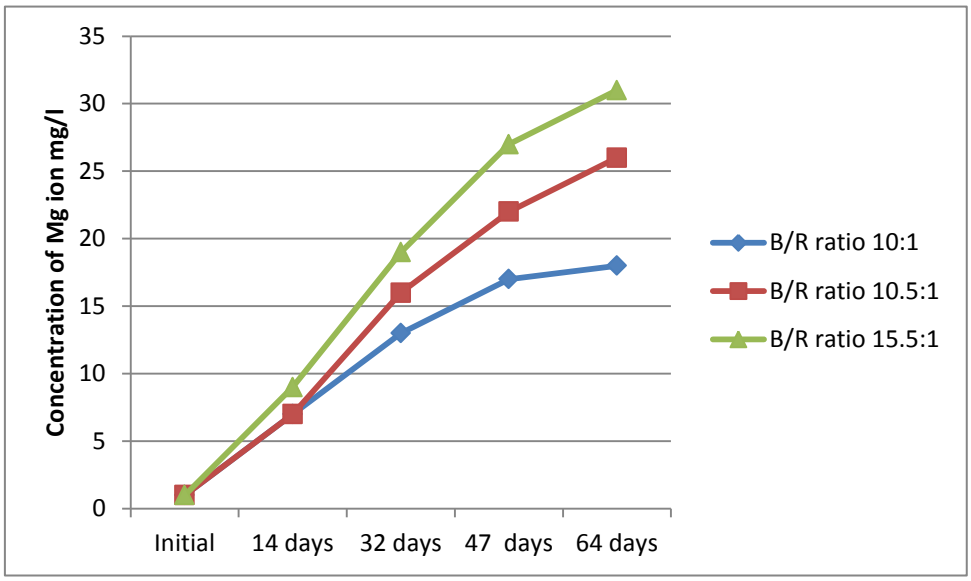

Figure 3- 47: Mg concentration for three B/R ratios.

4. GEOCHEMICAL MODELING

4.1. Introduction

Experimental analyses of the long-term behavior of CO_2 injected into saline aquifers are not possible with relatively short-term laboratory experiments. The fundamental issues of long-term geological carbon sequestration, which are the key to full-scale CO_2 injection into a geological repository, can be understood through simulation and geochemical modeling. Comprehensive numerical models that incorporate the physics of CO_2 behavior in porous media and the geochemical interactions of free and dissolved CO_2 in the brine with the host rock are necessary to effectively monitor the fate of injected CO_2 on geological time scales. These geochemical models must accurately represent the underlying processes over a broad range of spatial and temporal scales. They should also successfully integrate short-term injection with long-term transport and reaction.

Several models are available to calculate batch geochemical reactions among CO_2, brine, and minerals at elevated temperatures and pressures. These models do not consider the dynamics of flow and reactive transport. In this study, a batch reaction geochemical model was used to assess the fate of CO_2 injected into geologic formations. This chapter introduces the batch geochemical code as well as the compositional and geochemical parameters used in modeling and also presents the results of the

geochemical model. Since the analytical measurements were carried out at ambient conditions after degassing the reactors, degassing simulations were also carried out to assess the retrograde reactions that might occur when the reactor was depressurized and also long-term quenching reactions that might have taken place during this process. An attempt has also been made to compare the modeling results with the experimental results described in Chapter 3. The degassing simulations also provided the corrections that need to be taken into account before the comparison between the modeling and experimental results could be made. Batch geochemical modeling was conducted using the commercially available, flexible, and multipurpose geochemical software Geochemists WorkBench (GWB) [76]). Simulations of water-rock-gas interactions under no flow conditions are important for identifying the reactions that are most important for trapping CO_2 in the geological formations and for identifying the parameters that have the greatest influence on the quantity and form of sequestration. Detailed descriptions of the modeling are given below.

4.2. Geochemists WorkBench

Geochemists WorkBench (GWB) is a chemical reactor type, module-based software that simulates chemical reactions under both equilibrium and kinetic conditions. It is a set of software tools for manipulating chemical reactions, calculating stability diagrams and the equilibrium states of natural waters, tracing reaction processes, modeling reactive transport, and plotting the results of these calculations. The GWB package was developed at the Department of Geology of the University of Illinois at Urbana-Champaign under the guidance of Craig Bethke.

GWB can be used for equilibrium, reaction path, and kinetic modeling of CO_2-

brine-mineral reactions. Equilibrium modeling can be used to determine the ultimate fate of CO_2 in the aquifer. Kinetic modeling calculates the pace of the reactions based on the appropriate kinetic parameters, i.e., reactive surface areas and kinetic rate constants. It also calculates the time it takes to approach dynamic equilibrium.

Since the geochemical modeling was an attempt to verify the numerous experimental cases discussed in Chapter 3, the modeling conditions were chosen to match those of the experiments. Reactions involving the gases CO_2 and CO_2+ SO_2 were modeled. The temperature of the system was assumed to be isothermal and set at 100^0C for reaction path and kinetic modeling. This geochemical modeling for the arkose was used to investigate the impact of CO_2 fugacity, mineralogy, temperature, and pressure on mineral dissolution and precipitation and the mode of sequestration in each case. This model is based on the thermodynamic and kinetic data for the minerals involved in the reaction. The main constraints are the mass of water, amount of minerals in the system, fugacities of any gases at their known partial pressure, the amount of any component dissolved in the fluid, and the activities of species such as H^+ as determined by pH measurement. The intermediate products from a complex set of sequestration reactions can be evaluated using reaction path modeling. The progress of the possible reactions is traced by reacting several minerals with CO_2 enriched brine. This is important to investigate the precipitation and dissolution of phases as the reaction progresses because this has implications on the porosity evolution and integrity of the geochemical repository.

The GWB has a rich database that is capable of simulating many common chemical reactions. The database is compiled from work done at the Lawrence Livermore

National Laboratory. In the modeling, the equilibrium constants are tabulated based on eight principal temperatures for any given reaction. For temperatures outside of the principal values, a polynomial fit was used to calculate the equilibrium constants. The GWB provides default datasets where the equilibrium constants are only valid at 1 bar from 0-100°C and steam saturation pressures thereafter. These geochemical models do not have a built-in method to adjust the values of the equilibrium constants as a function of temperature and pressure explicitly.

Kinetic modeling considers the rates of reactions based on appropriate rate constants and reactive surface areas. The algorithm computes the time needed by the system to initiate CO_2 consumption and CO_2 trapping as mineral precipitates. The time required by the system to approach steady state or dynamic equilibrium is also calculated. The GWB has an internal thermodynamic database and requires user input of kinetic rate data. The following rate equation was adopted for the modeling [77]:

$$Rate = \frac{dn_i}{dt} = KA_{\min} \exp\left(\frac{-E_a}{RT}\right)\left(\frac{Q}{K_{eq}} - 1\right) \tag{4.1}$$

where, K is the rate constant (mol/cm^{2}s), A_{min} is the reactive surface area (cm^2), E_a is the activation energy (J/mol), R is the gas constant (J/Kmol), T is the absolute temperature (K), Q is the activity product, and K_{eq} is the equilibrium constant. This rate law assumes that the surface reaction is the rate-controlling step in the reaction mechanism chain. It is derived from the transition rate theory, which states that the mineral dissolves, by a mechanism involving the creation and subsequent decay of an activated complex. The rate at which the activated complex decays controls how quickly the mineral dissolves.

The dissolution rates of the minerals do not depend on the saturation state. The precipitation rate, on the other hand, varies strongly with saturation exceeding the dissolution rate only when the mineral is supersaturated. It is also of interest that when A_{min} is zero, the reaction rate vanishes. Therefore, a mineral that does not exist cannot begin to precipitate unless crystal nuclei form.

Rate constants for the kinetic reactions were compiled from the published literature based on laboratory experiments. However, these rates can be several orders of magnitude greater than the rates of weathering measured in the field [77]. To check the validity of the model and the kinetic parameters used in this model, the modeling results were compared to the experimental results. It was observed that the rate constants for the same mineral varied greatly depending on the literature source. Hence, kinetic parameters from different sources were used and the results were compared with each other and also with the experimental results. The measured rate constant reflects the dominant reaction mechanism in the experiment from which the constant was derived.

The GWB requires that the CO_2 pressure be input directly as fugacity. The fugacity (f_{CO2}) was calculated using the CO_2 solubility model developed by Duan and Sun [78]. The investigation of how geochemical reactions vary as a function of f_{CO2} can approximate the sequence of reactions and the reaction progress as fugacity decreases with increasing distance from the injection site and also over time. Reactive surface areas were calculated from geometric approximations and also adopted from laboratory measurements from the literature. For the geometric approximations, the grains were assumed to have a spherical geometry and an average diameter of 100 μm was assumed. For a spherical grain, the specific surface area is given by $A*\nu/V*MW$, where A is the

sphere area, ν is the molar volume, V is the sphere volume, and MW is the molecular weight. For sheet silicate minerals like clinochlore (chlorite), an average grain diameter of 2μm was assumed, which corresponds to sheet silicate size. Interactions with the minerals are generally expected to occur only at selected sites on the surface and the difference between total surface area and the reactive surface area can be between 1 to 3 orders of magnitude [79]. Hence, a scaling factor of 0.001 was used for all minerals to account for this difference.

Activity coefficients were calculated using the B-dot equation (an extension of the Debye Huckle equation) [80]. The virial method (Pitzer equations) is better suited to high ionic strength solutions such as the brine under consideration [80], but the GWB's application of the Pitzer equations does not take into account the distribution of species in solution, only recognizes free ions as if each salt has fully dissociated in solution, nor does it take into consideration SiO_2 and Al^{3+} species. Those assumptions preclude use with minerals like albite, quartz, and feldspar [61].

4.3. Mineral Stability Diagrams

This class of diagrams shows the relationship between mineral stabilities and predominance of aqueous species. Species activity, gas fugacity, activity or fugacity ratio, pH, Eh, or pE may serve as an axis variable. These stability diagrams were plotted using Act2, a program that calculates and plots activity-activity diagrams. These diagrams are useful for determining the stability regimes in the experiments and for evaluating the reaction mechanisms for minerals of interest. Hellevang et al. [25] calculated the relative stability of dawsonite with respect to other Na and Al bearing

phases using logarithmic activity-fugacity diagrams such as those illustrated in Figure 4-1. The relationships presented in this figure illustrate phase relations in the system Na_2O-Al_2O_3-SiO_2-CO_2-H_2O balanced on aluminum and with SiO_2 activity fixed by quartz saturation. The solid lines in this activity diagram represent fluid compositions in equilibrium with the two minerals adjoining these lines and are computed from the law of mass action for reactions among these minerals. For example, equilibrium between albite and dawsonite can be represented by:

$$NaAlSi_3O8 + H_2O + CO_2(aq) \leftrightarrow NaAl(OH)_2CO_3 + 3SiO_2(aq) \quad (4.2)$$

(Albite) (Dawsonite) (quartz)

Increasing CO_2 fugacity in this system leads to calcite dissolution and consumption of some aqueous CO_2. At 40°C, dawsonite is stable in this fluid at all CO_2 fugacities greater than 0.1. At higher temperatures, higher CO_2 fugacities are required to stabilize dawsonite. At 80°C, dawsonite stability requires a CO_2 fugacity of approximately 6.3, corresponding to a partial pressure of 10 bars. The stability of dawsonite at elevated CO_2 pressures has led numerous scientists to propose dawsonite as a potential long-term CO_2 storage host, particularly in divalent-cation-poor sedimentary basins. In contrast, as injected CO_2 gas disperses, dissolves in, or leaks from the sequestrating formation following its injection, CO_2 fugacity would decrease, potentially destabilizing dawsonite relative to aluminosilicate phases. Thus, the formation regimes of many minerals can be determined and the dissolution rates of the ephemeral phases can be calculated by laboratory measurements to be used as input for different geochemical calculations.

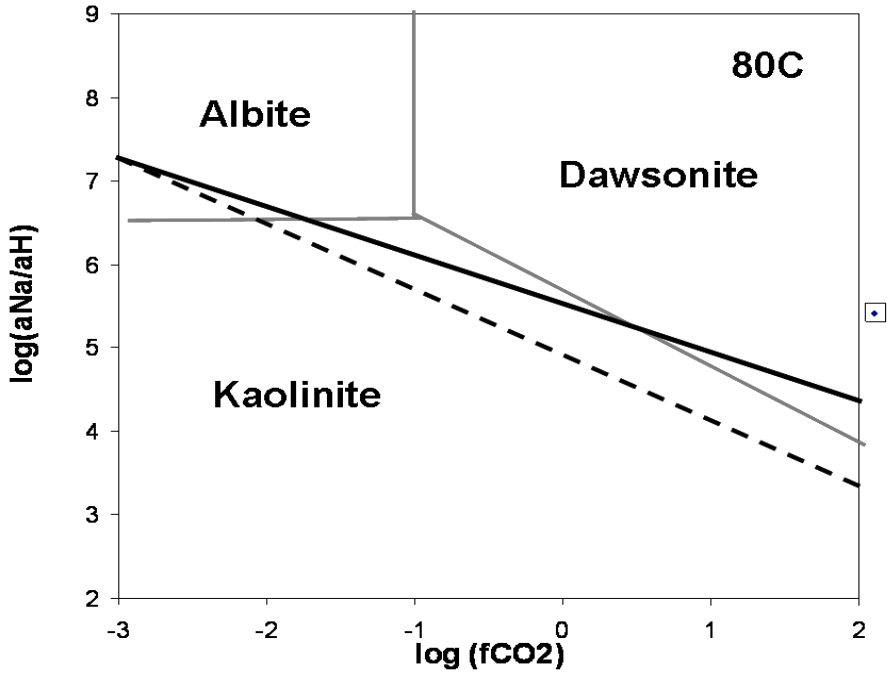

Figure 4- 1: Log fugacity-activity diagram depicting mineral stability fields in the system Na_2O Al_2O_3 SiO_2 CO_2 H_2O at 80°C. The dashed line was computed by equilibrating the formation water with varying CO_2 fugacities, whereas the solid line was computed by equilibrating the formation water with varying CO_2 fugacities, whereas the solid line was computed by equilibrating seawater with calcite [25].

The solubility of aluminum hydroxide is complicated by the fact that dissolved aluminum can exist in several forms in solution. In the absence of other ligands, the most important are Al^{3+} and its hydrolyzed forms $Al(OH)_2+$, $Al(OH)^{2+}$, $Al(OH)_3$, and $Al(OH)_4^-$. The activity of Al^{3+} in equilibrium with gibbsite is given by

$$Al(OH)_3 + 3H^+ \quad \leftrightarrow \quad Al^{3+} + 3\ H_2O \qquad (4.3)$$

The presence of feldspars (aluminosilicates) in the arkose makes it necessary to identify the stable forms of aluminum in the solution in our experiments. The carbonation reactions of feldspars usually yield kaolinite, which is a stable mineral at high activities of H_4SiO_4 like those in our experiments ($10^{-4.4}$ at 100^0C). It is impossible to determine

whether or not a particular solution is in equilibrium with kaolinite or any other mineral without knowing the dissolved aluminum concentration. Hence, the activity diagram shown in Figure 4-2 provides an understanding of the stability regimes and the stable minerals like kaolinite at a known pH and Al^{3+} ion activity.

Another important system is that of K_2O Al_2O_3 -SiO_2 -CO_2 -H_2O. Mineral pairs in this system include:

$$2KAl_3Si_3O_{10}(OH)_2 + 2\ H^+ + 3H_2O \leftrightarrow 3\ Al_2Si_2O_5(OH)_4 + 2\ K^+ \quad (4.4)$$

(muscovite) (kaolinite)

$$2KAlSi_3O_8 + 2\ H^+ + 9\ H_2O \leftrightarrow Al_2Si_2O_5(OH)_4 + 2\ K_+ + 4H_4SiO_4 \quad (4.5)$$

(K-feldspar) (kaolinite)

$$3\ KAlSi_3O_8 + 2\ H^+ + 12\ H_2O \leftrightarrow KAl_3Si_3O_{10}(OH)_2 + 2\ K^+ + 6\ H_4SiO_4 \quad (4.6)$$

(K-feldspar) (muscovite)

$$KAl_3Si_3O_{10}(OH)_2 + 2\ H^+ + 12\ H_2O \leftrightarrow 3\ Al(OH)_3 + K^+ + 3\ H_4SiO_4 \quad (4.7)$$

(K-feldspar) (gibbsite)

The mineral stability diagram for these reactions is displayed in Figure 4-3 with the slopes of the lines determined by the stoichiometry of the equations.

The area kaolinite represents the solution composition in which kaolinite is the most stable of the minerals considered in constructing the diagram. It is conceivable that a mineral exists that would be more stable than kaolinite over part of the kaolinite field. The minerals used in these diagrams are the most common forms in natural environments. In our experiments with arkose, the log SiO_2 is around -3.37 and log aK+/H+ is around 0.9. This indicates that the most stable form of alumino silicate mineral in the system is kaolinite.

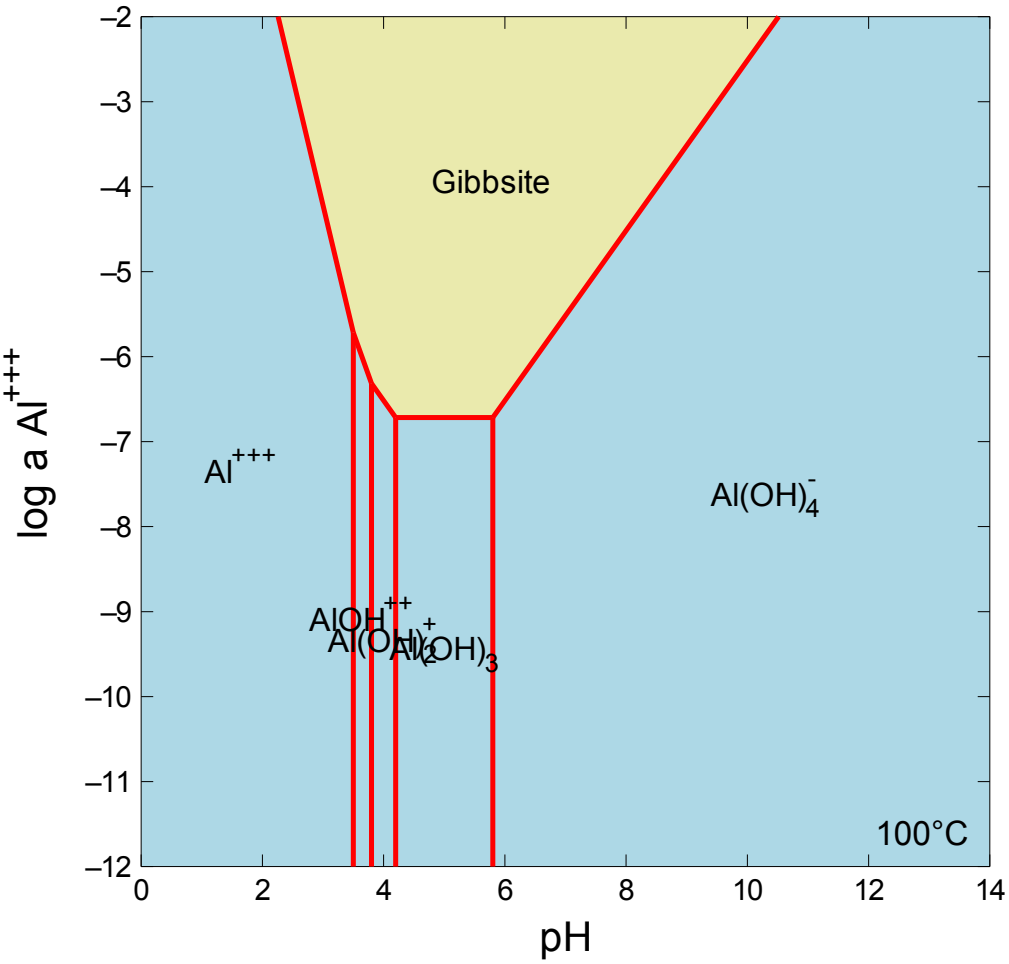

Figure 4- 2: Stability regimes of different aluminum hydroxide species as a function of pH and activity of aluminum ion

Analogous stability diagrams can be constructed for system Na_2O-Al_2O_3-SiO_2-H_2O (Figure 4-4). Na bearing feldspars like albite are an important source of cations required for secondary precipitation reactions of carbonates. Hence, identification of stable phases in these environments is very important. Again for our experiments, the most important stable aluminosilicate phase is kaolinite, which is the primary product in the dissolution of orthoclase feldspar. This was evident in the experimental results where kaolinite was identified by XRD and SEM analysis.

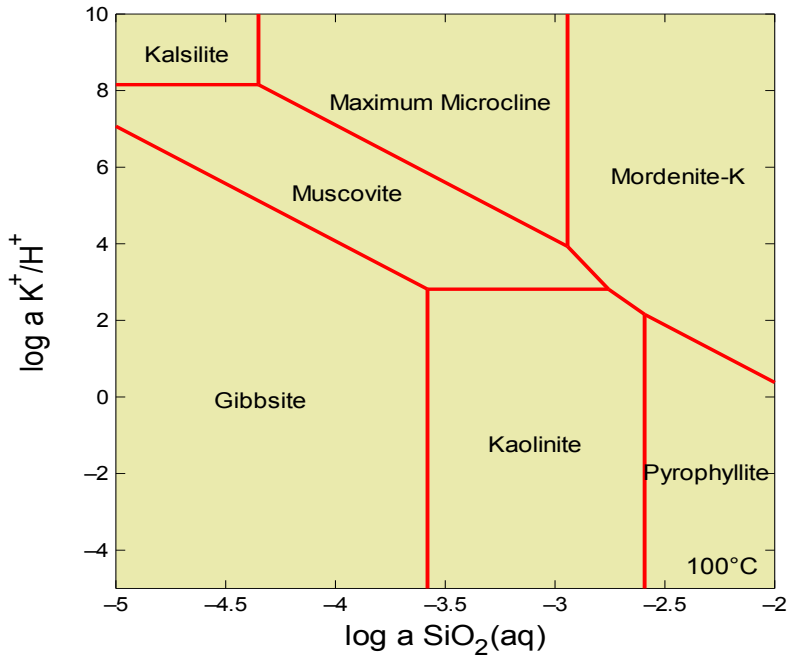

Figure 4- 3: Stability relationships among some minerals in the system K_2O-Al_2O_3 -SiO_2 -CO_2 -H_2O at 100^0C

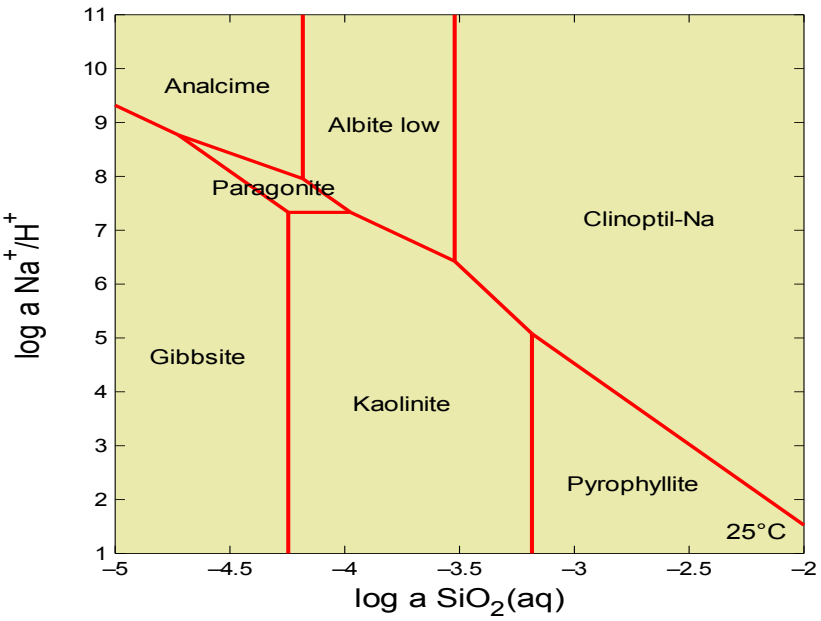

Figure 4- 4: Stability relationships among some minerals in the system Na_2O Al_2O_3 - SiO_2 -H_2O at 100^0C

4.4. Modeling Sequestration Experiments

A batch geochemical model was developed using the Geochemists WorkBench version 7.0. The initial brine chemistry used for these models was identical to the brine used for experiments and described in Table 3-5. The temperature was assumed to be isothermal at 100^0C for all the simulations.

The operational parameter set and kinetic parameters used for the model are described in Tables 4-1 and 4-2, respectively.

The following cases are discussed in the sections to follow:

1. Arkose as the host rock and CO_2 as the feed gas
2. Arkose as the host rock and CO_2 + SO_2 as the feed gas
3. Limestone as the host rock and CO_2 as the feed gas
4. Sandstone as the host rock and CO_2 as the feed gas
5. Peridotite as the host rock and CO_2 as the feed gas

Table 4- 1: Parameter set used for the simulations

Parameters used	Description
Temperature	100^0C
CO_2	Dissolved in brine
Activity coefficient	B Dot equation
Reactive surface area	Table 4.2
Kinetic rate constants	Table 4.2
Fugacity coefficient	Based on Duan and Sun algorithm
CO_2 fugacity	113.08 bar

Table 4- 2: Kinetic parameters used for the model

Mineral	Surface Area	kinetic rate constant
	cm^2/g	mol/cm^2sec
Calcite	711	3.16E-14
Dolomite	635	4.17E-12
Quartz	686	1.86E-16
Chlorite	1130	2.34E-16
Microcline	720	1.60E-13
Andesine	637	1.80E-13

4.4.1. Degassing Simulations

One of the main objectives of this study is to compare the experimental results with the results generated from the geochemical model in the GWB. Brine chemistry is used as the comparison parameter for the modeling and the experimental results. The rock chemistry was also quantified in the experiments using XRD but the intermediate (new) minerals precipitated could not be quantified since very small amounts of precipitates were detected and their composition was well within the range of uncertainty for XRD measurements.

All the experimental analyses were carried out at ambient conditions after the reactor was depressurized. This degassing process would lead to numerous retrograde reactions and also long-term quenching reactions. Several changes take place during this process like the change in the pH of the system because of a decrease in f_{CO2}, change in the saturation states of the minerals in the brine, spontaneous dissolution, and precipitation of new phases. In order to compare the experimental results with the modeling, a correction factor need to be introduced for this degassing process. Using the sliding fugacity module in GWB, we can predict the changes that this change in f_{CO2}

would introduce into the system. Following is the procedure that is followed for these simulations:

- The final output at the end of a particular time interval from the geochemical model is the input as the initial basis for the degassing simulation.
- The change in the concentrations of the principal ions is calculated and catalogued.
- The behavior of principal ions with their respective minerals in the event of a sudden decrease in f_{CO2} is used as a basis for calculating the in-situ elemental composition of the ion in the fluid.
- This concentration is then marked on the same plot as the modeling results.
- The concentrations of all the principal ions at the time intervals of degassing are calculated similarly and plotted.

All the results discussed henceforth and the comparisons are corrected for degassing.

4.4.2. Experiments with Arkose as Host Rock and CO_2 as Feed Gas

These experiments are described in Section 3.3.4. Arkose was reacted with CO_2 and brine (Table 3-5) at 100^0C and 2000 psi. The initial dissolution and re-precipitation of calcite and the precipitation of analcime were the key features in this experiment. The brine chemistry in these experiments is described in Figure 3-23. The degassing simulations were conducted with the procedure mentioned in Section 4.4.1 and the experimental results were corrected for degassing.

The model captured the initial increase in the Ca, (Figure 4-5) which occurs due to the dissolution of the carbonate minerals calcite and dolomite and also the dissolution of plagioclase feldspar. The Ca concentration was found to decrease in the latter stages of

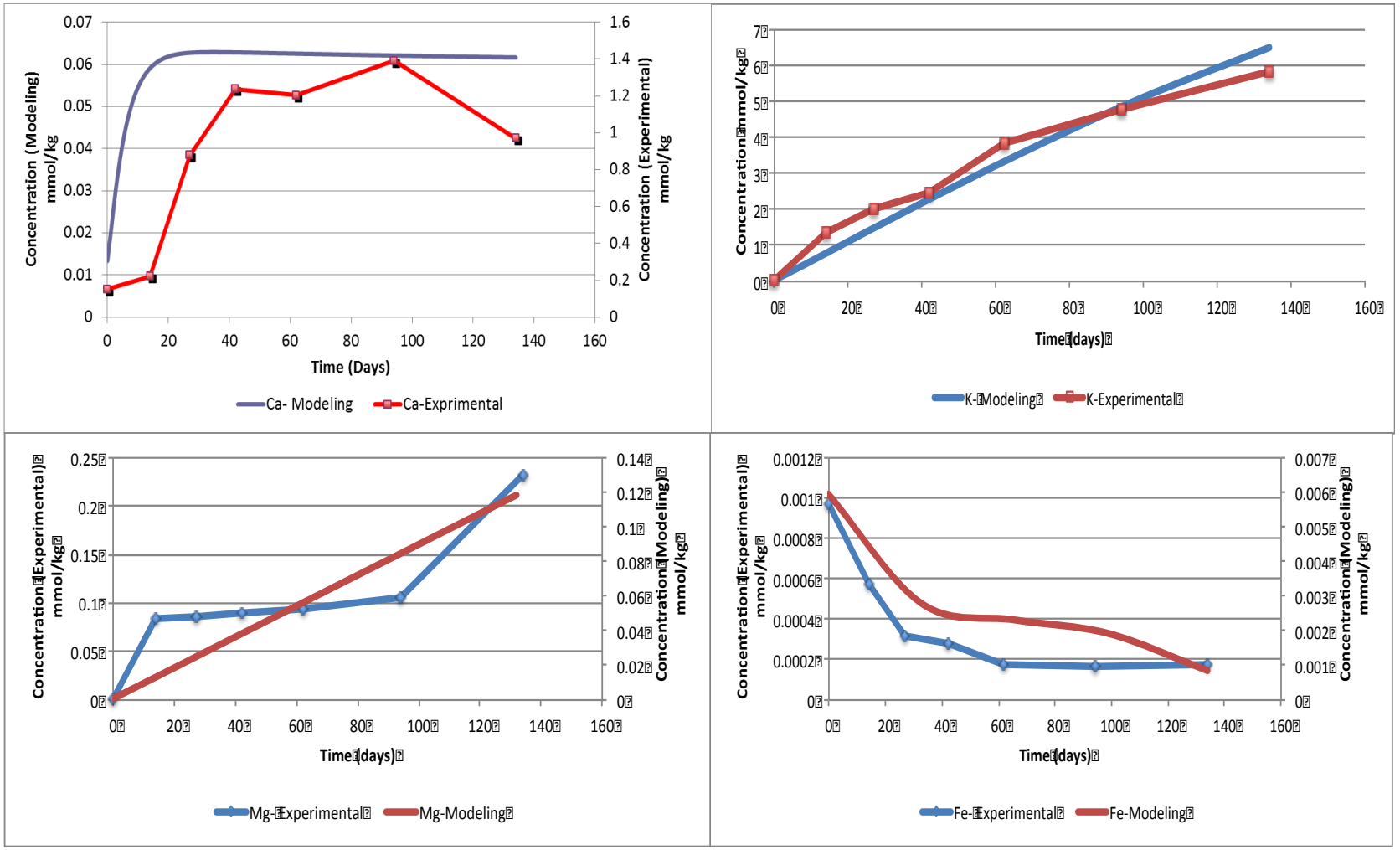

Figure 4- 5: Comparison of experimental and modeling results for arkose + CO_2

the reaction as seen in the experiments, which led to the precipitation of calcite. In spite of the degassing correction, there is a difference of about an order of magnitude for this case. There can be two possible reasons for this deviation. The first one is multiple sources for Ca in the starting mineral (calcite, dolomite, and Ca-feldspar) with different kinetic parameters and the latter is the behavior of these Ca bearing minerals during degassing. The rates of dissolution of Ca bearing minerals in the experiment were higher in the experiments than in the model. Hence, the Ca activity in the brine in experiments is higher than in the modeling. If these were adjusted to match the experimental results, the concentrations of other ions in the brine would deviate much further.

The Mg concentrations increased due to dissolution of dolomite in the initial stages of the experiment. It should also be noted that the dissolution rate of dolomite is significantly higher (two orders of magnitude greater than calcite), which could have led to the immediate dissolution of dolomite. The deviation observed in this case was about 22%. K concentrations increased throughout the experiment in response to the dissolution microcline. There was excellent agreement between the experimental and modeling concentrations for K with a deviation of about 2%. Fe concentration decreases rapidly in the latter stages because of the precipitation of iron carbonates like (ankerite or siderite). The difference between the experimental and modeling results were about 30%. Figure 4-6 shows the precipitation of analcime in the solid phase in the model.

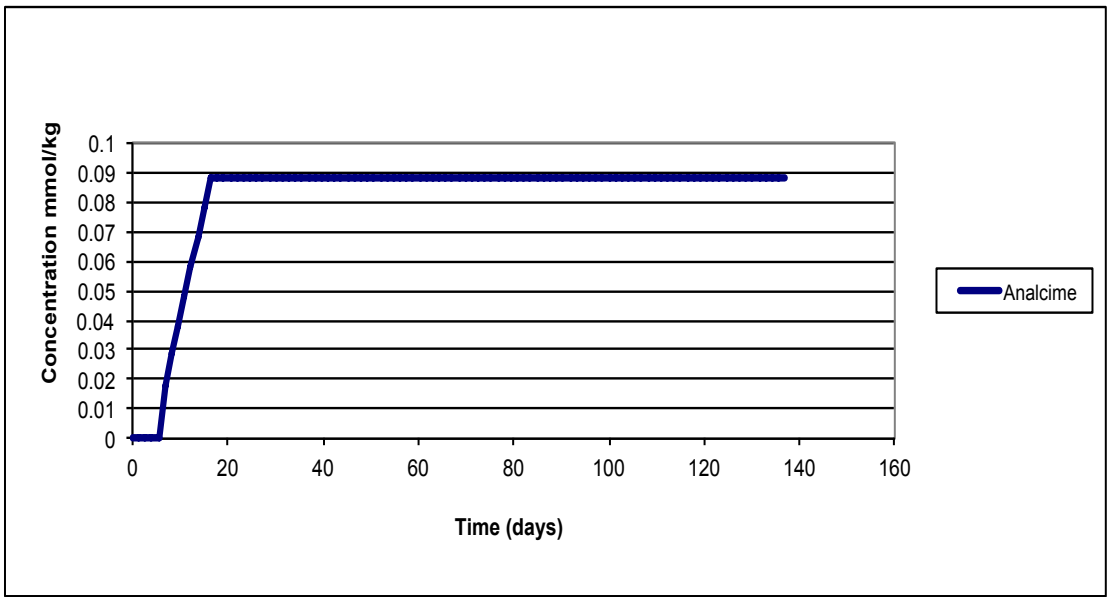

Figure 4- 6: Precipitation of analcime in the model

4.4.3. Experiments with Arkose as Host Rock and CO_2 + SO_2 as Feed Gas

These experiments are described in Section 3.4.3. Arkose was reacted with 90% CO_2 and 10% SO_2 and brine (Table 3-5) at 100^0C and 2000 psi. Pronounced dissolution of all the minerals in the host rock and precipitation of anhydrite and kaolinite were the key features in this experiment. The brine chemistry in these experiments is described in Figure 3-39. The degassing simulations were conducted with the procedure mentioned in Section 4.4.1 and the experimental results were corrected for degassing. Figures 4-7 and 4-8 show the output of the model for this case in both aqueous phase and solid phase.

In the model, Ca ion concentration increases due to the dissolution of calcite and dolomite and also the silicate dissolution plagioclase feldspar. In this case, the dissolution rate is fast due to the acidity of the brine (presence of SO_2 in the gas stream).

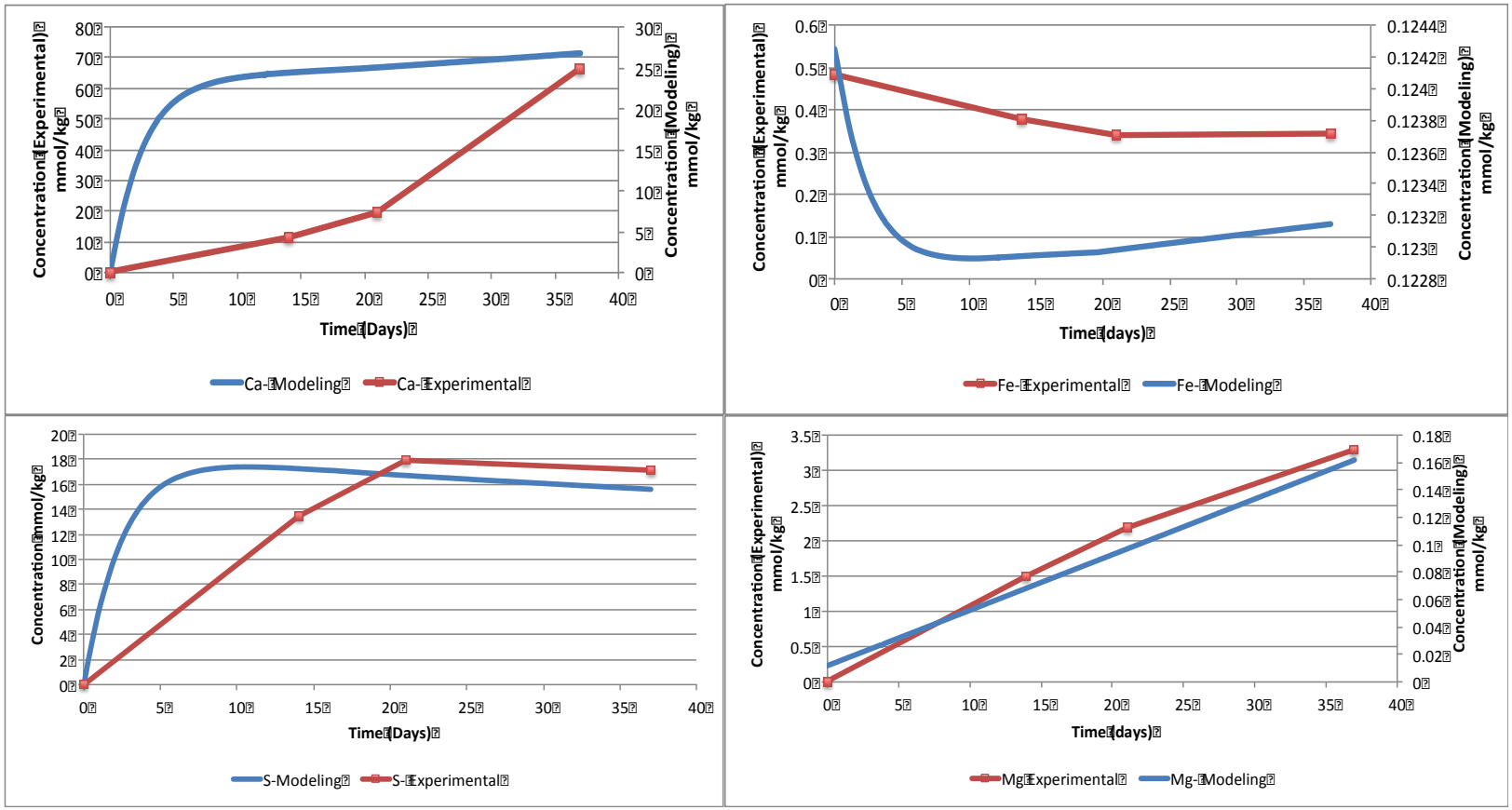

Figure 4- 7: Comparison of experimental and modeling results for arkose +CO_2 +SO_2

There is a good agreement between the simulations and the experimental results for Ca with a maximum difference of 32%. The reasons for the deviation mentioned above further intensified in this case. The multiple sources of Ca and degassing effect still hold true, but the precipitation of anhydrite further increases the deviation. The dissolution rates of calcite are pretty high in this relatively lower pH system, but the precipitation rates of anhydrite are also high compared to the precipitation of calcite. The Mg concentrations increased in the experiment and this increase is greater than that of Ca. This supports the "dolomotization of calcite" mechanism by Rosenbauer et al. [27], brines with high sulfate concentrations. K ion concentration increases and continues to increase because of the dissolution of microcline. In the experiment, the Al bearing mineral kaolinite was found in trace amounts. Fe concentrations decreased, consistent with the experimental observations. Its decrease can be attributed to the dissolution of ankerite or siderite. S concentrations increased in the initial stages of the experiment, but in the latter stages of the experiment, S decreased because of the precipitation of anhydrite, gypsum, or bassanite. These observations are consistent with the experimental results. Degassing corrections reduce the error to very acceptable value for geochemical simulations. The agreement in the sulfur ion concentration was very good with an initial deviation of 24% and the difference decreases to 4% in the latter stages of the experiment because the only source of sulfur in the brine is the feed gas, whereas Ca in the brine can come from calcite, dolomite, or plagioclase feldspar. The behavior of these minerals when f_{CO2} decreases is different. Hence, when the correction factor is calculated, it leads to a marginally larger error in the case of cations, which are contributed by multiple minerals. Figure 4-8 shows the precipitation of anhydrite and dissolution of calcite in the

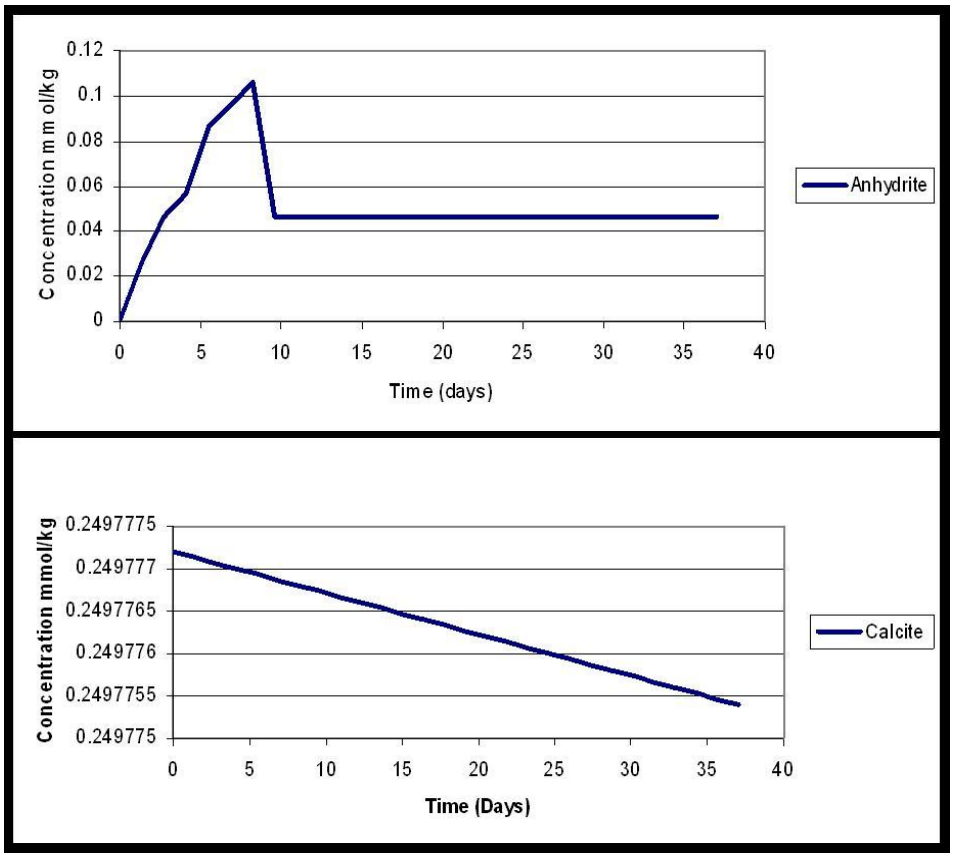

Figure 4- 8: Precipitation of anhydrite and pronounced dissolution of calcite in the model

experiments. The mechanisms for these reactions are listed in Section 3.4.3. Anhydrite was seen as euhedral crystals growing in the pore spaces of primary minerals. Dissolution patterns of calcite and dolomite were ubiquitous in addition to the precipitated anhydrite crystals. All the mineral surfaces were rough and pitted. Due to the increased acidity following the injection of the gas mixture, primary calcite and dolomite underwent dissolution and this led to secondary precipitation of anhydrite. There were traces of gypsum and bassanite identified in the XRD analysis, but the amount of these precipitates was very small.

4.4.4. Experiments with Limestone as Host Rock and CO_2 as Feed Gas

These experiments are described in Section 3.3.1. Limestone was reacted with CO_2 and brine (Table 3-5) at 100^0C and 2000 psi. Pronounced dissolution of the host rock was the key feature in this experiment. The brine chemistry in these experiments is described in Figure 3-11. The degassing simulations were conducted with the procedure mentioned in Section 4.4.1 and the experimental results were corrected for degassing.

The Ca concentration is the only comparison parameter used in this case. The agreement between the experimental and modeling values is very good (Figure 4-9) with a maximum deviation of 22%. The Ca concentration increased because of the dissolution of limestone driven by the acidic brine. The absence of cations for secondary precipitation reactions precludes the chance of any mineral sequestration in this case. The rate of increase of Ca decreases with time temporally because the pH of the brine increases with calcite dissolution, but no precipitation reactions were observed in the time scale of this experiment.

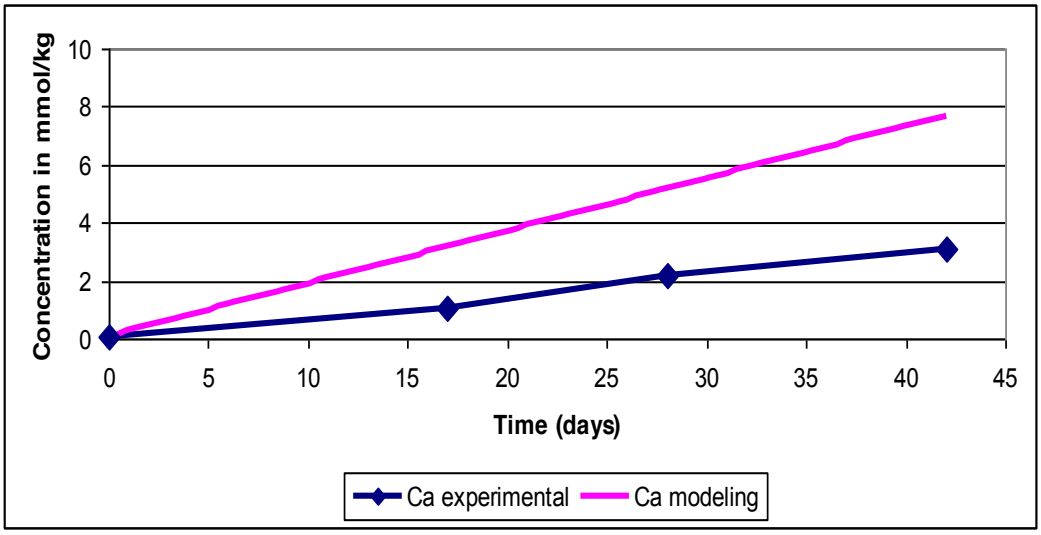

Figure 4- 9: Comparison of experimental and modeling results for limestone experiments

4.4.5. Experiments with Sandstone as Host Rock and CO_2 as Feed Gas

These experiments are described in Section 3.3.2. Sandstone was reacted with CO_2 and brine (Table 3-5) at 100^0C and 2000 psi. Dissolution of the host rock and precipitation of halite kaolinite were the key features in this experiment. The brine chemistry in these experiments is described in Figure 3-15. The degassing simulations were conducted with the procedure mentioned in Section 4.4.1 and the experimental results were corrected for degassing.

Brine chemistry is again chosen as the comparison parameter for this case. Ca concentrations progressively increased due to the dissolution of plagioclase feldspars (Figure 4-10). The initial deviation of 18% decreased to 3% in the final stages of the experiment. The experimental results agree very well with the modeling results. In the case of K, a maximum deviation of 12% is observed. Dissolution of microcline leads to an increase in the K concentration in the brine. Kaolinite precipitation is observed in the experiments. As mentioned earlier in Figure 4-3, the mineral that is most stable in the activity regime in the experimental conditions is kaolinite. The silica saturation, driven by the dissolution of feldspars, is the principal factor governing the mineral that would precipitate in this experiment. Analcime was detected in the XRD analyses but its precipitation was not observed in the reacted samples during the SEM analyses. Si concentrations increased continuously in the samples because of the dissolution of the aluminosilicate minerals. The deposition of amorphous silica is an indication of a very high silica activity in these experiments.

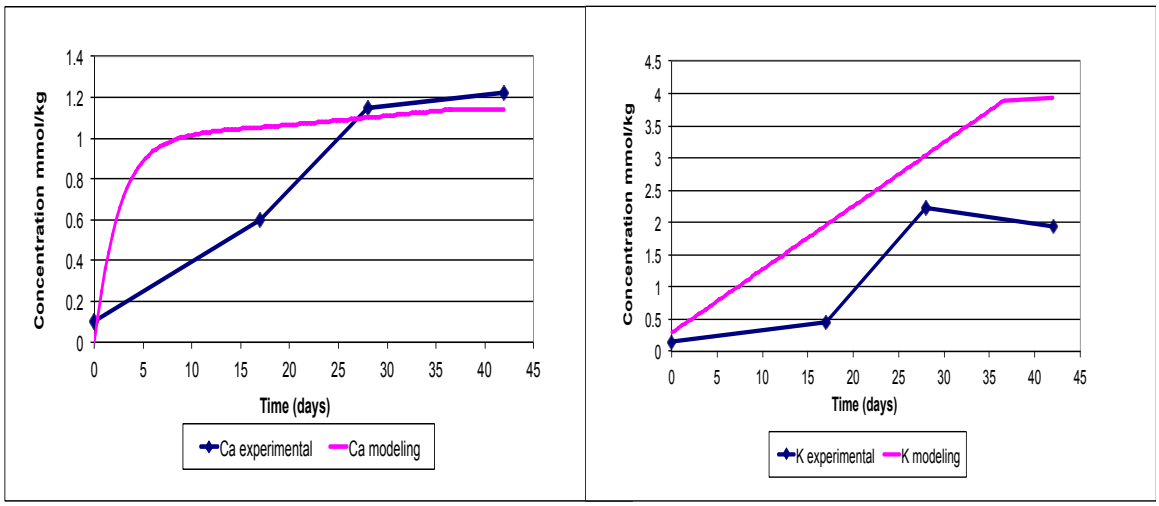

Figure 4- 10: Comparison of experimental and modeling results for the sandstone experiments

4.4.6. Experiments with Peridotite as Host Rock and CO_2 as Feed Gas

These experiments are described in Section 3.3.3. Sandstone was reacted with CO_2 and brine (Table 3.2) at 100^0C and 2000 psi. Dissolution of the host rock, magnesite precipitation, and heterogeneous deposition of amorphous silica were the key features in this experiment. The degassing simulations were conducted with the procedure mentioned in Section 4.4.1 and the experimental results were corrected for degassing. In the case of calcium, the model captured the increase in Ca, which occurs due to the dissolution of silicate minerals (Figure 4-11). The initial deviation of 26% decreased to 2% at the end of the experiment. The Mg ion concentration followed an increasing trend, initially indicating dissolution of olivine in the initial stages of the experiment with a maximum deviation of 34%. The decrease in Mg in the latter stages of the experiment is a result of precipitation of magnesite ($MgCO_3$), which is a product of carbonation reactions. The precipitation of analcime is shown in Figure 4-12. Due to the presence of excess CO_2 in the reactor, carbonation of olivine dominates the hydration reactions.

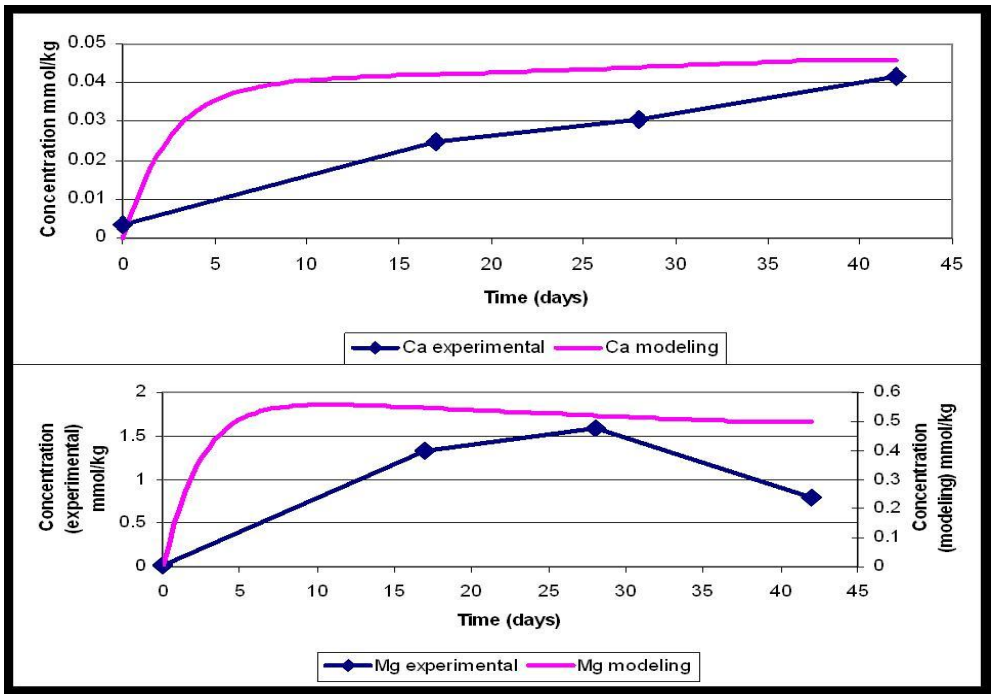

Figure 4- 11: Comparison of experimental and modeling results for peridotite experiments

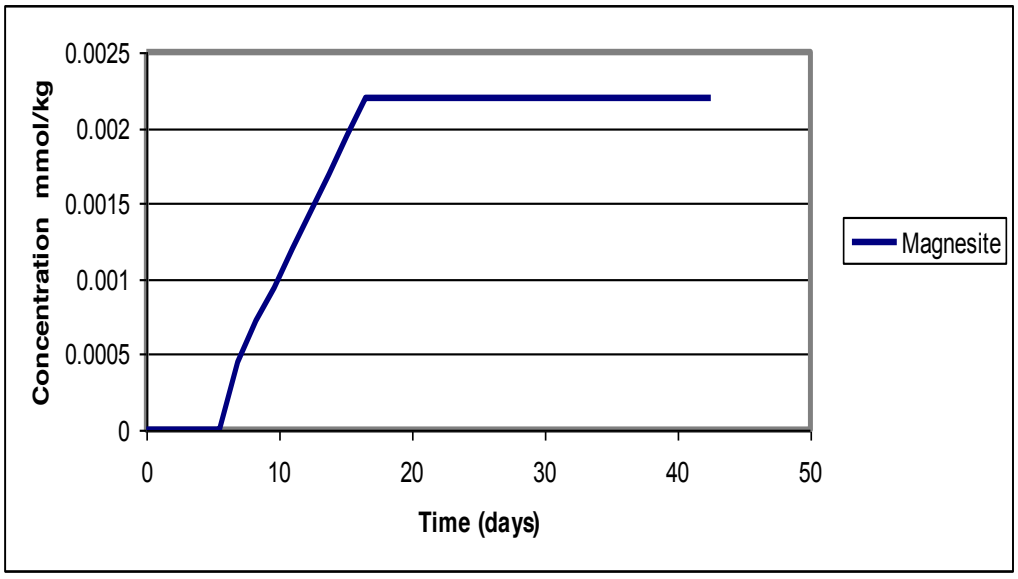

Figure 4- 12: Precipitation of analcime in peridotite experiments

4.5.Parameter Sensitivity Analysis

4.5.1. Theory

By definition, a factorial design consists of all contributions of the factor levels of two or more factors. Since frugality is a major virtue in any practical situation, it is advisable to run the fewest number of levels of the factors and learn about their impacts on the final output. The two levels of each factor are denoted symbolically by a"+" or a"-" to indicate a high and low level of each particular factor.

For example, in the case of a two factorial design, the layout of the experimental design is shown in Table 4-3. Plotting the experimental design allows us to look at all of the extreme points in the experimental region. After the experiments are run and a measured response at each set of conditions is obtained, the data must be analyzed to determine the impact of each of the factors under study. The average effect of X1 and X2 in a two factorial design can be stated as

$$\text{Average effect of X1} = [(Y2-Y1) + (Y4-Y3)]/2 \quad (4.8)$$

$$\text{Average effect of X2} = [(Y3-Y1) + (Y4-Y2)]/2 \quad (4.9)$$

These concepts can be readily extended to factorial designs with more than two factors.

Table 4- 3: Two level factorial design for two factors

Run	X1	X2	Output Y
1	-	-	Y1
2	+	-	Y2
3	-	+	Y3
4	+	+	Y4

4.5.2. Application to Sequestration Experiments

In the experiments using arkose as the starting mineral assemblage, there are six different minerals involved. Hence, there are six different kinetic rate constants and six different reactive surface areas corresponding to each case, to be fed as input to the model in the GWB. To evaluate the variation or the uncertainty in the model both qualitatively and quantitatively with the variation in these kinetic parameters, a fifteen factorial sensitivity analysis and a full factorial sensitivity analysis were run. This analysis takes into account the contribution of each parameter to the desired output and weighs it on a pareto chart.

This analysis requires us to choose the highest and lowest values for each parameter. All the possible values for that particular parameter fall within this range. The desired output is selected. Then, following the methodology for the analysis, these parameters are lined up and the model is run for the desired output for the various cases in the analysis. For the arkose, there are twelve different parameters, which are designated as X1, X2, X3…….X12. The desired output is selected as Y. This setup is described in Table 4-4.

The following two cases are studied using the parameter sensitivity analysis:

1. Arkose as host rock and CO_2 as feed gas
2. Arkose as host rock and 90% CO_2 +10% SO_2 as feed gas

The key factors that affect the output in each case are identified. Brine chemistry is once again used as the primary parameter. The concentrations of principal ions in the brine are selected as the desired output from the model and the important parameters from Table 4-4 are identified.

Table 4- 4: Parameters for the sensitivity analysis

Factor	Parameter
X1	Reactive surface area for Calcite
X2	Reactive surface area for Quartz
X3	Reactive surface area for Dolomite
X4	Reactive surface area for Chlorite
X5	Reactive surface area for Microcline
X6	Reactive surface area for Andesine
X7	Kinetic rate constant for Calcite
X8	Kinetic rate constant for Quartz
X9	Kinetic rate constant for Dolomite
X10	Kinetic rate constant for Chlorite
X11	Kinetic rate constant for Microcline
X12	Kinetic rate constant for Andesine

As mentioned earlier, the main source of error in batch geochemical modeling arises from the uncertainty in kinetic parameters. There is a wide range of rate constants and the reactive surface areas in the literature. In addition to this, the measured rate constants are usually two to three orders of magnitude greater than the rates of weathering usually observed in the field. With the help of this sensitivity analysis, we can identify the key contributors and concentrate on the parameters that contribute to the final outcome of the model. This analysis also helps in confirming the validity of the reaction mechanisms put forth in this study.

4.5.3. Arkose as Host Rock and $CO_2 + SO_2$ as Feed Gas

The key parameters affecting the concentration of Ca in the brine are kinetic rate constant for microcline, the reactive surface area for calcite, and reactive surface area for andesine (Figure 4-13). This output is actually intuitive because dissolution of feldspars

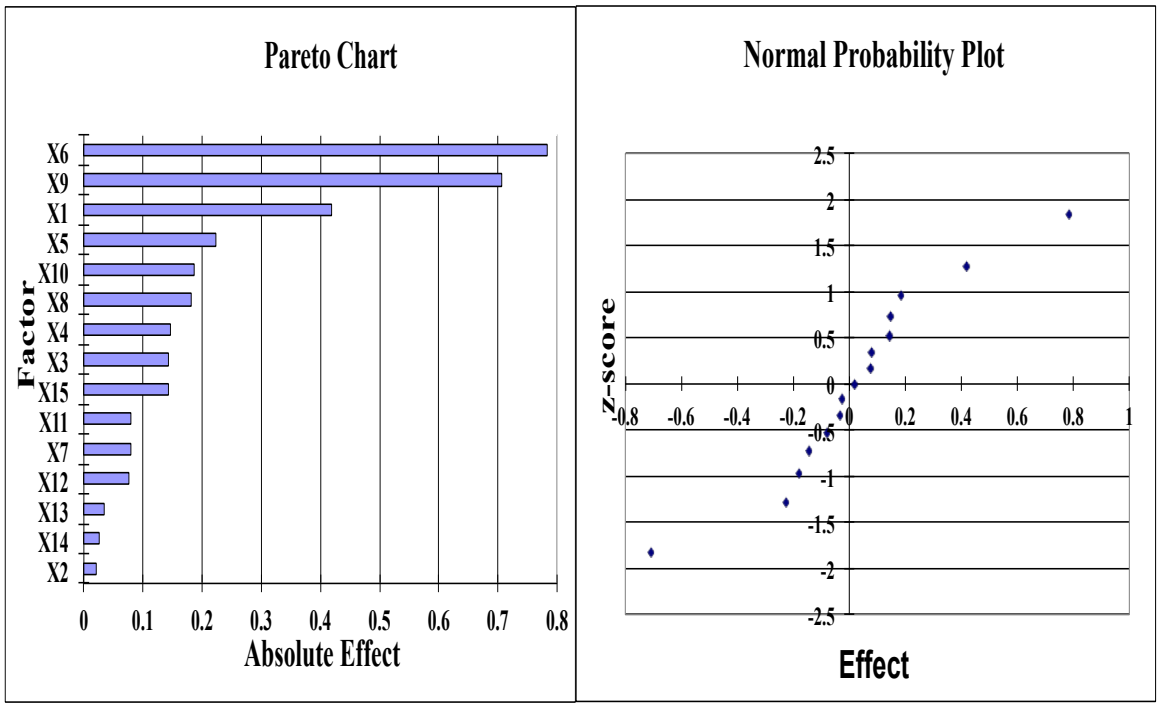

Figure 4- 13: Pareto chart weighing the key factors in experiment with arkose + CO_2 with Ca concentration in brine as key output

and dissolution of carbonates governs the pH of the brine. The Ca concentration is governed by carbonate and silicate geochemistry. Kinetic rate constant of microcline governs the rate of dissolution of microcline, which in turn drives the pH of the system. In the case of K, the key parameters are kinetic rate constant for microcline, the reactive surface area for calcite, and reactive surface area of microcline (Figure 4-14). The rate of dissolution of microcline governs the release of K in brine. It is also governed by the top contributor to the pH of the system, which is reactive surface area of calcite. The outputs and the top three key factors affecting their outcome are described in Table 4-5.

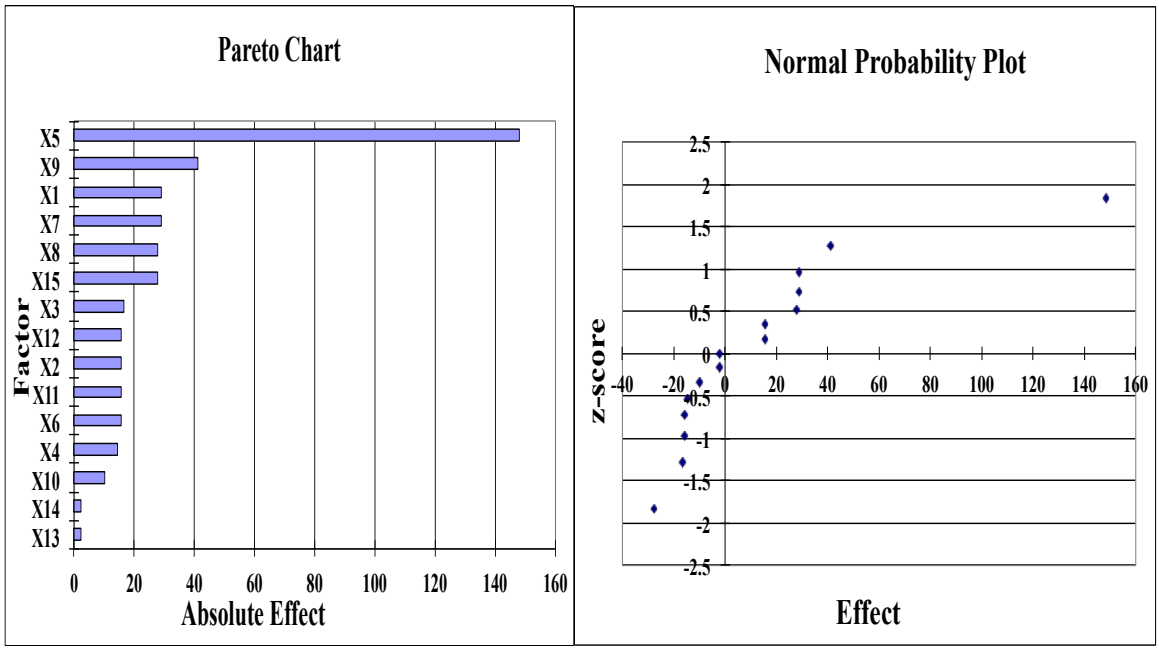

Figure 4- 14: Pareto chart weighing the key factors in experiment with arkose + CO_2 with K ion concentration in brine as key output

Table 4- 5: Contribution of key parameters to the desired outputs in the model for Arkose+CO_2 experiment

Output	Contributor 1	Contributor 2	Contributor 3
Ca	Kinetic rate constant for microcline	reactive surface area for calcite	reactive surface area for andesine
K	Kinetic rate constant for microcline	reactive surface area for calcite	reactive surface area for microcline
Mg	Kinetic rate constant for dolomite	reactive surface area for dolomite	reactive surface area for microcline
Al	Kinetic rate constant for andesine	reactive surface area for calcite	reactive surface area for microcline
Fe	Kinetic rate constant for calcite	reactive surface area for chlorite	reactive surface area for andesine
Si	Kinetic rate constant for microcline	reactive surface area for calcite	reactive surface area for andesine

4.5.4. Arkose as Host Rock and $CO_2 + SO_2$ as Feed Gas

The key parameters affecting the concentration of Ca in the brine are kinetic rate constant for microcline, kinetic rate constant for andesine, and kinetic rate constant for calcite (Figure 4-15). This output is also intuitive because the dissolution of feldspars microcline and andesine occurs at a rapid pace in highly acidic conditions in the system. Hence, it is the silicate geochemistry, which drives the pH of the system overriding carbonate geochemistry.

Kinetic rate constant of microcline governs the rate of dissolution of microcline, which in turn drives the pH of the system. In the case of K ion, the key parameters are kinetic rate constant for microcline, reactive surface area for microcline, and reactive surface area of andesine (Figure 4-16). The rate of dissolution of microcline governs the release of K ion in brine. It is also governed by another top contributor to the pH of the system, which is reactive surface area of andesine. The outputs and the top three key factors affecting their outcome are described in Table 4-6. The kinetic parameters used for generating the modeling results in Section 4.4 (Table 4-2) have been derived based on the sensitivity analysis results. Hence, it is imperative to use parameter sensitivity analysis to eliminate the factors that do not contribute to the changes in the system. In the case of arkose used in these experiments, quartz is the inert mineral in the assemblage, which is evident from the results of parameter sensitivity analysis.

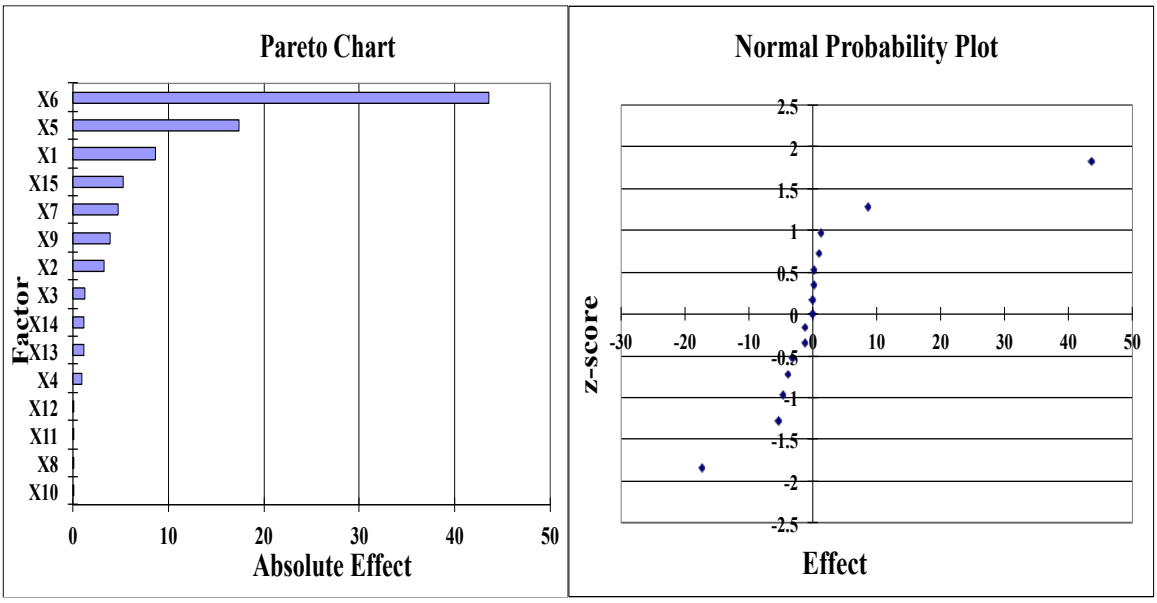

Figure 4- 15: Pareto chart weighing the key factors in experiment with arkose + CO_2 + SO_2 with Ca ion concentration in brine as key output

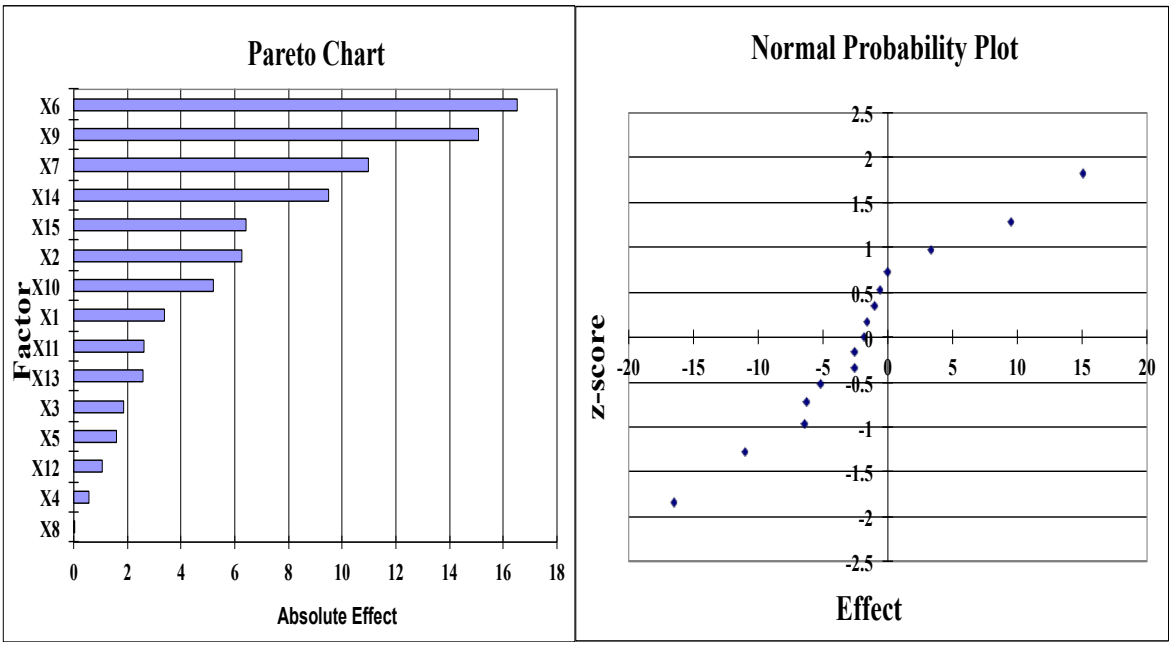

Figure 4- 16: Pareto chart weighing the key factors in experiment with arkose+CO_2+SO_2 with K ion concentration in brine as key output

Table 4- 6: Contribution of key parameters to the desired outputs in the model for Arkose+CO_2+SO_2 experiment

Output	Contributor 1	Contributor 2	Contributor 3
Ca	Kinetic rate constant for microcline	Kinetic rate constant area for andesine	Kinetic rate constant area for calcite
K	Kinetic rate constant for microcline	reactive surface area for microcline	reactive surface area for calcite
Mg	reactive surface area for microcline	Kinetic rate constant for dolomite	reactive surface area for dolomite
Al	Kinetic rate constant for andesine	reactive surface area for microcline	reactive surface area for calcite
Fe	Kinetic rate constant for microcline	reactive surface area for chlorite	reactive surface area for andesine
Si	Kinetic rate constant for microcline	reactive surface area for calcite	reactive surface area for andesine

5. SUMMARY

Storing carbon dioxide generated by fossil fuel utilization will provide means of reducing CO_2 emissions into the atmosphere as the transition to carbon-neutral energy technologies unfolds. CO_2 injection into oil reservoirs has been carried out for enhanced oil recovery for several decades – hence, there is considerable knowledge about the process. There are major differences between CO_2 EOR and large-scale CO_2 injection into saline aquifers. The scale and scope of a meaningful CO_2 sequestration project are much larger than CO_2 EOR projects currently underway. CO_2 EOR is accompanied by production (of oil, water, and CO_2 (after breakthrough)), as a result of which the operation dynamics and associated risks are different. Sequestration must provide reasonably secure storage of CO_2. Otherwise, the energy penalty incurred in separating and storing CO_2 may result in net CO_2 emissions into the atmosphere, basically negating the original objective. The sequestration physical processes must be understood to ensure that the process is engineered correctly.

This study is an attempt to answer two major questions that may have significant implications on the economic and safety implications of the sequestration process. They are:

1. What is the effect of the reservoir rock mineralogy on the ultimate fate of CO_2?

2. What are the implications of co-injecting trace amounts of gases such as SO_2 and NH_3 with CO_2 into formations of interest?

The experimental investigation of the effect of reservoir rock compositions on the sequestration reactions has not yet been reported in the literature. Zerai et al. [61] investigated the effect of mineral assemblages on the ultimate fate of CO_2. Their study concluded that the mixed assemblages (carbonate + sandstone) and sandstone aquifers sequester CO_2 as mineral carbonates, primarily dawsonite and siderite, whereas in a carbonate aquifer, the primary modes of trapping are structural and ionic. This experimental study provides a means of comparing those modeling results with experimental data. The three formations, limestone, sandstone, and arkose were chosen because of their common occurrence and their proximity to coal fire power plants [1]. Peridotite was chosen because of its high reactivity.

Calcite undergoes dissolution releasing Ca ion and CO_3^{2-} or HCO_3^- ions, depending on the stage of deprotonation, and pH when CO_2 and brine are brought into contact with limestone. Cations required for precipitation are not present either in sufficient concentration or diversity. Hence, addition of CO_2 to a carbonate reservoir increases acidity and causes dissolution, not precipitation of carbonate minerals. Dissolution of calcite and increase in the concentration of Ca in the brine were the principal observations in the experiments with CO_2 and limestone. Sequestration of CO_2 in these reservoirs must be accomplished by structural and ionic trapping mechanisms.

In sandstone reservoirs, the dissolution of the silicate minerals overrides the relatively slow carbonation reactions, and hence, the role of silicates in bringing about mineralization is not realized. The carbonation step in this sequence of reactions is

usually the rate-controlling step since silicate dissolution rates are relatively rapid. Precipitation of kaolinite in the experiments with CO_2 + sandstone is the evidence of carbonation reactions. Calcite and kaolinite precipitation was detected in the XRD analyses. The abundance of cations for secondary precipitation reactions combined with initially acidic conditions drives the complex set of carbonation and hydration reactions. Silica is also released into the brine because of feldspar dissolution. The brine becomes sufficiently saturated with silica. When the sample is cooled for analysis, the brine becomes supersaturated with silica at the lower temperature. This silica in the brine undergoes heterogeneous deposition as amorphous silica, which was evident in the EDS analysis on all reacted samples.

Experiments with peridotite were conducted because of its relatively rapid reactive tendency with CO_2 rich brine. The rates of carbonation of peridotite have been reported in the literature [36] and are three to four orders of magnitude higher than carbonation rates of feldspars. Peridotite used in this study had traces of iron in it, giving it a distinct green color. Precipitation of magnesite, siderite, and pronounced deposition of silica were the principal observations in these experiments. Orthorhombic crystals of magnesite were observed with pitted rough faces, indicating that brine was undersaturated with respect to magnesite when the experiment was concluded. The amorphous silica deposition resulted from the significant dissolution of olivine (from the peridotite).

Arkose (or dirty sands) are the most common reservoir rock types in major saline formations (Ohio Rose Run, Mt. Simon, Sleipner aquifer, etc.). The synthetic arkose used in this study was prepared by mixing equal proportions of pure calcite, quartz, microline,

anorthite, chlorite, and dolomite. Hence, this synthetic arkose represents a mixed assemblage of carbonates, sandstone, and sheet silicates (clay minerals). Because of the complexity of the starting mineral, identifying the initial mineral signature of the mineral was essential. The initial analysis (XRD and SEM) revealed the presence of the above-mentioned minerals with a reasonably uniform distribution. The experiments at 200^0C yielded precipitation of ankerite and calcite. The source of iron for ankerite was the dissolution of chlorite; magnesium rich phase in the initial sample. Halite deposits were also observed on the reacted mineral as a result of brine desiccation during degassing. In the experiments at 100^0C, initial dissolution of carbonate minerals (calcite and dolomite) was observed. Although there were numerous angular pits in the initial calcite grains, these pits are more enlarged and distinct in the reacted samples. There was an evident increase in the number of pores in the reacted samples because of the mild acid attack. This relatively quick dissolution is followed by reprecipitation of calcite in the latter stages of the experiment. Calcite is seen growing as tightly packed polymorph of calcium carbonate. These layers of calcite are seen growing as an amorphous mass intergrown with the starting minerals (especially quartz). These calcite crystals are highly irregular in shape and show no consistency in size. Deposition of a new phase, analcime or kaolinite on the reacted surface was also observed.

In the experiments with spent shale as the host rock, Ca-zeolite precipitates were observed in the reacted sample. This precipitation was observed relatively quickly (two weeks) since these experiments were carried out at 200^0C, which accelerated the silicate dissolution rates. These zeolite crystals were observed as an amorphous mass grown into crystals on weathering orthoclase. Alteration of clays, illite to chlorite was also observed

in the reacted samples. Reprecipitation of some carbonate phases such as dolomite and magnesite were observed in the sample after four weeks.

Arkose was selected as the host rock to investigate the gas compositional effects due to its common occurrence and geochemical complexity. The experiments with 10% SO_2 with CO_2 were dominated by pronounced dissolution of all primary minerals followed by growth of anhydrite crystals. The presence of anhydrite in these experiments confirms the recent modeling (reference) results in other studies. The precipitation of kaolinite was also observed in these experiments. The pronounced dissolution patterns of the host rock pose concerns for the safe injection of CO_2+ SO_2 into the formations. In experiments with CO_2+NH_3, precipitation of calcite and ammonium zeolites was observed. Dissolution and precipitation patterns have direct consequences on petrophysical properties and on the integrity of the storage system as a whole. For example, anhydrite precipitation in the near well bore region may impact gas injectivity. For these reasons, the reaction chemistry of the sequestration system with the targeted gas species like SO_2 and NH_3 must be carefully evaluated prior to the commencement of the injection process. This study also highlights the importance of silica and clay chemistry in determining dissolution/precipitation balance in sequestration repository. All the results from the mineralogical analyses were correlated with the changes in the brine chemistry for all the cases.

The effect of brine to rock (B/R) ratio was studied with three different B/R ratios 10:1, 10.5:1, 15.5:1. Zerai et al. [61] concluded from modeling studies that increasing B/R ratio increases the amount of CO_2 sequestered. The experiments show that the amount of initial dissolution increases with an increase in B/R ratio. The presence of

more amount of dissolved CO_2 in the brine for the same amount of rock leads to this increase.

Geochemists WorkBench was chosen to develop batch models to simulate the experiments and also compare the experimental results with modeling. Rate constants for the kinetic reactions were compiled from the published literature based on laboratory experiments. However, these rates can be several orders of magnitude greater than the rates of weathering or dissolution measured in the field. The reason for this discrepancy arises from the particle size used in the measurements in the laboratory experiments. To measure the dissolution rates in the laboratory, the rocks are usually ground very fine (100 μm) to increase the reactive surface area of the pure minerals. This process is necessary to record the dissolution rates at measurable time scales, but these rates do not reflect the actual dissolution of the same minerals in the field.

There is also considerable discrepancy in kinetic parameters adopted from different sources in the literature. This arises from various factors. The primary source for these factors is the method used for measuring these dissolution rates. The common method used is the rotating disk technique. The use of different rotation speeds, size of the disks, buffers (to maintain the pH) which can accidentally inhibit or promote the dissolution reactions, grain sizes of the minerals, reaction time periods, and variation in the purity of the minerals can be listed as some of the important factors that contribute to the huge difference between the kinetic parameters of the same mineral from different literature sources.

The kinetic parameters used in this study were collected from Gaus et al. [57] after an exhaustive literature review. The fugacity coefficient was calculated using the

Duan and Sun algorithm. B dot equation was used to calculate the activity coefficients. B dot equation is not accurate for solutions with high ionic strength, but the virial equation does not take into account the distribution of species in the solution. This would lead to some very inaccurate conclusions because the choice of a different species in the solution could lead to a completely different precipitate in the solid phase. Hence, after weighing the pros and cons, B dot equation was used in the model.

All the experimental analyses were carried out at ambient conditions after the reactor was depressurized. This degassing process would lead to numerous retrograde reactions and also long-term quenching reactions. Several changes take place during this process like the change in the pH of the system because of a decrease in f_{CO2}, change in the saturation states of the minerals in the brine, spontaneous dissolution, and precipitation of new phases. To correct for degassing, the sliding fugacity module in GWB was used. All the experimental results were corrected for degassing and compared with the modeling results.

In the experiments with CO_2+arkose, there was reasonable agreement between the modeling and experimental results for all the ions except Ca ion which differed by an order of magnitude. There can be two reasons for this deviation. The first one is multiple sources for Ca in the starting mineral (Calcite, dolomite, and Ca-feldspar) with different kinetic parameters and the latter is the behavior of these Ca bearing minerals during degassing. The dissolution rates for the minerals were measured using pure minerals. Each mineral behaves in a different manner in each assemblage. For example, consider calcite as an individual mineral and calcite in the arkose. The chemical composition of the mineral is the same, but the overall mineral assemblage within which it is placed

plays the governing role in its ultimate fate. Hence, the presence of multiple sources of Ca (carbonates and feldspars with very different kinetic behavior), and their largely different behavior when the experimental results are corrected for degassing, are the primary reasons for the deviation between the experimental and modeling results.

In the comparison of CO_2+ SO_2+arkose experiments, again reasonable agreement was observed except for Ca ion. The reasons for the deviation mentioned above are further intensified in this case. The multiple sources of Ca and degassing effect still hold true, but the precipitation of anhydrite further increases the deviation. The dissolution rates of calcite are higher in this relatively lower pH system, but the precipitation rates of anhydrite are also high compared to the precipitation of calcite. This effect combined with the degassing correction produces a relatively high deviation of Ca ion from the modeling results. The Mg concentrations increased in the experiment and this increase is greater than that of Ca. This supports the "dolomotization of calcite" mechanism by Rosenbauer et al. [27], in brines with high sulfate concentrations.

There was very good agreement in the modeling and simulation results for experiments with CO_2 as the feed gas and limestone, sandstone, and peridotite as host rocks with a maximum error of 34% in the case of peridotite experiments. This is partly due to the reason that these minerals were relatively pure when compared to the synthetic arkose, which was used in the other comparisons.

In the experiments using arkose as the starting mineral assemblage, there are six different minerals involved. Hence, there are six different kinetic rate constants and six different reactive surface areas corresponding to each case, to be fed as input to the model in the Geochemists WorkBench. To evaluate the variation or the uncertainty in the model

both qualitatively and quantitatively with the variation in these kinetic parameters, a fifteen factorial sensitivity analysis and a full factorial sensitivity analysis is necessary. This analysis takes into account the contribution of each parameter to the desired output and weighs it on a pareto chart. The key parameters affecting the concentration of Ca in the brine, in CO_2, and arkose experiments are kinetic rate constant for microcline, the reactive surface area for calcite, and reactive surface area for andesine. The key factors for other ions were also identified.

An exhaustive literature review, leading to an in-depth understanding of the gaps to be filled and the questions to be answered, was identified in this study. The fundamental experimental results for the mineralogical reactions in a variety of scenarios encountered in geological sequestration of CO_2 have been discussed. Dissolution and precipitation scenarios provide in this study will have profound implications on the porosity, permeability, and other petrophysical properties of the formation, which in turn have an effect on the integrity of the geological repository on the whole. These experimental results have been backed up by batch geochemical modeling results and a comparison with experimental results has also been provided. A statistical analysis, to understand the key contributors to the uncertainty in the model, was identified using full factorial sensitivity analysis.

Future Work

This experimental study would provide the basis for designing and fabricating a similar experimental setup with in-situ measurements of pH and selective ion concentrations. These experiments would enable us to directly compare the experimental results with those of the modeling results, thereby avoiding the correction factors through

degassing simulations. Simple experiments with pure minerals having one primary cation (Ca) like calcite would be helpful in calibrating the electrodes. These experiments can be carried out at different temperatures between 50^0C-100^0C and no pressure and with different initial pH values. It will be a lot easier with dissolution experiments of $CaCO_3$ at mild pH conditions to monitor the pH and brine chemistry, to find out the mechanism through which the brine is buffered due to carbonate geochemistry. Since carbonate geochemistry is well documented in the literature, these experiments will be also useful to calibrate the instruments if necessary. The longevity and reliability of the ion electrodes can also be evaluated with these simple dissolution experiments. The experiments with slightly complex minerals with multiple primary cations like dolomite ($CaMg(CO_3)_2$) and plagioclase ($KAlSi_3O_8$) feldspar should be carried out after the calibration experiments. Here we would study, at room temperature and pressure, the in-situ pH and concentrations of the primary cations. These simple dissolution experiments would give us valuable insight into dissolution mechanisms of different minerals under different pH conditions. The next set of experiments - high temperature, high-pressure experiments (with injection of CO_2) with in-situ measurements - would be the first of its kind. In this scenario, a gradual pH change would be observed due to CO_2 dissolution in brine as well as the dissolution of carbonates and feldspars. Hence, these data would yield a clear picture of the pace and sequence of reactions in this complex geochemical system.

APPENDIX

A.1. List of important sequestration reactions

1) The dissolution of carbon dioxide in the formation brine and the following deprotonation reactions leading to decrease in pH

$$CO_2\,(g) \quad \leftrightarrow \quad CO_2\,(aq)$$

$$H_2O + CO_2 \quad \leftrightarrow \quad H_2CO_3$$

$$H_2CO_3 \quad \leftrightarrow \quad H^+ + HCO_3^-$$

2) The dissolution of calcite liberating Ca ion into the brine

$$CaCO_3 + H^+ \quad \leftrightarrow \quad Ca^{2+} + HCO_3^-$$

3) The dissolution of Calcium feldspar leading to the formation of kaolinite

$$2H^+ + CaAl_2Si_2O_8 + H_2O \quad \leftrightarrow \quad Ca^{2+} + Al_2Si_2O_5(OH)_4$$

$$CaAl_2Si_2O_8 + H_2CO_3 + H_2O \quad \leftrightarrow \quad CaCO_3 + Al_2Si_2O_5(OH)_4$$

4) Phase transformation of albite

$$NaAlSi_3O_8 + 3\,H_2O \quad \leftrightarrow \quad NaAlSi_2O_6.H_2O \; + H_4SiO_4$$

5) Dissolution of microcline yielding kaolinite

$$2KAlSi_3O_8 + 9H_2O + 2H^+ \quad \leftrightarrow \quad Al_2Si_2O_5(OH)_4 + 2\,K^+ + 4H_4SiO_4$$

6) Hydration of olivine to serpentine

$$2Mg_2SiO_4 \quad + \quad Mg_2Si2O_6 + 4\,H_2O \quad \leftrightarrow \quad 2Mg_3Si_2O_5(OH)_4$$

7) Carbonation of olivine to form magnesite

$$Mg_2SiO_4 + 2CO_2 \leftrightarrow 2MgCO_3 + SiO_2$$

8) Carbonation of Olivine and Ca-Mg pyroxene to yield calcite and magnesite

$$Mg_2SiO_4 + CaMg_2Si_2O_6 + 2CO_2 + 2H_2O \leftrightarrow Mg_3Si_2O_5(OH)_4 + CaCO_3 + MgCO_3$$

9) Secondary precipitation reaction of calcite

$$Ca^{2+} + CO_3^{2-} \rightarrow CaCO_3$$

10) Formation of kaolinite from albite

$$NaAlSi_3O_8 + CO_2 + 5.5H_2O \leftrightarrow Na^+ + HCO3^- + 2\ H_4SiO_4 + 0.5\ Al_2Si_2O_5(OH)_4$$

11) Formation of anhydrite and gypsum

$$Ca^{2+} + SO_4^{2-} \leftrightarrow CaSO_4$$

$$CaSO_4 + 2H_2O \leftrightarrow CaSO_4.\ 2H_2O$$

12) Dolomotization of calcite

$$Mg^{2+} + CaSO_4 \leftrightarrow Ca^{2+} + MgSO_4$$

$$Mg^{2+} + 2CaCO_3 \leftrightarrow Ca^{2+} + CaMg(CO_3)_2$$

13) Precipitation of siderite

$$Fe^{2+} + CO_3^{2-} \leftrightarrow FeCO_3$$

14) Dissolution of dawsonite

$$NaAlCO_3\ (OH\ )_2 + 4H^+ \rightarrow Na^+ + Al^{3+} + CO2_{(aq)} + 3H_2O$$

14) Precipitation of magnesite

$$Mg_3Si_2O_{6.76}(OH)_{0.48} + 3CO_2 \leftrightarrow 3MgCO_3 + 2SiO_2 + 0.24H_2O$$

REFERENCES

[1] S. Bachu and J.J. Adams, "Sequestration in geological media in response to climate change: Capacity of deep saline aquifers to sequester CO_2 in solution," *Energy Conversion Management,* vol. 44, pp. 3151-3175, 2002.

[2] S. Holloway, "Storage of fossil fuel-derived carbon dioxide beneath the surface of the earth," *Annual reviews in Energy and Environment,* vol. 26, 2001.

[3] K. Bateman, G. Turner, D.J. Noy, D. Birchall, and C.A. Rochelle, "Large Scale Column Experiment: Study of CO_2, pore water, rock reactions and model test case," *Oil Gas and Technology,* vol. 60, pp. 161-175, 2005.

[4] J. P. Kaszuba, D.R. Janecky, and M.G. Snow, "Carbon Dioxide reaction processes in a model brine aquifer at 200^0C and 200 Bar: Implications for geologic sequestration of carbon," *Applied GeoChemistry,* vol. 18, pp. 1065-1080, 2003.

[5] "An assessment of the Intergovernmental panel on climate change," ed, 2007. Available at www.ipcc.ch/piblications_and_data/publications.shtml

[6] S. Holloway and D. Savage, "The potential for aquifer disposal of carbon dioxide in the UK," *Energy Converse Manage,* vol. 34, 1997.

[7] "Carbon Sequestration Atlas of the United States," N.E.T.L, U.S. Department of Energy, Ed., ed, 2007.

[8] "Carbon Sequestration Atlas of the United States, Version 2, ," N.E.T.L, U.S. Department of Energy, Ed., ed, 2008.

[9] "Storage of Captured Carbon Dioxide on Federal Lands," N.E.T.L, U.S. Department of Energy, Ed., ed, 2009.

[10] T. Xu, J.A. Apps, and K. Pruess, "Mineral Sequestration of carbon dioxide in a sandstone-shale system," *Chemical Geology,* vol. 217, pp. 295-318, 2005.

[11] E. Lindeberg, "Escape of CO_2 from aquifers," *Energy Converse Manage,* vol. 38, pp. S235-S240, 1997.

[12] P.D. Bergman and E.M. Winter, "Disposal of CO_2 in aquifers in the U.S," *Energy Conversion Management,* vol. 36, pp. 523-526, 1995.

[13] S. Bachu, J.J. Adams, and E.H. Perkins, "Aquifer disposal of CO_2: Hydrodynamic and mineral trapping," *Energy Converse Manage,* vol. 35, pp. 269-279, 1994.

[14] R. Span and W. Wegner, "A new equation of state for carbon dioxide covering the fluid region from the triple point temperature to 1100K at pressures up to 800 MPa," *Journal of Physical Chemistry,* vol. 25, pp. 1509-1596, 1996.

[15] J.A.O. Lohuis, "Carbon dioxide disposal and sustainable development in The Netherlands," *Energy Converse Manage,* vol. 34, pp. 815-821, 1993.

[16] W.D. Gunter, E.H. Perkins, and T.J. McCann, "Aquifer disposal of CO_2 rich gases: Reaction design for added capacity," *Energy Converse Manage,* vol. 34, pp. 941-948, 1993.

[17] E.H. Perkins and W.D. Gunter, "A users manual for PATHARC.94: A reaction path-mass transfer program," A.R.C. Report, Ed., ed: ENVTR, 1995, pp. 95-111.

[18] W.D. Gunter, S.Bachu, D.H.S. Law, V.Marwaha, D.L. Drysdale, D.E. MacDonald, and T.J. McCann, "Technical and economic feasibility of CO_2 disposal in aquifers within the Alberta Sedimentary Basin, Canada," *Energy Converse Manage,* vol. 37, pp. 1135-1142, 1996.

[19] W.D. Gunter and E.H. Perkins, "Aquifer disposal of CO_2 rich green house gases: Extension of the time scale experiment for CO_2 sequestration reactions by geochemical modeling," *Mineralogy and Petrology,* vol. 59, pp. 121-140, 1997.

[20] J. Gale, N.P. Christensen, A. Cutler, and T.A. Torp, "Demonstrating the potential for geologic storage of CO_2: The Sleipner and GESTCO projects," *Environmental Geosciences,* vol. 8, pp. 160-165, 2001.

[21] J.P. Kaszuba, D.R. Janecky, and M.G. Snow, "Experimental evaluation of mixed fluid reactions between supercritical carbon dioxide and NaCl brine: Relevance to the integrity of a geologic carbon repository," *Chemical Geology,* vol. 217, pp. 277-293, 2005.

[22] J.R. Seyfried, W.E. Janecky, and D.R. Berndt, *Rocking Autoclaves for Hydrothermal Experiments, II. The Flexible Reaction Cell System*: Ulmer, G.C; Barnes, H.L, 1987.

[23] J.W. Johnson, J.J. Nitao, C.I. Steefel, and K.G. Knauss, "Reactive transport modeling of geologic CO_2 sequestration in saline aquifers: The influence of intra aquifer shales and the relative effectiveness of structural solubility and mineral trapping during prograde and retrograde sequestration," in *National Conference on Carbon Sequestration*, 2001.

[24] K.G. Knauss, J.W. Johnson, and C.I. Steefel, "Evaluation of the impact of CO_2, co-contaminant gas, aqueous fluid and reservoir rock interactions on the geologic sequestration of CO_2 " *Chemical Geology,* vol. 217, pp. 339-350, 2005.

[25] H. Hellevang, P. Aagaard, E.H. Oelkers, and B.Kvamme, "Can Dawsonite Permanently trap CO_2?," *Environ. Sci. Technol,* vol. 39, pp. 8281-8287, 2005.

[26] Y. Soong, A.L. Goodman, S.W. Hedges, J.R. Jones, and D.K. Harrison, "CO_2 sequestration and importance of pH," *American Chemical Society,* vol. 47, pp. 43-48, 2002.

[27] R.J. Rosenbauer, T. Koksalan, and J.L. Palandri, "Experimental investigation of CO_2–brine rock interactions at elevated temperature and pressure: Implications for CO_2 sequestration in deep-saline aquifers," *Fuel Processing Technology,* vol. 86, pp. 1581-1597, 2005.

[28] M. L. Druckenmiller, M. Maroto-Valer, and M. Hill, "Investigation of carbon sequestration via induced calcite formation in natural gas well brine " *Energy and Fuels,* pp. 1481-1492, 2005.

[29] G.H. Wolf, A.V.G. Chizmeshya, J. DiefenBacher, and M.J. McKelvy, "Insitu observation of CO_2 sequestration reactions using a novel micro-reaction system," *Environ. Sci. Technol,* vol. 38, pp. 932-936, 2004.

[30] T.P. Wellman, R.B. Grigg, B.J. McPherson, R.K. Svec, and P.C. Lichtner, "Evaluation of CO_2-brine-reservoir rock with laboratory flow tests and reactive transport modeling," in *SPE International Symposium on Oil FIeld Chemistry*, Houston, Texas, 2003.

[31] J.N. Moore, W.B. Christensen, R. Allis, L.R. Browne, and S. Lutz, "The mineralogical consequences and the results of descending acid sulphates water: An example from the Karaha–Telaga-Bodas Geothermal system, Indonesia," *Canadian Mineralogy,* vol. 42, pp. 1483-1499, 2004.

[32] N. Jacquemet, N. Pironon, and J.S. Marc, "Mineralogical changes of a well cement in various H_2S-CO_2 (brine) fluids at high pressure and temperature," *Environ. Sci. Technol,* vol. 42, pp. 282-288, 2008.

[33] D.H. Bacon, M.B. Sass, M. Bhargava, J. Sminchak, and N. Gupta, "Reactive transport modeling of CO_2 and SO_2 injection into deep saline formations and their effect on the hydraulic properties of host rocks," *Energy Procedia,* pp. 3283-3290, 2009.

[34] C. Taberner, G. Zhang, L. Cartwright, and T. Xu, "Injection of supercritical CO_2 into deep saline carbonate formations: Predictions from geochemical modeling," in *Society of Petroleum Engineers*, New Orleans, Louisiana, 2009.

[35] W.K. O'Connor, D.C. Dahlin, and D.N. Nielsen, "Continuous studies on direct aqueous mineral carbonation for CO_2 sequestration " in *27th International Conference on Coal utilization & Fuel systems*, Clear Water, Florida, 2002.

[36] P.B. Kellemen and J. Matter, "Insitu carbonation of peridotite for CO_2 storage," *Proceedings of National Academy of Sciences,* vol. 105, pp. 17295-17300, 2008.

[37] O. Izgec, B. Demiral, H. Bertin, and S. Akin, "CO_2 injection into saline carbonate aquifer formations: Laboratory investigation," *Transport in Porous Media,* vol. 72, pp. 1-24, 2008.

[38] J. Krumhasl, R. Grigg, H. Westrich, N. Warpinski, and D. Zhang, "Geological sequestration of CO_2 in a depleted oil reservoir," *Society of Petroleum Engineers,* pp. 752-756, 2002.

[39] P. Egermann, B. Bazin, and O. Vizika, "An Experimental Investigation of reaction–transport phenomena during CO_2 Injection," *Society of Petroleum Engineers,* pp. 936-942, 2005.

[40] S.A. Caroll and J.V. Walther, "Kaolinite dissolution at 25^0C, 60^0C and 80^0C" *American Journal of Science,* vol. 290, pp. 797-810, 1990.

[41] M. Alkattan, E.H. Oelkers, J.L. Dandurrand, and J. Schott, "An experimental study of calcite and limestone dissolution rates as a function of pH from -1 to 3 and temperature from 25^0C to 80^0C," *Chemical Geology,* vol. 151, pp. 199-214, 1998.

[42] D.P. Gregory and A. C. Riddiford, "Transport to the surface of a rotating disc," *Journal of Chemical Society of London,* vol. 3, pp. 3756-3764, 1956.

[43] Y.V. Pleskov and V. Filinovski, *The Rotating Disc Electrode* vol. 402: New York Publications, 1976.

[44] R. S. Arvidson and F.T. Mackenzie, "The dolomite problem: Control of precipitation kinetics by temperature and saturation state," *American Journal of Science,* vol. 299, pp. 257-288, 1999.

[45] A.C. Lasaga and R.J. Kirkpatrick, "Kinetics of geochemical processes," in *Reviews in Mineralogy*, ed: Mineralogical society of America, 1981.

[46] M. Gautelier, E.H. Oelkers, and J. Schott, "An experimental study of dolomite dissolution rates as a function of pH from -0.5-5 and temperature from 25^0C to 80^0C," *Chemical Geology*, vol. 157, pp. 13-26, 1999.

[47] O.S. Pokrovsky and J. Schott, "Kinetics and Mechanism of Dolomite dissolution in neutral to alkaline solutions revisited," *American Journal of Science*, vol. 301, 2001.

[48] Z. Liu, D. Yuan, and W. Dreybrodt, "Comparative study of dissolution rate-determining mechanisms of limestone and dolomite," *Environmental Geology*, vol. 49, pp. 274-279, 2005.

[49] O.S. Pokrovsky, J. Schott, and S.V. Golubev, "Dissolution kinetics of calcite, dolomite and magnesite at 25^0C and 0 to 50 atm P_{CO2}," *Chemical Geology*, vol. 217, pp. 239-255, 2005.

[50] O.S. Pokrovsky, J. Schott, and F. Thomas, "Processes at the magnesium bearing carbonates/solution interface: A surface speciation model of magnesite," *Geochemica Coscochemica Acta*, vol. 63, pp. 863-880, 1999a.

[51] O.S. Pokrovsky, J. Schott, and F. Thomas, "Dolomite surface speciation and reactivity in aquatic systems," *Geochemica Coscochemica Acta*, vol. 63, pp. 3133-3143, 1999b.

[52] T. Xu, J.A. Apps, and K. Pruess, "Reactive geochemical transport simulations to study mineral trap for CO_2 disposal in deep arenaceous formations," *Geophysical Research Letters*, vol. B2, 2003.

[53] T. Xu, J.A. Apps, and K. Pruess, "Numerical simulation to study mineral trapping for CO_2 disposal in deep aquifers," *Applied GeoChemistry*, vol. 19, 2004.

[54] K. Pruess, C. Oldenburg, and G. Moridis, "TOUGH2 User's guide, Version 2," 1999.

[55] D.E. Allen, B.R. Stazisar, Y. Soong, and S.W. Hedges, "Modeling carbon dioxide sequestration in saline aquifers: significance of elevated pressures and temperatures," *Fuel Processing Technology*, vol. 86, 2005.

[56] F. Cipolli, B. Gambardella, L. Matrini, G. Ottonello, and M.V. Zuccolini, "Geochemistry of high pH waters from serpentines of the Gruppo Di Votri (Genova, Italy) and reaction path modeling of CO_2 sequestration in serpentine aquifers," *Applied GeoChemistry*, vol. 19, pp. 787-802, 2004.

[57] I. Gaus, M. Azaroual, and C.I. Lauriol, "Reactive transport modeling of the impact of CO_2 injection on the clayey cap rock at Sleipner (North Sea)," *Chemical Geology,* vol. 217, pp. 319-337, 2005.

[58] C.I. Steefel. (2001). *CRUNCH*.

[59] V. Lagneau and H. Catalette, "Reactive transport modeling of CO_2 sequestration in deep saline aquifers," *Chemical Geology,* vol. 217, 2005.

[60] S. White, R. Allis, J.N. Moore, T. Chidsey, C. Morgan, W. Gynn, and M. Adams, "Simulation of reactive transport of injected CO_2 on the Colorado plateau, Utah, USA," *Chemical Geology,* vol. 217, pp. 387-405, 2005.

[61] B. Zerai, B. Z. Saylor, and G. Matisoff, "Computer simulation of CO_2 trapped through mineral precipitation in the Rose Run Sandstone, Ohio," *Applied GeoChemistry,* vol. 21, pp. 223-240, 2006.

[62] A. Battistelli, C. Calore, and K. Pruess, "The simulator TOUGH2/EWASG for modeling geothermal properties with brines and non-condensible gas," *Geothermics,* vol. 26, pp. 144-164, 1976.

[63] G. Yousuf, G.A. Pope, and K. Sepehrnoori, "Hysteresis and field scale optimization of WAG injection for coupled CO_2-EOR and sequestration," presented at the Society of Petroleum Engineers, 2000.

[64] K. Jessen and E. Stenby, "Fluid characterization for miscible EOR projects and CO_2 sequestration," presented at the Society of Petroleum Engineers, 2001.

[65] E. Shtepani, "CO_2 sequestration in depleted gas/condensate reservoirs," presented at the Society of petroleum Engineers, 2004.

[66] S.W. Neal, G. Brromhal, O. Odusote, S. Jikich, T. Ertekin, and D.H. Simth, "Simulating carbon dioxide sequestration/ECBM production in coal seams: Effects of coal properties and operational paramaters," in *Society of Petroleum Engineers*, 1999.

[67] M. Saikat, A. Karnik, and G.H. Wolf, "Swelling of coal in response to CO_2 sequestration for ECBM and its effect on fracture permeability," in *Society of Petroleum Engineers*, 2001.

[68] D. Siriwardene, F. Smith, C. Gorucu, and T. Ertekin, "Influence of shrinkage and swelling of coal on production of coalbed methane and sequestration of carbon dioxide," in *Society of Petroleum Engineers*, 2001.

[69] R. Allis, S. White, T. Chidsey, W. Gwynn, C. Morgan, and M. Adams, "Natural CO_2 reservoirs on the Colorado plateau and southern Rocky mountains: candidates for CO_2 sequestration," in *First National Conference on Carbon Sequestration*, Washington, DC, May 2001, 2001, pp. 243-253.

[70] W.J. Werner, "Petrology of the Cutler formation (Pennsylvanian-permian) near Gateway, Colorado and the Fisher towers, Utah," *Journal of Sedimentary Petrology,* vol. 44, pp. 292-298, 1974.

[71] J. Lefever and L. Helms, "Bakken Formation Reserve Estimates, North Dakota ", D. North, Geological, Survey, Report Ed., ed, 2007.

[72] J.N. Moore, M. Adams, R. Allis, S. Lutz, and S. Rauzi, "Mineralogical and geochemical consequences of long term presence of CO_2 in natural reserviors: An example from the Springerville-St.Johns field, Arizona and New Mexico, U.S.A," *Chemical Geology,* vol. 217, pp. 365-385, 2005.

[73] R. Krueger, M. LoParco, and J. Bhattacharya, "Strike Variability Within a Wave-influenced Delta, The Gallup Sandstone, Shiprock, New Mexico," in *AAPG Annual Convention and Exhibition*, 2010.

[74] J.I. Dreever, *The Geochemistry of Natural Waters: Surface and Groundwater Environments*. Prentice Hall, INC., 1988.

[75] S.P. Neuhoff, L.G. Hovis, G. Balassone, and F.J. Stebbnis, "Thermodynamic properties of analcime solid solutions," *American Journal of Science,* vol. 304, pp. 21-66, 2004.

[76] C. M. Bethke, *Geochemical and Biogeochemical Reaction Modeling*. Cambridge, 1998.

[77] A.C. Lasaga, "Chemical kinetics of water rock interactions," *Journal of Geophysics,* vol. 89, pp. 4009-4025, 1995.

[78] Z. Duan and R. Sun, "An improved model calculating CO_2 solubility in pure water and aqeous NaCl solutions from 273 to 5333 K and from 0 to 2000 bar," *Chemical Geology,* vol. 193, pp. 257-271, 2003.

[79] A.F. White, "Chemical weathering rates of silicate minerals in soils," *Mineralogical Soceity of America,* vol. 31, pp. 407-461, 1995.

[80] K.S. Pitzer and L. Brewer, *Thermodynamics*. McGraw-Hill, 1961.